MDOT RC-1514

Combining Link Slab, Deck Sliding over Backwall, and Revising Bearings

FINAL REPORT – AUGUST 2008

Western Michigan University
Department of Civil & Construction Engineering
College of Engineering and Applied Sciences

Research

Intentionally left blank

Technical Report Documentation Page

1. Report No. **Research Report RC-1514**	2. Government Accession No.	3. MDOT Project Manager **Roger Till, P.E.**	
4. Title and Subtitle **Combining Link Slab, Deck Sliding over Backwall, and Revising Bearings**		5. Report Date **August 31, 2008**	
7. Author(s) **Dr. Haluk Aktan, Dr. Upul Attanayake, and Mr. Evren Ulku**		6. Performing Organization Code **WMU**	
9. Performing Organization Name and Address **Department of Civil and Construction Engineering** **College of Engineering and Applied Sciences** **Western Michigan University** **1903 W. Michigan Ave, Kalamazoo, MI 49008**		8. Performing Org Report No.	
12. Sponsoring Agency Name and Address **Michigan Department of Transportation** **Construction and Technology Division** **PO Box 30049, Lansing MI 48909**		Work Unit No. 11. Contract Number : **2006-0415** 11(a). Authorization Number: **1**	
15. Supplementary Notes		13. Type of Report and Period Covered **Final Report, 2006-2008** 14. Sponsoring Agency Code	

16. Abstract

The new bridge design trend is to avoid having expansion joints over piers and abutments to prevent premature deterioration of bridges due to faulty joints. For this purpose joints over the piers are eliminated using link slabs where the deck is continuous and the underlying girders are simply supported. The expansion joints over the abutments are also eliminated by allowing the deck to slide over the backwall or by allowing the deck-backwall combined system to slide over the abutment (semi-integral abutments). Consequently, the movement of the superstructure is transferred to the ends of the approach slab that sits on a sleeper slab.

The research was designed to respond to the concerns of the designers in terms of the design of specific components and field performance of a limited number of bridges retrofitted with the link slab deck system. Three tasks were performed in this project. The first task was to review and synthesize information related to the behavior, performance, design, and analysis of jointless bridges with link slabs. The second task was to document the distress at the sleeper slab and bearings in Michigan jointless bridges associated with the link slab, approach slab, abutments, pier caps, and expansion joints. The third and final task was to develop analysis models of the jointless bridge deck system including link slab, bearings, abutment types (deck sliding over backwall and backwall sliding over abutment), approach slab, and sleeper slab.

Based on literature reviewed, field inspection data analysis, finite element modeling, and subsequent simulations of the numerous models developed in this project, four design recommendations are developed. One recommendation deals with the link slab design and the remaining three deal with the backwall and approach slab region. Current link slab design is solely based on the moment demand due to live load, but AASHTO LRFD (2004) Service I limit state requires a combined effect of live and thermal load in calculating link slab moment demand. Hence, a new analysis procedure is proposed for calculating link slab design moment and axial load from thermal gradient load.

17. Key Words: **Approach Slab, Abutment, Concrete, Deterioration, Finite Element, Jointless Bridge, and Link Slab.**		18. Distribution Statement **No restrictions. This document is available to the public through the Michigan Department of Transportation.**	
19. Security Classification (report) **Unclassified**	20. Security Classification (Page) **Unclassified**	21. No of Pages **195**	22. Price

Intentionally left blank

COMBINING LINK SLAB, DECK SLIDING OVER BACKWALL, AND REVISING BEARINGS

Project Manager: Mr. Roger Till, P.E.

Submitted to:

MDOT

Submitted by

Dr. Haluk Aktan, P.E.
Professor & Chair
(269) – 276 – 3206
haluk.aktan@wmich.edu

Dr. Upul Attanayake, E.I.T
Assistant Professor
(269) – 276 – 3217
upul.attanayake@wmich.edu

Mr. Evren Ulku
Graduate Research Assistant
(313) – 577 – 3785
evren@eng.wayne.edu

Western Michigan University
Department of Civil & Construction Engineering
College of Engineering and Applied Sciences
Kalamazoo, MI 49008
Fax: (269) – 276 – 3211

Intentionally left blank

DISCLAIMER

The content of this report reflects the views of the authors, who are responsible for the facts and accuracy of the information presented herein. This document is disseminated under the sponsorship of the Michigan Department of Transportation in the interest of information exchange. The Michigan Department of Transportation assumes no liability for the content of this report or its use thereof.

Intentionally left blank

ACKNOWLEDGEMENTS

This project is funded by the Michigan Department of Transportation. The authors would like to acknowledge the support and effort of Mr. Roger Till for initiating this research. The authors also wish to acknowledge the continuing assistance of the Research Advisory Panel (RAP) members in contributing to the advancement of this study.

Intentionally left blank

EXECUTIVE SUMMARY

INTRODUCTION

The new bridge design trend is to avoid having expansion joints over piers and abutments to prevent premature deterioration of bridges due to faulty joints. For this purpose joints over the piers are eliminated using link slabs where the deck is continuous and the underlying girders are simply supported. The expansion joints over the abutments are also eliminated by allowing the deck to slide over the backwall or by allowing the deck-backwall combined system to slide over the abutment (semi-integral abutments). As a result the movement of the superstructure is transferred to the ends of the approach slab that sits on a sleeper slab. Integral abutments that are used in jointless bridge systems are not within the scope of this project.

This research was designed to respond to the concerns of the designers in terms of the design of specific components and field performance of a limited number of bridges retrofitted with the link slab deck system.

The objectives of this study were identified as follows:

1. Identify distress associated with the following: link slab, approach slab, abutments, pier caps, expansion joints at the sleeper slab, and bearings during field inspection of selected bridges.
2. Develop finite element models of selected components, or combinations of several components, of the link slab bridge deck system [including bearings, abutment types (deck sliding over backwall and backwall sliding over abutment), approach slab, and sleeper slab] to understand the behavior and interaction between components under various load conditions, including volume change load.
3. Develop recommendations for changes or modifications to the design of the link slab bridge deck system including bearings, abutment types, approach slab, and sleeper slab.

To satisfy the objectives, this project was organized into three main tasks: literature review, field inspection, and analytical modeling.

LITERATURE REVIEW

Review of analysis methods, design details, and performance of the link slab deck system with either deck sliding over backwall or backwall sliding over abutment was performed. Bridge superstructure retrofitting methods that eliminate deck joints were investigated. Furthermore, certain design configurations with records of satisfactory performance were identified. It was found that certain states such as North Carolina are implementing link slabs designed with two layers of continuous reinforcement. Regarding the deck sliding over a backwall configuration, Michigan uses a more favorable joint location than what is utilized in New York and Virginia. Consequently, the use of continuous bottom reinforcement instead of top layer through the construction joint is encouraged to prevent moment transfer between the span and approach slab. For integral and semi-integral abutment details, the use of diagonally placed reinforcement to tie the approach slab to the backwall is capable of reducing deck cracking in the vicinity of the abutment allowing the joint to behave as a hinge to accommodate the inevitable rotation over the backwall.

FIELD INSPECTION

Five unique and three similar bridges were selected for inspection in order to identify performance differences, if there were any. The thought behind the selection process was twofold. First, two repair categories such as deck replacement and deck overlay were considered. Second, three design categories were considered. The design categories were semi-integral with bearings redesigned, deck sliding over backwall with steel beams, and deck sliding over backwall with prestressed concrete beams. These design categories appeared to be the most common among the retrofit applications. A list of bridges identified for inspection is given in Table E1.

Table E1. Bridges Selected for Field Inspection - Inventory Information

No	Bridge ID	Year Built	Region	County	Feature Intersected	Facility	Main Spans	Max Span (ft)	Length (ft)	Skew (Deg.)	Girder Type
1	S04-1 of 63174[+]	2001	Metro	Oakland	13 Mile Road	I-75 NB	3	63	141	0	PC[++]
2	S04-2 of 63174[+]	2001	Metro	Oakland	13 Mile Road	I-75 SB	3	63	141	0	PC
3	S08 of 41027	1964	Grand	Kent	Monroe	I-196 EB M-21	3	72	179	Varies	ST*
4	B01 of 10042	2003	North	Benzie	Betsie River	M-115	3	50	150	20	ST
5	S12-3 of 25042[**]	1969	Bay	Genesee	I-75	I-69 EB	4	70	210	20	PC
6	S12-4 of 25042[**]	1969	Bay	Genesee	I-75	I-69 WB	4	70	210	20	PC
7	S12-7 of 25042[**]	1969	Bay	Genesee	I-75	I-69 Ramp E	4	70	210	20	PC
8	S12-8 of 25042[**]	1960	Bay	Genesee	I-75	I-69 Ramp F	4	70	210	20	PC

+ Identical bridges; ++ Prestressed concrete girders; * Steel girders; ** Identical bridges

The inspection looked into a series of performance issues: link-slab cracking, approach slab movement, approach slab cracking, deck condition near the construction joint adjacent to the backwall, backwall and girder end interface in case of a dependent backwall, and the condition of abutments, pier caps, and bearings. A predominant distress observed in all bridges was full- depth link slab cracking over the pier centerline irrespective of bridge girder type and span length and regardless of whether or not they had saw cuts. Vertical cracks in the abutment wall were also common to all inspected bridges. Abutment D-cracks were present only in two of the eight bridges; however, abutment performance was not affected by retrofit applications that eliminated deck joints. Six out of eight inspected bridges had short horizontal cracks near the bearings. Five bridges had distressed bearings. An overview of findings is presented in Table E2 and Table E3 below.

Table E2. Summary of Approach Slab Inspection Data

Bridge ID	Description	Saw cut over abutment	Cracks over abutment	Diagonal cracks	Expansion joint function	Skew (Deg.)
S04-1-63174	I-75 NB over 13 Mile Rd	No	No	No	Yes	0
S04-2-63174	I-75 SB over 13 Mile Rd	No	No	No	Yes	0
S08-41027	I-196 EB over Monroe Av	Deck top surface could not be inspected				Varies
B01-10042	M115 over Betsie River	Yes	Yes	No	Not observed[+]	20
S12-3-25042	I-69 EB over I-75	No	Yes*	Yes*	Yes	20
S12-4-25042	I-69 WB over I-75	No	No	Yes	Yes	20
S12-7-25042	I-69 EB Ramp over I-75	No	Yes*	Yes*	Yes	20
S12-8-25042	I-69 WB Ramp over I-75	No	No	Yes	Yes	20

* Only on one approach slab

+ Due to previous night rain cracks on dirt fill could not be seen

Table E3. Summary of Abutment and Backwall Inspection Data

Bridge ID	Description	Abutment wall cracks types		Backwall cracks		Distressed bearings	Bearing at abutment	Skew (Deg.)
		D	Vertical	General	Bearing vicinity			
S04-1-63174	I-75 NB over 13 Mile Rd	Yes	Yes	No	Yes	No	MF/MF[+]	0
S04-2-63174	I-75 SB over 13 Mile Rd	Yes	Yes	No	Yes	No	MF/MF	0
S08-41027	I-196 EB over Monroe Av	No	Yes	No	No	No	Fix/Exp[++]	Varies
B01-10042	M115 over Betsie River	No	Yes	Yes	Yes	Yes	Exp/Exp	20
S12-3-25042	I-69 EB over I-75	No	Yes	No	No	Yes	MF/MF	20
S12-4-25042	I-69 WB over I-75	No	Yes	No	Yes	Yes	MF/MF	20
S12-7-25042	I-69 EB Ramp over I-75	No	Yes	No	Yes	Yes	MF/MF	20
S12-8-25042	I-69 WB Ramp over I-75	No	Yes	No	Yes	Yes	MF/MF	20

+ MF: Modified-fixed bearing; ++ Fix: Fixed-bearing and Exp: Expansion bearing

ANALYTICAL MODELING

Finite element analysis was utilized to understand the behavior of the jointless bridge structural system with link slabs to verify the design assumptions and propose fine-tuning to the current design procedures. This task was accomplished by developing and analyzing refined finite element models representing link slab and abutment regions.

The objectives of the finite element modeling discussed in this report are to study the effects of various types and levels of loads on the design parameters of the jointless bridges, to understand the behavior of the bridge structural system, and to provide required fine-tuning to the current design for improved performance.

Link Slab Region

Single girder, two span assemblage models were developed evaluating the effects of various types and levels of loads on the design parameters of the link slab, understanding the behavior of the bridge structural system, and providing required fine-tuning to the current design for improved performance. The investigated design parameters of the link slab were as follows: the link slab debonded length with respect to adjacent span lengths, girder height, adjacent span ratio, and support conditions. Results of the link slab assemblage models showed that support conditions underneath the link slab had a great influence on the moments and axial forces developed within the link slab. Also, the deformation demand on the bearings due to uniform thermal loads was considered. Existing bearings had more than enough reserve capacity for girder-end displacements. Furthermore, bridge deck casting

sequence and drying and hydration thermal loads were evaluated using ACI 209 (1992) and CEB-FIP (1990) models. Thermal hydration and drying shrinkage strains resulted in cracks as wide as that may develop by live load. In addition, analyses of straight and 20^0 skew full-bridge models were conducted to investigate the load demand on link slabs. Another important consideration included in the analysis was the link slab torsion and twist that arise from asymmetric loading of single and two lane bridges. Full bridge link slab assemblage models revealed that torsion arises in link slabs of skew bridges irrespective of support conditions. Lower and upper bound bearing stiffness had a greater influence on torsion and twisting moments than bending moments and axial forces. Moreover, service and strength load demands of the link slab were calculated according to AASHTO LRFD (2004) procedures and compared to the capacity of a singly or doubly reinforced cross-section. Positive thermal gradient loading could alone exceed the section capacity creating positive moment at the link slab where only top reinforcement is continuous.

Approach Slab/Abutment Region

Assemblage models of the approach slab region with dependent and independent backwall arrangements were developed to investigate the load demands on approach slab, sleeper slab, backwall, and the abutment. The models consisted of a composite girder-deck cross-section that spans between the abutment and the first pier, approach slab, sleeper slab, and backwall. Also, two independent and four dependent backwall configurations were investigated to evaluate their comparative response and propose design modifications. Contact-interaction surfaces were utilized between various components such as approach slab-sleeper slab, deck-expanded polystyrene, and bearing plate-abutment to evaluate the effects of tangential friction under various loading conditions. In addition to the load cases given in MDOT Bridge Design Manual (2005), two other load cases were also considered to investigate the critical load demands. The effects of backfill and sleeper slab rocking were incorporated into the models. Backfill effects increased stress and force resultants of around 5% for its most critical scenario whereas sleeper slab rocking caused an increase in approach slab mid-span moments as much as 35%. The deformation demands on the bearings due to thermal loads and restraints that may stem from frozen aggregate base or bearings were also investigated. It was concluded that additional restraints that may arise from the threshold friction between

the approach slab and aggregate base or bearings would not cause any additional distress within the approach slab region. Implementation of construction joints between the approach and deck and use of reinforcement details that help the joint behave as a hinge under negative moments over the backwall is recommended. Finally, single girder assemblages were expanded to develop multi girder bridge superstructure models in order to investigate the effects of torsion, twist and skew. The demands obtained under various load cases were compared to the section capacity. The calculated moment demand exceeded the approach slab cracking moment capacity.

CONCLUSIONS

Based on literature review, field inspection, and finite element analysis results, it is recommended to provide continuous top and bottom reinforcements for resisting service live and thermal gradient loading. Three saw cuts are recommended: one at each end of link slab and the other is directly over the pier centerline. Current link slab design is based on the moment demand due to live load. AASHTO LRFD (2004) Service I limit state requires the combined effect of live and thermal load in calculating link slab moment demand. A new analysis procedure is proposed for calculating link slab design moment and axial load from thermal gradient load as presented in Appendix F. Proposed detail is shown in Figure E1.

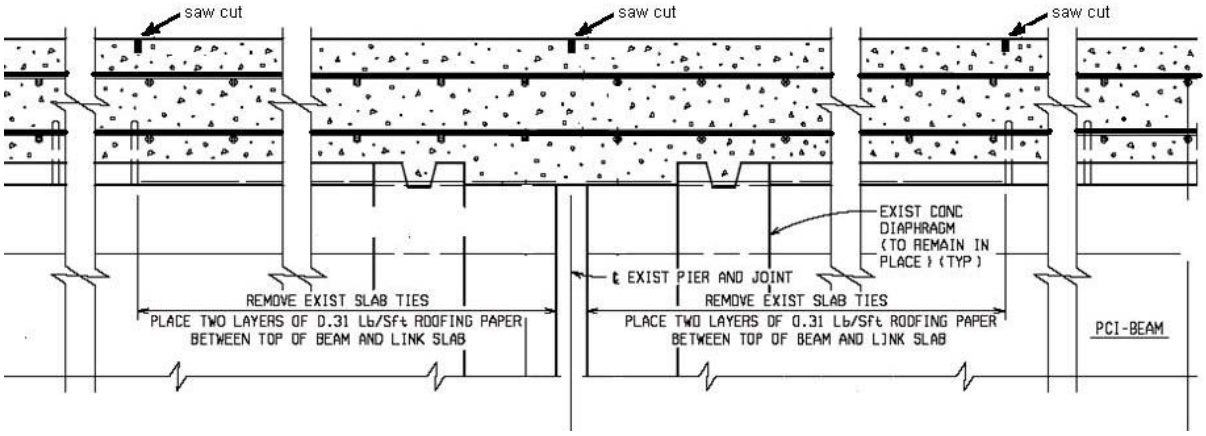

Figure E1. Proposed link slab details: both reinforcement layers are continuous with three saw cuts

Current Michigan details of deck sliding over independent backwall configuration utilize continuous top reinforcements through the construction joint. This configuration allows negative moment transfer through the joint defeating the purpose of providing a construction joint. Refined finite element analysis shows that greater stresses develop over the backwall

with the current configuration. The modification proposal to MDOT Bridge Design Guide 6.20.03A is shown in Figure E2. The proposed detail in standard MDOT Bridge Design Guide format is presented in Appendix G.

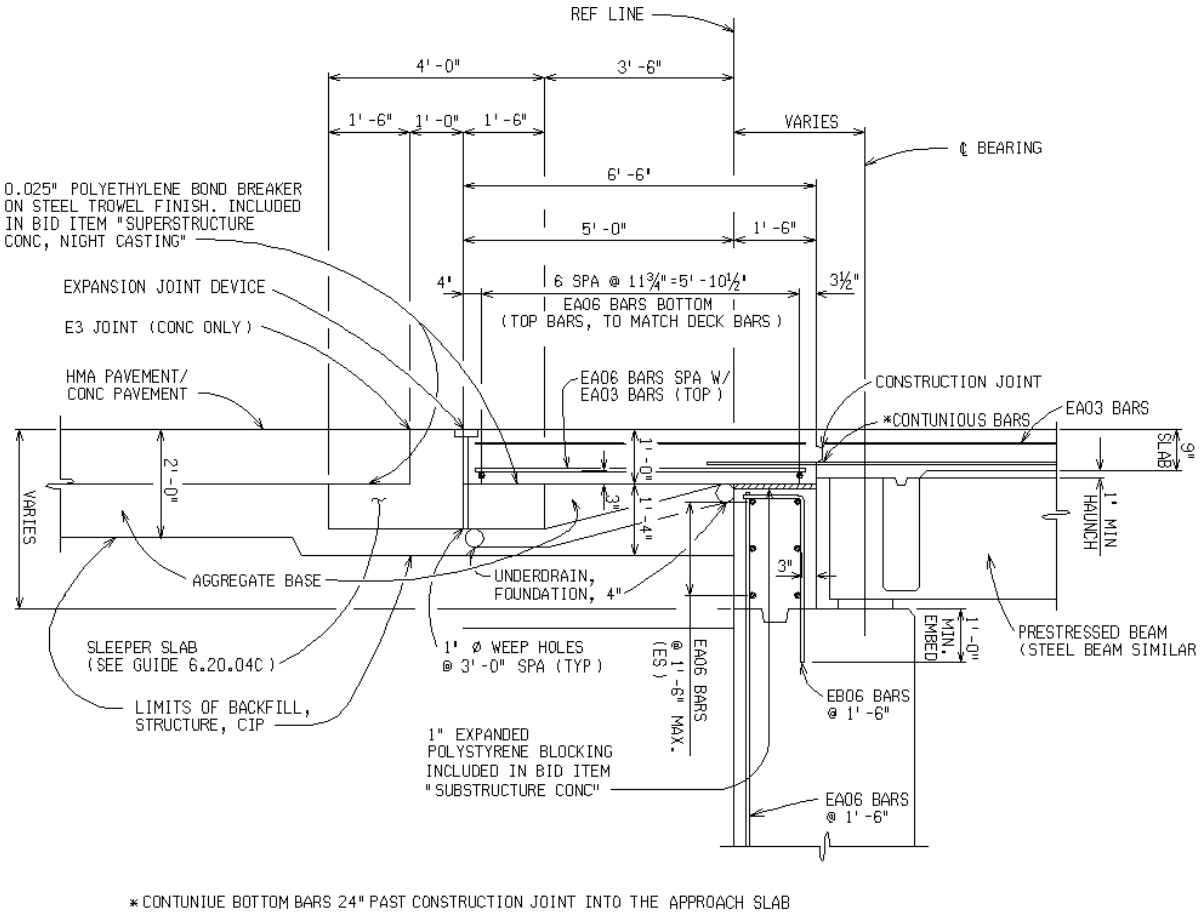

Figure E2. Proposed independent backwall configuration with deck sliding over backwall, i.e. continuous bottom layer reinforcement through the construction joint

Finite element analysis results showed that utilization of a hinge at the deck over the backwall face at the span side reduces the stresses at regions over the backwall of the current retrofit configuration. Utilization of a construction joint in conjunction with a saw cut and continuous bottom layer reinforcement is recommended. The proposed detail is shown in Figure E3. The proposed detail in standard MDOT Bridge Design Guide format is presented in Appendix G.

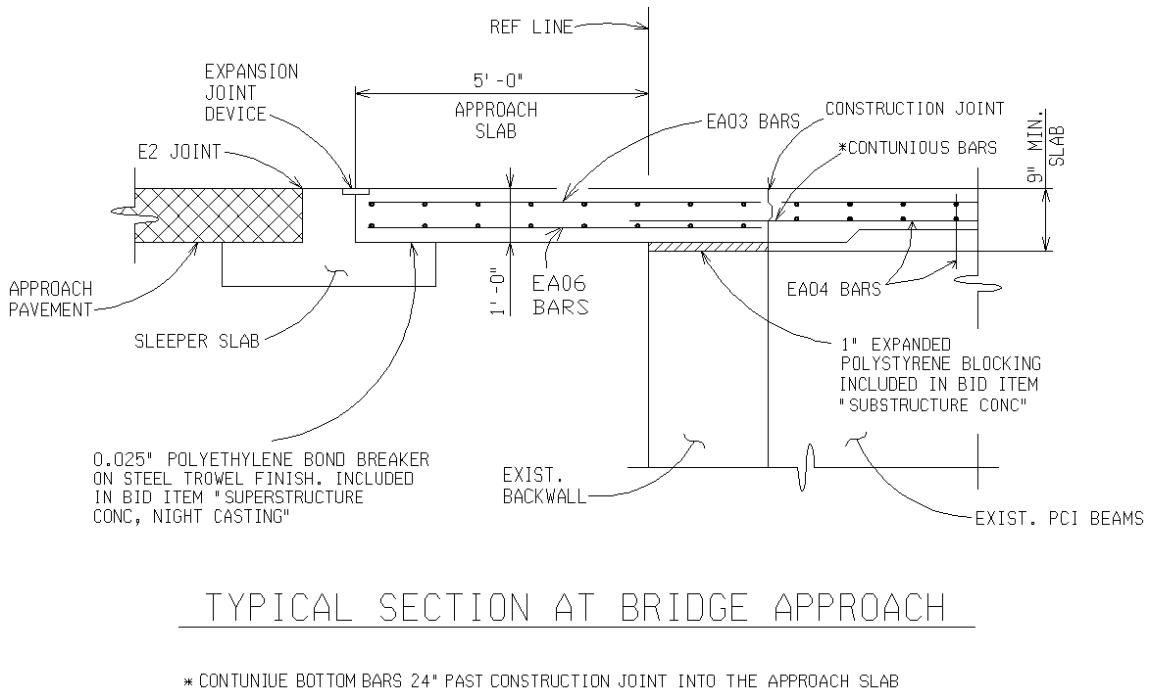

Figure E3. Proposed dependent backwall configuration for retrofit application, i.e. construction joint over the backwall face at the span side with continuous bottom layer reinforcement

Current MDOT standard abutment detail for semi-integral bridges uses a construction joint between approach slab and the deck. Refined FE analysis showed that the use of a hinge connection (i.e., a construction joint) helps relieve the stresses developed at the connection. Current MDOT detail shows a continuous bottom reinforcement layer through the construction joint. Literature reviewed shows that the NYDOT experienced cracking in the vicinity of the joint with a continuous bottom reinforcement layer and recommended discontinuing bottom reinforcement while using diagonal reinforcements connecting the approach slab and the backwall. This detail helps to develop a perfect hinge connection and is recommended for consideration. The modification proposal to MDOT Bridge Design Guide 6.20.04 is shown in Figure E4. The proposed detail in standard MDOT Bridge Design Guide format is presented in Appendix G.

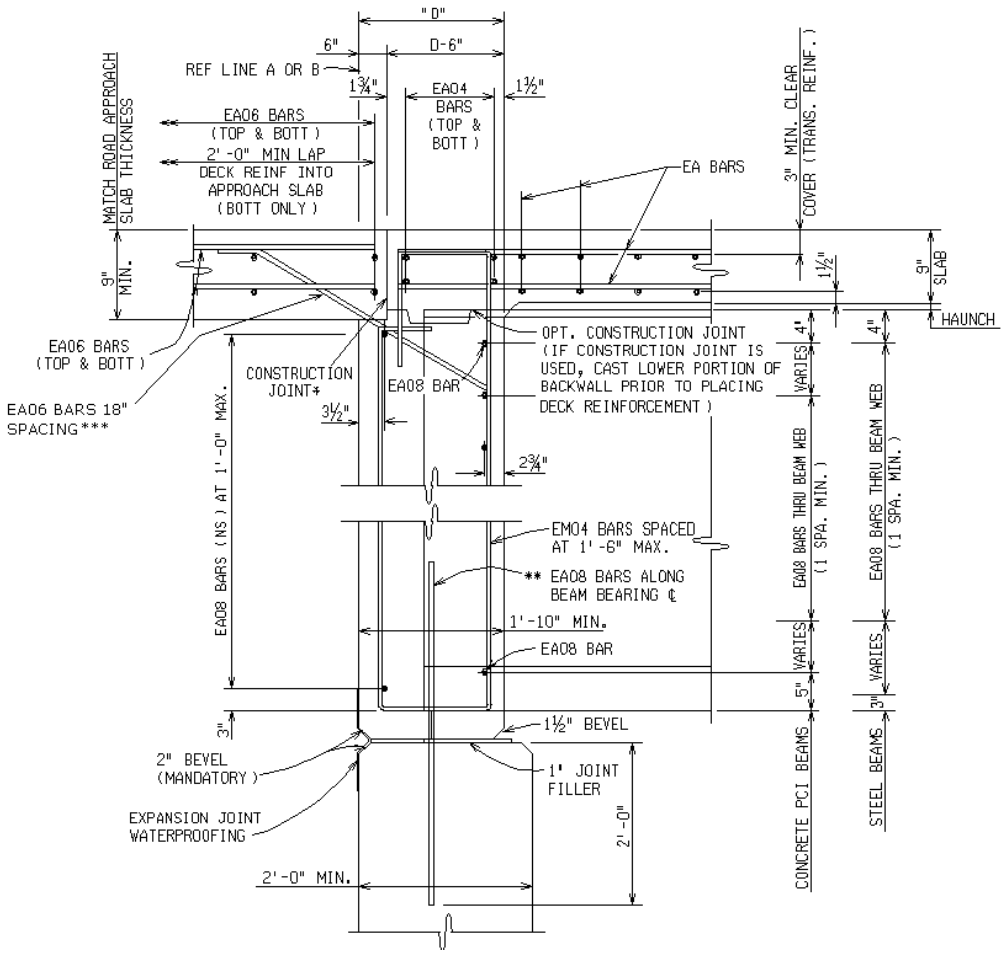

Figure E4. Proposed dependent backwall details for new construction; i.e., top and bottom reinforcements are discontinued at the construction joint and diagonal reinforcements are provided connecting approach slab and backwall.

Intentionally left blank

Contents

Intentionally left blank

TABLE OF TABLES

TABLE OF FIGURES

Intentionally left blank

1 INTRODUCTION

1.1 BACKGROUND

Jointless bridge deck systems are developed to resolve issues related to expansion joint performance. As shown in Figure 1-1 and Figure 1-2, joints over the piers are eliminated using link slabs where the deck is continuous and the underlying girders are simply supported. The link slab is the continuous cast-in-place deck portion joining the adjacent spans. Link slabs can be utilized with repair activities. The expansion joints over the abutments can also be eliminated by making the approach slab and the deck continuous and allowing the deck to slide over the backwall (Figure 1-3). An additional design for eliminating the abutment joint is by designing an approach slab-deck-backwall monolithic system, which slides over the abutment (often defined as semi-integral abutments) (Figure 1-4).

Deck sliding over a backwall or a backwall sliding over the abutment design is implemented with the deck to include the approach slab either monolithically or with a construction joint. The movement of the superstructure is transferred to the end of the approach slab that is supported by a sleeper slab (Figure 1-5). Link slabs, having the deck slide over a backwall, and semi-integral abutment are design options for bridge repair categories such as deck overlay and deck replacement.

The integral abutment bridge structure, which requires a flexible foundation structure, is also classified as a jointless bridge system. The integral abutment system is outside the scope of this project, since they can only be integrated in full bridge replacement or new constructions.

Current MDOT link slab design is based on the procedure described by Caner and Zia (1998). This project is designed to respond to designers' concerns regarding the performance of jointless bridges with link slabs and design details of other specific components of jointless bridges. Specific components are: link slab, backwall, approach slab, sleeper slab, and bearings (Figure 1-1).

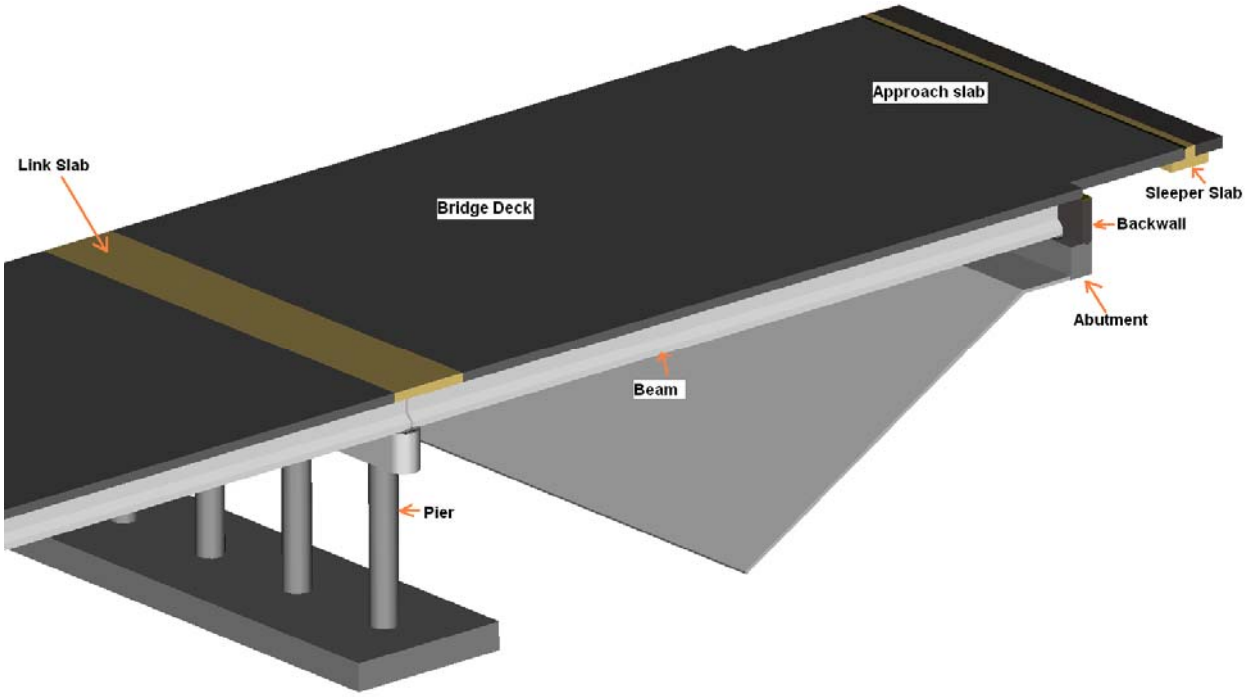

Figure 1-1. Jointless bridge deck

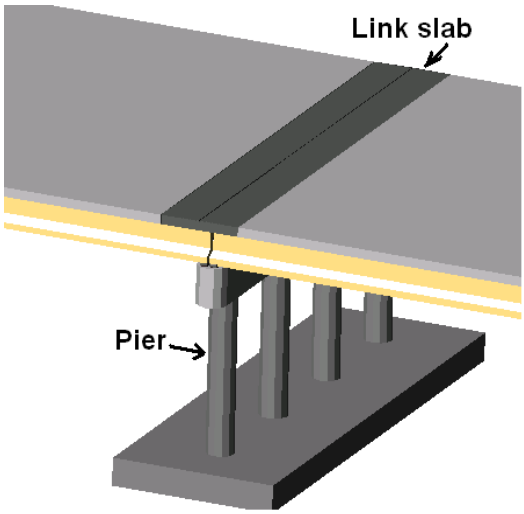

Figure 1-2. Link slab over the pier

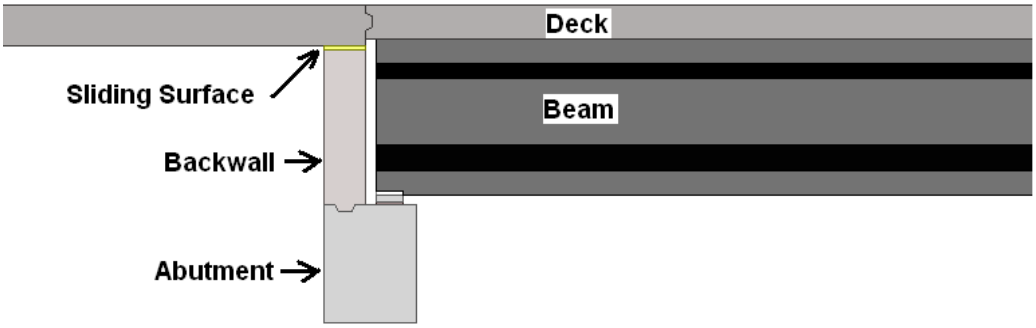

Figure 1-3. Independent backwall (deck slides over the backwall)

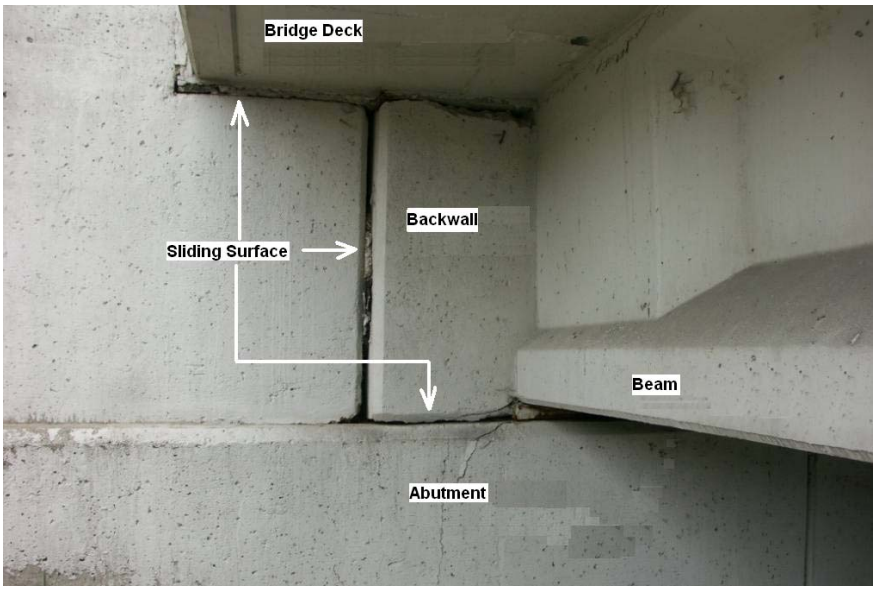

Figure 1-4. Dependent backwall (deck-backwall combination slides over the abutment)

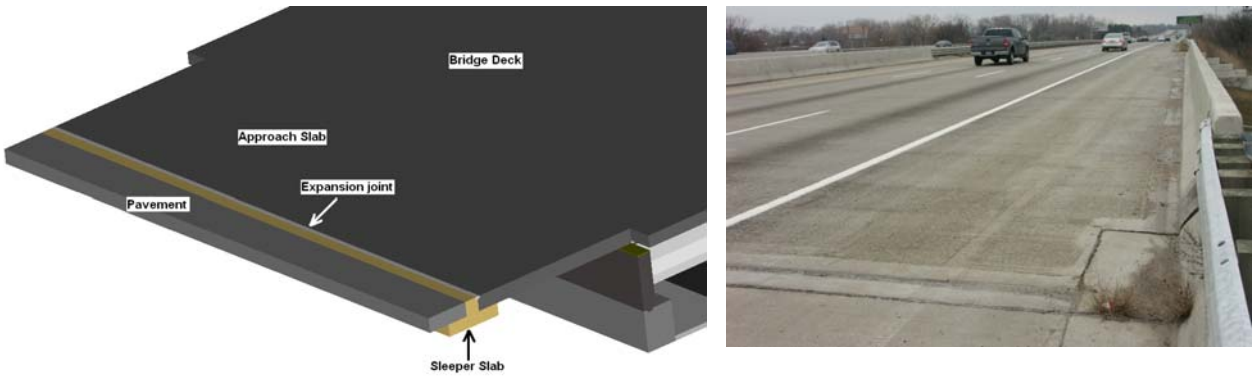

Figure 1-5. Expansion joint at the sleeper slab

1.2 PROJECT OBJECTIVE AND TASKS

The objective of this project is to evaluate the performance of jointless bridge systems/components, verify the design assumptions, and develop design recommendations for link slab, approach slab, sleeper slab, backwall and bearings. The project tasks are as follows: (1) literature review including evaluation of current design, field performance of jointless bridges, and analytical and numerical modeling techniques; (2) field inspection for performance assessment of jointless bridges; and (3) analytical and numerical modeling of jointless bridge structural systems with link slabs.

This report is organized with seven chapters.

The literature review is presented in Chapter 2 covering jointless bridge superstructure component behavior and design, behavior of straight and skew jointless bridges, performance of jointless bridges, and modeling and analysis of bridge structural system/components.

Chapter 3 includes the field inspection of five unique and three identical link slab bridges with either the deck sliding over a backwall or a backwall sliding over an abutment (semi-integral abutments). The bridge selection criteria for inspection were based on repair and design categories. Eight bridges were selected based on (1) two repair categories: deck replacement and deck overlay and (2) three design categories: semi-integral with redesigned bearings, deck sliding over backwall with steel beams, and deck sliding over backwall with prestressed concrete beams. The field inspection documented cracking within the link region as well as in the approach slab (especially over the backwall). The field assessment involved the movement and apparent rotation at the approach slab ends. Further, the bearing and substructure condition was documented. The compiled inspection data is included in Appendix A, B, C, and D.

Analytical modeling presented in Chapter 4 deals with the development and analysis of 3-dimensional refined finite element (FE) models for the link-slab, as well as full bridge models. The analysis of specific design parameters was performed. The design parameters were: link slab length, debonded length of the link slab over the piers, movement and rotation of the bridge deck with different support conditions (fixed or expansion) over the piers, girder size, and adjacent span ratio. FE model description and analysis results are presented in Chapter 4.

Furthermore, detailed analysis results and stress contours are included in Appendix E. Current link slab design is based on girder end rotations under live loads. ASHTO LRFD (2004) Service I limit state requires combined effect of live and thermal loads. Appendix F presents a detailed calculation procedure for moment and axial load demand under thermal gradient loading that can be incorporated into the current link slab analysis procedure.

Chapter 5 deals with the development and analysis of 3-dimensional refined FE models for the abutment region as well as full bridge models. The design parameters considered in the analysis are: movement and rotation of the bridge deck over the backwall or a deck-backwall combined system over the abutment, and movement and rotation of approach slab over the sleeper slab. Analysis models and results are presented in Chapter 5

Chapter 6 presents the comprehensive results and recommendations.

Chapter 7 discusses the need for further work on this topic.

Intentionally left blank

2 LITERATURE REVIEW

2.1 OBJECTIVE AND APPROACH

The objective of the literature review presented in this chapter is to identify, review, and synthesize information related to jointless bridges with simply supported girders. Concentration areas for the review are established for the project as follows, and are discussed within this chapter.

- Jointless bridge component behavior and design
- Longitudinal behavior of jointless bridge
- Behavior of jointless bridges with skew
- Performance of jointless bridges
- Modeling and analysis of jointless bridges

2.2 OVERVIEW

Most highway bridges in the United States have been designed as multiple simple-spans with either prestressed concrete or steel girders incorporating a cast-in-place concrete deck since the 1950s. Expansion joints are provided at each end of the span in order to accommodate movement due to thermal loads, creep, shrinkage, etc. Major problems associated with expansion joints are short life-span and subsequent inability to prevent the surface water runoff to the girder ends, bearings, and substructure leading to premature deterioration due to repeated and prolonged moisture exposure. These are more serious problems in states within low temperature zones similar to Michigan (Zones C and D defined by AASHTO) where a large amount of deicing salt application is required for controlling icing of the bridge deck. Additionally, debris accumulation at the joints restrains deck movement developing forces that were not accounted for.

As alternative options for the construction of jointless bridges, integral or semi-integral abutments with joints off of bridge abutments have been developed. The sliding deck that extends over the top of the backwall allowing joints to be placed away from the abutment backwall is another commonly applied type of jointless bridge (Maruri et al. 2005). Joints over the piers can be eliminated using link slabs where the cast-in-place deck is continuous while the underlying girders remain simply supported (Gilani and Jansson 2004). Semi-

integral and sliding deck abutment configurations are used by the Michigan Department of Transportation (MDOT) in some repair designs.

Jointless bridges have brought in many advantages as well as addressed a few performance issues in conventional jointed bridges. These advantages are improved riding quality, lower impact loads, and reduced snowplow damage. However, with eliminating joints, additional loads need to be dealt with in design. Thermal movements, which are accommodated by multiple joints in a conventional bridge, must now be accommodated by the joints provided at the ends of the bridge or by building flexibility into the support structures while providing sufficient strength for restraining forces. The magnitude of the forces generated through restraints and stiffness of the restraining elements are uncertain. Design of jointless bridges has primarily been based on designer judgment, empirical rules, technical references, and experience rather than scientific and engineering understanding of material and structural responses. Design and detail practices have varied among state highway departments (Oesterle et al. 2005 and Tabatabai et al. 2005).

2.3 JOINTLESS BRIDGE COMPONENT BEHAVIOR AND DESIGN

2.3.1 General

Link slabs are incorporated in bridge repair activities. Examples of some Michigan bridges are S04 of 63174, S12-8 of 25042, S04 of 70063, B01 of 10042 and B01 of 51041. In the case of full bridge replacement, the design incorporates integral abutments. Also, in the case of full bridge or superstructure replacement, the bearings can be redesigned to accommodate the link slab as well as the changes to the abutment design. For partial or full-depth deck replacement, the deck can be connected to the approach slab and designed to slide over the backwall. The design uncertainties other than link slab include the design of the approach slab, sleeper slab, backwall, and bearings.

2.3.2 Link Slabs

The link slab is designed using a rational procedure (Caner and Zia, 1998). The original design procedure was proposed by Gastal and Zia (1989). The link slab is modeled as a one dimensional beam system. It is assumed that the flexural stiffness of the link slab would be very low compared to that of girders, thus it cannot provide continuity between the girders.

Hence each span behaves as simply-supported, and the end-rotations of two adjacent girders under live load will generate the design moment at the connecting section of the deck - link slab. Therefore, the link slab is analyzed as a beam subjected to the adjacent girder end rotations. The link slab length (L in Figure 2-1), which is the debonded zone, is assumed to be 5% of each adjacent span plus the gap between the adjacent beam ends (Caner and Zia 1998). The maximum of 5% of debonded length is assumed to reduce the flexural stiffness of the link slab so as to minimize stress development at the connecting region (El-Safty 1994).

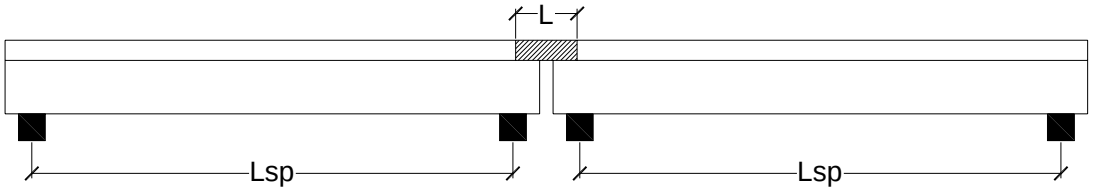

Figure 2-1 Length of link slab, L

The first link slab implemented in North Carolina was designed using the procedure set forth by Carner and Zia (1998). In this procedure, the deck with stay-in-place forms is detached by placing roofing paper over the girder to develop debonded region over the pier. Link slab is designed with two layers of continuous reinforcements (Figure 2-2) (Wing and Kowalsky 2005)).

Though utilized in many bridges, link slab detail is not standardized in Michigan. link slab details implemented in S12-25042 bridge is shown in Figure 2-3. Details show a debonded region where slab ties are removed, and two layers of roofing paper are placed over the beam. Bottom reinforcement is discontinued over the pier centerline.

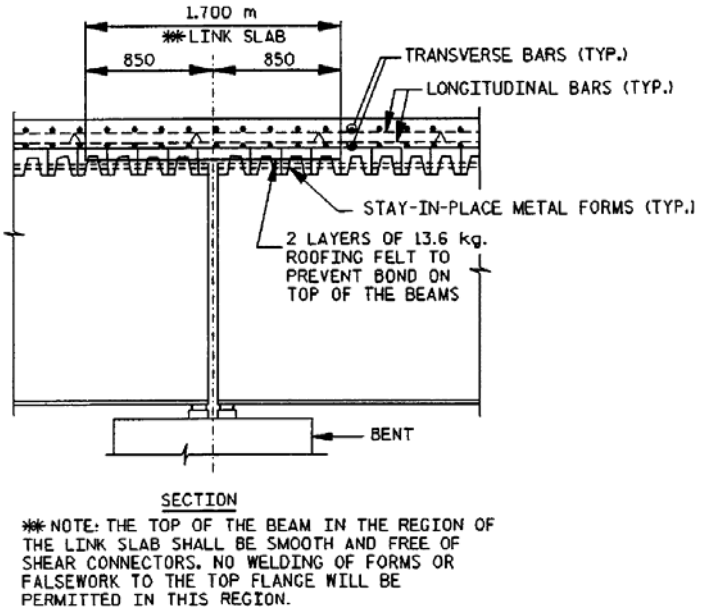

Figure 2-2. Details of the first link slab design implemented in North Carolina

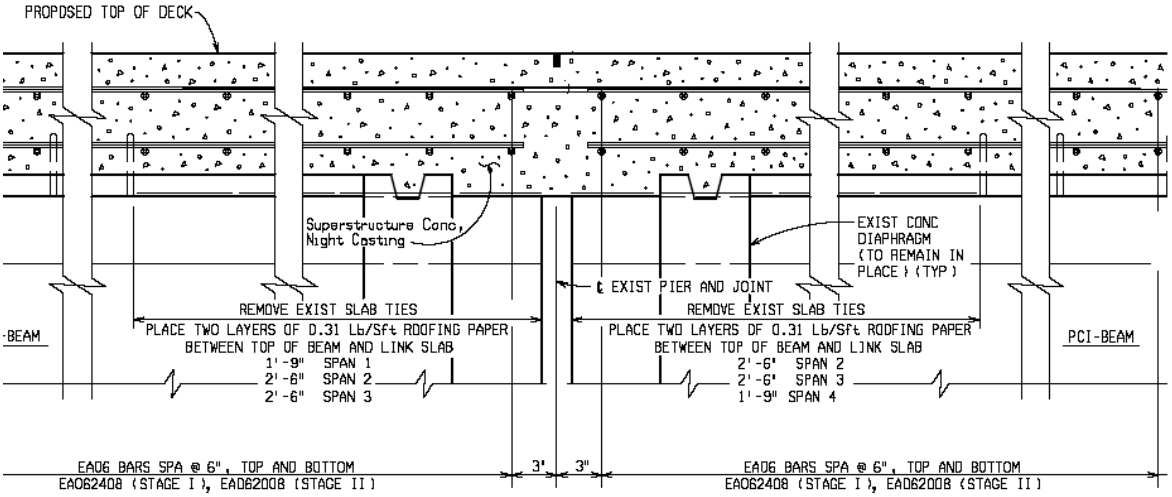

Figure 2-3. Longitudinal section through link slab (S12-25042)

2.3.3 Abutments

Three types of abutment details are used by MDOT in jointless bridges. The first two are the well defined semi-integral and integral abutment details. The third detail is similar to that described in the FHWA survey as "deck extensions" (Maruri and Petro 2005). "Deck extensions", which is also referred as "deck sliding over backwall," is incorporated in retrofit applications where the deck is placed continuously over the backwall with conventional abutments and independent backwalls (Figure 2-4). According to Michigan Bridge Design

Guide Sheet 6.20.03A (2006), sliding surfaces are developed with an expanded polystyrene (EPS) layer placed between the deck and backwall.

NYDOT also uses deck sliding over backwall design in retrofit applications (Alampalli and Yanotti 1998). The similarities in the details of MDOT and NYDOT designs are the use of a bond breaker between the deck and the backwall. The primary difference between the two applications is the location of the construction joint. While MDOT uses a construction joint aligned with the span side of the backwall, NYDOT extends the deck to the centerline of backwall (Figure 2-4). A study by Burke (1997) supports the MDOT detail. Virginia DOT utilizes a deck extension configuration similar to that of NYDOT. A ½-inch layer of EPS is placed between the backwall and the deck to seal the gap and provide vertical flexibility as well as allow longitudinal movement. Virginia DOT recommends using soft material such as EPS to reduce the load demand on the cantilever portion of the deck (Weakley 2005). A similar configuration was proposed by Wetmore and Peterson (2005).

An additional difference between MDOT and NYDOT design is the reinforcement details at the joint between the deck and the approach. MDOT uses continuous top reinforcement through the construction joint while NYDOT uses continuous bottom reinforcements. Continuous top reinforcement allows negative moment transfer across the joint. Strictly speaking, the construction joint is intended to act as a hinge and prevent negative moment transfer. Continuity for axial loads through the joint is central to the design. The change in bridge superstructure section from composite girder-deck section to a standard slab at the beam ends results in changing axial and flexural capacity; thus, this change develops strain concentrations. Providing a construction joint or a saw cut as shown in Figure 2-4 (b) is desirable for crack control.

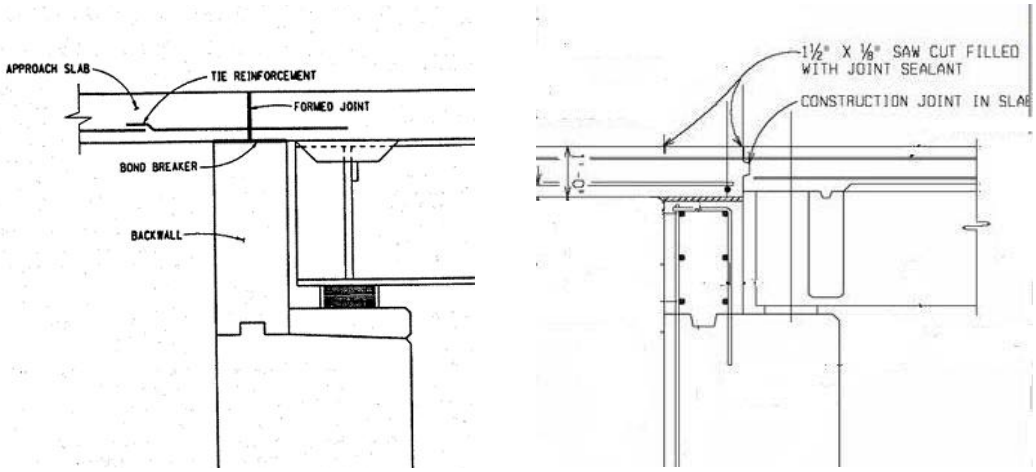

(a) (b)

Figure 2-4. Deck sliding over backwall: (a) NYDOT and (b) MDOT

An additional retrofit design detail is to embed the girder ends into the backwall (dependent backwall) while the deck is isolated from backwall using one-inch thick EPS layer between the backwall and the slab as a bond breaker (Figure 2-5). The purpose of the EPS layer appears to be for isolating the backwall from the approach slab. The sliding under thermal loads will take place between the backwall and the abutment. This particular detail is not considered as a standard in Michigan. MDOT standard details of a semi-integral bridge abutment are shown in Figure 2-6. Ohio and Virginia DOTs use somewhat different details from Michigan by placing diagonal reinforcement to tie the approach slab to the backwall (Figure 2-7). This detail allows the joint between the approach and the slab-backwall system to act as a hinge and accommodates the rotation over the backwall (Burke 1999 and Weakley 2005). Yannotti et al. (2005) provide improved details shown in Figure 2-8(b) for reducing deck cracking improving the earlier NYDOT details in Figure 2-8(a). The details given in Figure 2-8(b) prevent direct load transfer between the approach slab and the deck.

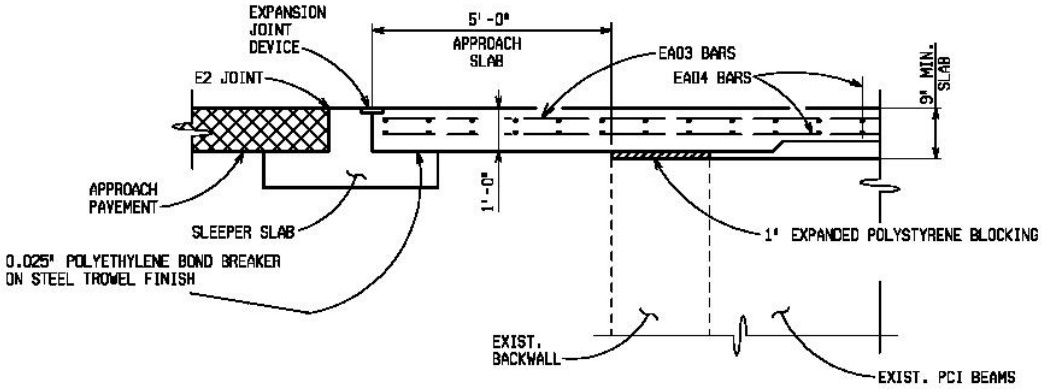

Figure 2-5. MDOT dependent backwall configuration used for retrofit applications

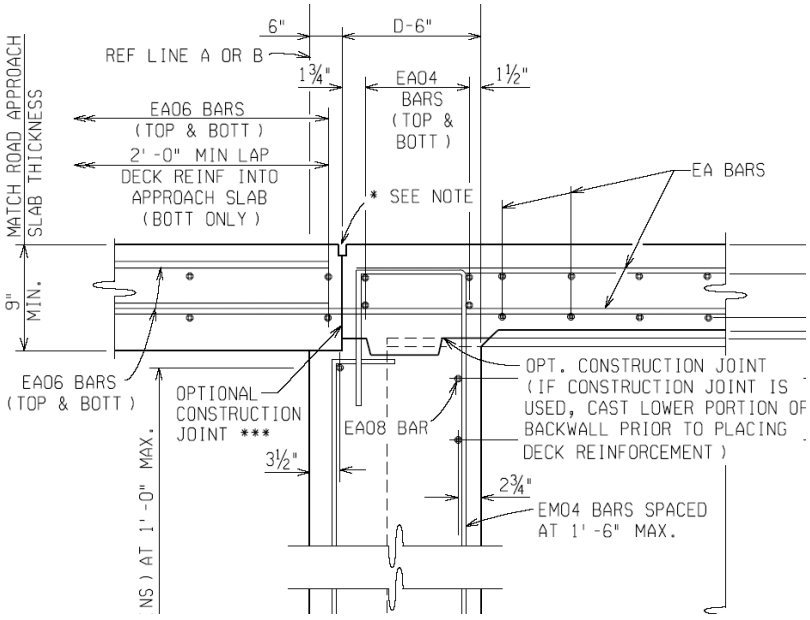

Figure 2-6. MDOT standard integral and semi-integral abutment details

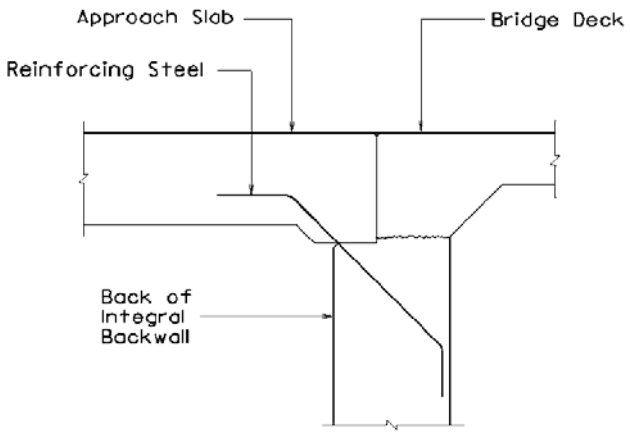

Figure 2-7. ODOT and VDOT approach slab-backwall connection detail

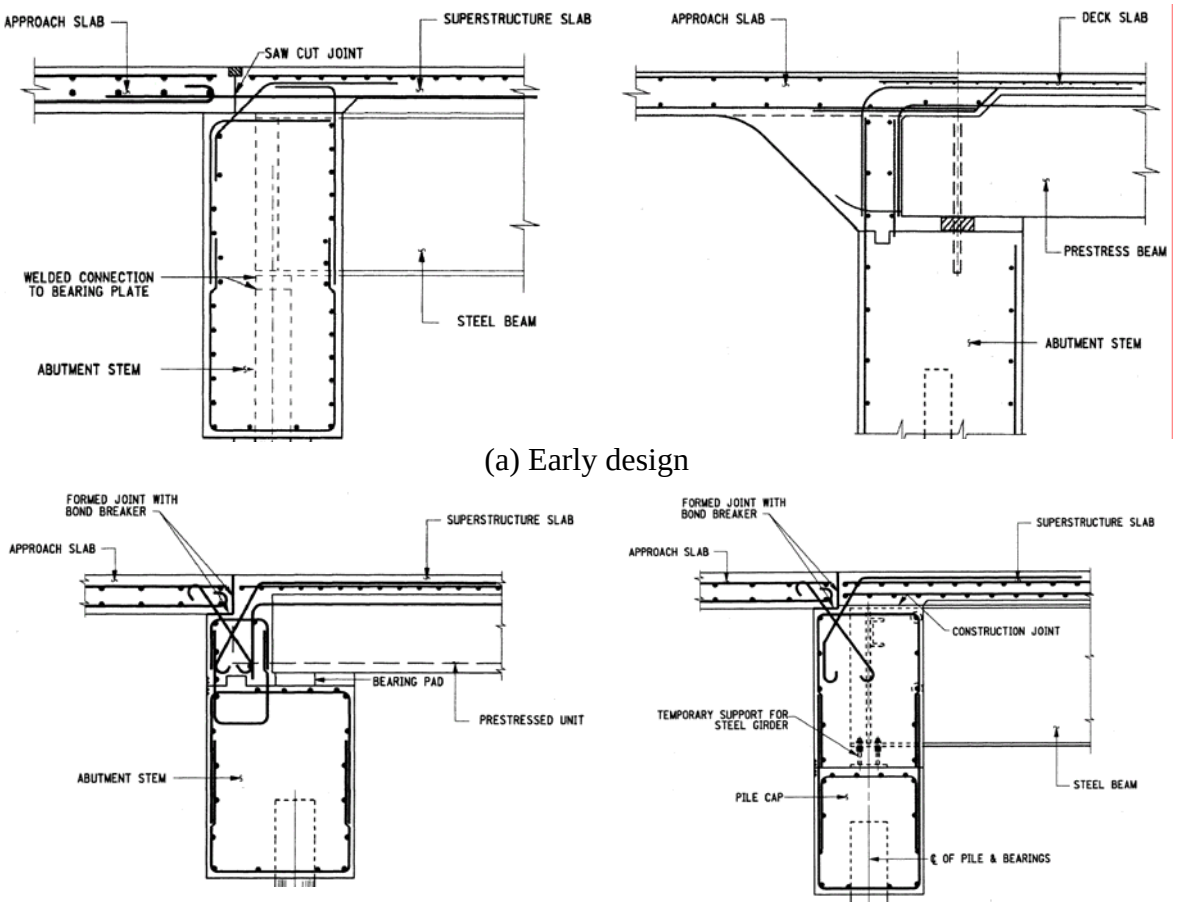

Figure 2-8. NYDOT integral abutment details

In semi-integral bridges, a sliding surface is provided between the backwall and abutment wall. Laminated elastomeric bearings are provided so that the superstructure can move over the rigid abutment. A watertight expansion seal is provided since the movable bridge seat

joint is buried within the backfill and consequently is not accessible for repair or replacement (Figure 2-9). Otherwise, backfill may wash into the joint, clogging it and limiting its function. The backwall should be able to expand adequately to withstand differential abutment-superstructure movement (Burke 1994). MDOT detail shows that the beam end is tied to the backwall using horizontal dowel bars placed through holes of the girder web. Similar detail is used by the Massachusetts and Vermont DOTs (Conboy and Stoothoff 2005). NYDOT has developed a significantly different semi-integral abutment detail that also accommodates bridge movement without backfill intrusion into the joints (Figure 2-10) (Yannotti et al. 2005).

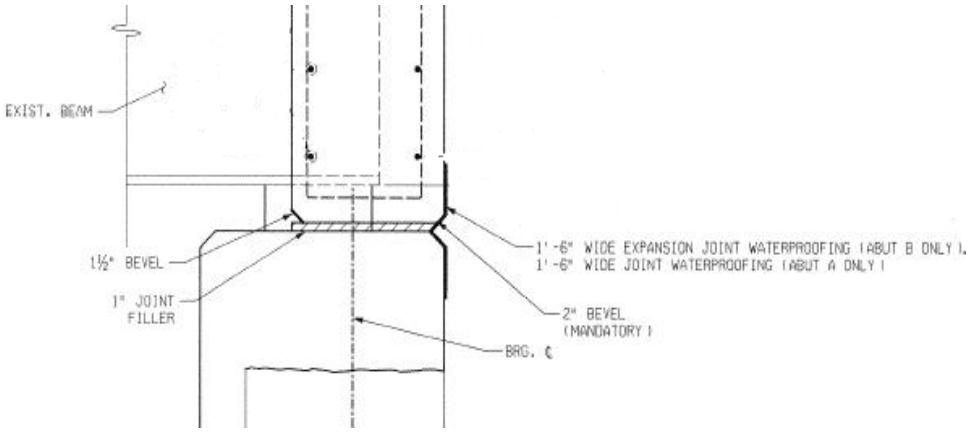

Figure 2-9. Expandable watertight seal in a semi-integral abutment

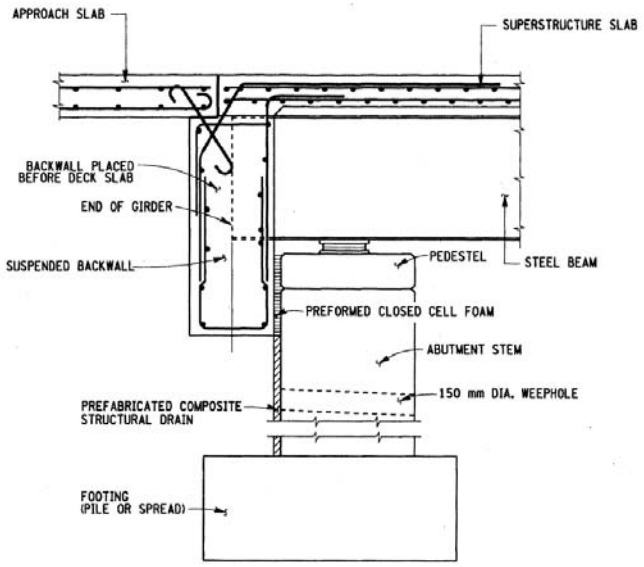

Figure 2-10. NYDOT semi-integral abutment detail

2.3.4 Approach and Sleeper Slabs

MDOT currently utilizes integrated approach slabs in all jointless bridges. An approach slab of 5 ft in length is used for deck sliding over backwall whereas a 20 ft approach slab is used for integral and semi-integral bridges. A sleeper slab with a stub in the middle is provided for supporting the approach slab on one side of the stub while the pavement rests on the opposite side (MDOT Bridge Design Guide 2006). An expansion joint is provided at the approach slab over the sleeper slab to accommodate bridge superstructure movements (Figure 2-5). Joints at the sleeper slab also help relieve the longitudinal pressures generated by the restrained growth of jointed rigid pavement (Burke 1998). An earlier detail did not utilize the sleeper slab and placed the approach slab adjacent to compressible hot-mix asphalt (HMA) pavement. Upon thermal cycles, irregular cracks formed at the interface, and also pavement settlement typically developed at the interface of the approach slab and the approach pavement (Mistry 2005). Wassermann and Walker (1996) proposed using a sleeper slab to support the approach slab with the design details shown below in Figure 2-11:

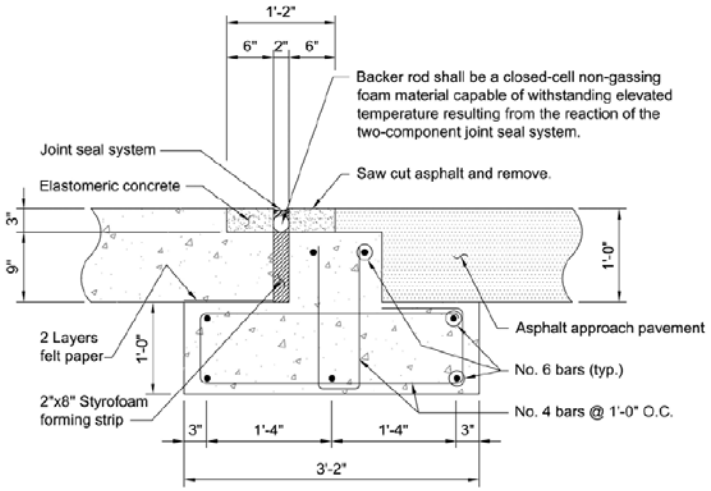

Figure 2-11. Sleeper slab details proposed by Wassermann and Walker (1996)

2.4 LONGITUDINAL MOVEMENTS OF JOINTLESS BRIDGES

In conventional bridges, the movements due to volume changes such as temperature, creep, and shrinkage are compensated by expansion joints. Once the joints are eliminated at the piers and/or abutments, these movements now must be accommodated elsewhere in order to prevent or reduce resulting restraining forces. Piers and abutments must be designed to

accommodate the anticipated movement, and the superstructure must be capable of carrying the forces induced by the stiffness of the piers and abutments (Oesterle et al. 2005). The restraints to the longitudinal movement are developed by active and passive earth pressures, shearing stiffness of elastomeric bearings, friction between approach slabs and sub-base, and friction at the other sliding surfaces (Burke 1997). Also, the use of turn-back wingwalls cantilevered from the superstructure in place of straight wingwalls would provide additional longitudinal restraint by mobilizing the resistance of backfill-wingwall friction (Burke 1994).

Once anticipated movement is calculated, the longitudinal movement can be incorporated in the design in a more comprehensive manner. Oesterle et al. (2005) proposed a methodology to calculate the anticipated longitudinal movements. Effect of coefficient of thermal expansion, effective temperature range including annual and diurnal temperature variations, creep and shrinkage on thermal expansion, and foundation, abutment, and pier rigidities on the structural system are considered for evaluating longitudinal movement and the resultant forces developed in the system.

The effective bridge temperature, which is also referred to as the mean or average bridge temperature, is the temperature that governs the overall longitudinal movement of the superstructure. Determination of the effective bridge temperature is influenced by many factors such as shade temperature, solar radiation, wind speed, material properties, surface characteristics, and section geometry. Many of these factors are highly variable and not necessarily related. Oesterle et al. (2005), like a number of other researchers, attempted to develop a relationship between the shade temperature and effective temperature (Emerson 1976 and Imbsen 1985). He proposed a linear relationship between the minimum and maximum effective bridge temperatures and the minimum and maximum shade temperatures adopted from American Society of Heating, Refrigerating, and Air-Conditioning Engineers (ASHRAE 1993) handbook. Accordingly, minimum and maximum effective bridge temperatures are calculated as follows:

For concrete bridges:

$$T_{min,eff} = 1.00\, T_{min,shade} + 9°F\ (5°C) \quad (2\text{-}1)$$

$$T_{max,eff} = 0.97\, T_{max,shade} - 3°F\ (2°C) + \Delta\overline{T}_{solar} \quad (2\text{-}2)$$

For composite steel bridges:

$$T_{min,eff} = 1.04\,T_{min,shade} + 3°F\ (2°C) \quad (2\text{-}3)$$

$$T_{max,eff} = 1.09\,T_{max,shade} - 3°F\ (0°C) + \Delta\overline{T}_{solar} \quad (2\text{-}4)$$

where,

$T_{min,eff}$ = minimum effective bridge temperature
$T_{max,eff}$ = maximum effective bridge temperature
$T_{min,shade}$ = minimum shade temperature from the weather data based on bridge location
$T_{max,shade}$ = maximum shade temperature from the weather data based on bridge location
$\Delta\overline{T}_{solar}$ = uniform temperature change from direct solar radiation based on girder type and bridge location

Minimum and maximum air shade temperatures as well as mean construction temperatures for various locations in the US are provided by ASHRAE (1993).

For a specific bridge, the available data may be interpolated between the State and nearest station values as needed. Additional uniform temperature increment caused by solar radiation can be determined by selecting the solar zone for the bridge location from AASHTO LRFD Specifications (1998). According to the solar zone, $\Delta\overline{T}_{solar}$ can be determined from Table 2-1.

Table 2-1. Solar Increment Values Based on Girder Type and Bridge Location (Oesterle et al. 2005)

Zone	T_1	Concrete $\Delta\overline{T}$	Composite Steel $\Delta\overline{T}$
1	17°F	4°F	3°F
2	14°F	4°F	3°F
3	13°F	3°F	2°F
4	12°F	3°F	2°F

Typical design values used are: 6.0×10^{-6} /°F (10.8×10^{-6} /°C) for the coefficient of thermal expansion of concrete, creep and shrinkage constants from ACI 209R-92 (1992), and the modulus of elasticity of concrete as 57,000 $\sqrt{f'_c}$, psi (4700 $\sqrt{f'_c}$, MPa).

Total length of the structure is calculated as the distance between the point of fixity to the end of bridge (Zederbaum 1969). According to Zederbaum (1969), the point of fixity can be determined for jointless bridges with pinned bearings on the piers as follows:

$$\bar{x} = \frac{\sum K_x L_x}{\sum K_x} \tag{2-5}$$

Where, $\bar{x}$ is the coordinate of the point of fixity, L_x is the horizontal distance along the longitudinal axis from the centerline of the piers/abutments to the zero point on the axis, K_x is the stiffness of the piers/abutments in the x direction (taking into account the effect of foundation rotation and bending in the pier).

The following equations are used to calculate the maximum end movement for a prestressed concrete bridge:

$$\varepsilon_{th} = \alpha \, \Delta T \tag{2-6}$$

$$\varepsilon_{sh} = \varepsilon_{sh_{girder}} + \frac{\varepsilon_{sh_{deck}} - \varepsilon_{sh_{girder}}}{1 + \frac{(EA)_{girder}}{(EA)_{deck}}} \tag{2-7}$$

$$\varepsilon_{cr} = \varepsilon_{cr_{girder}} \left[\frac{1}{1 + \frac{(EA)_{girder}}{(EA)_{deck}}} \right] \tag{2-8}$$

$$\Delta \ell = \Gamma \varepsilon_{total} \ell \tag{2-9}$$

where,

ε_{th} = thermal strain
ε_{sh} = shrinkage strain
ε_{cr} = creep strain
α = coefficient of thermal expansion
E = modulus of elasticity
A = cross-sectional area
ℓ = length from calculated point of fixity to end of bridge. Note that, for a nonsymmetrical bridge, two different lengths are involved.
Γ = magnification factor to account for uncertainty

$$\varepsilon_{total} = \varepsilon_{th} - \varepsilon_{sh} - \varepsilon_{cr} \text{ for expansion} \tag{2-10}$$

$$\varepsilon_{total} = -\varepsilon_{th} - \varepsilon_{sh} - \varepsilon_{cr} \text{ for contraction} \tag{2-11}$$

$\Delta\ell$ = maximum end movement

$\Delta T = T_{max,eff} - T_{mean,construction}$ for bridge expansion (2-12)

$\Delta T = T_{mean,construction} - T_{min,eff}$ for bridge contraction (2-13)

$\Delta T = T_{max,eff} - T_{min,eff}$ for re-expansion after full contraction (2-14)

Γ, magnification factor to account for uncertainty (Table 2-2), is calculated for prestressed concrete, cast-in-place concrete, and composite steel bridges for both bridge expansion and contraction using Monte Carlo simulation of statistical data.

Table 2-2. Values for Γ Magnification Factor. (Oesterle et al. 2005)

Design Condition	For Bridge Expansion		For Bridge Contraction	
	Total	End	Total	End
Conventional Design of Prestressed Bridge	1.50	1.60	1.30	1.35
Cast-in-Place Concrete Bridge	1.50	1.60	1.30	1.40
Composite Steel Bridge	1.50	1.70	1.45	1.50
Re-expansion After Full Contraction	1.10	1.20	—	—

A similar procedure can be used for a reinforced concrete bridge in establishing the maximum expansion and contraction end movements. However, creep shortening is not included as a factor. The procedure to estimate maximum end movements for composite steel bridges is similar to the procedure for prestressed concrete bridges, except that modulus of elasticity of 29×10^6 psi (20×10^4 MPa) and coefficient of thermal expansion of 6.5×10^{-6} /°F ($11.7\text{x}10^{-6}$ /°C) is used as recommended by AASHTO for structural steel.

2.5 JOINTLESS SKEW BRIDGE BEHAVIOR

AASHTO LRFD (2004) section C4.6.2.1.1 indicates that about two-thirds of bridges in the U.S. are skewed. Characteristics of skewed bridges are: reduction in maximum mid span moments compared to that of straight bridges under similar loads, negative moments at corners, torsional moments in the end zones, and redistribution of reaction forces. Skewed bridges develop high reactions and shear forces near wide corners and low reactions and

possibly uplift at narrow corners (Hambly 1991). When the deck uplifts and cantilevers off at the narrow corner, under live loads, cracking could be a possibility. According to Hambly (1991), skew issues are more critical in solid and cellular bridges than the multi beam bridge decks.

The effect of skew can be neglected when the skew angle is less than 20 degrees. However, for continuous bridges the lower skew angle effects are still critical particularly at the intermediate supports. Skewed bridges also exhibit a different response pattern with regard to both bearing displacements and restraint forces. Transverse movement may be observed in wider bridges, which tend to rotate with respect to the vertical axis, creating additional design issues. Restraint forces vary considerably with skew angles and show nonlinear behavior (Tindal and Yoo 2003).

Menassa et al. (2007) investigated the effects of different skew angles on reinforced concrete slab bridges. FE analyses results of skewed bridges were compared to the reference straight bridges as well as the AASHTO Standard Specifications (2003) and LRFD procedures (2004). Under live load, maximum longitudinal moment values decreased, whereas, maximum transverse moment increased with increasing skew angles. The variation in moment values was significant for skew angles greater than 20^{o}.

Oesterle et al. (2005) performed a detailed study of skewed jointless bridges; however, a majority of the structures covered in that study are integral or semi-integral bridge systems. According the study conducted by Oesterle et al. (2005), a skew angle of 20 degrees can be considered to be the upper limit for integral skew bridges. Unfortunately, there is no documentation on the behavior of high skew link slab bridges with deck extension.

2.6 JOINTLESS BRIDGE PERFORMANCE

In the 1930s and 1940s, Ohio, Oregon and South Dakota appear to have pioneered the use of jointless concrete bridges that are made continuous for live load (CLL). CLL deck bridges were introduced in California in the mid-1950s. By the mid-1960s, Tennessee and five other states had adopted CLL deck bridges with integral abutments as standard construction (Wasserman and Walker 1996). Since 1987, numerous states have adopted integral abutment bridges as structures of choice when conditions allow, and currently more than 40 states are

implementing some form of jointless bridges (Mistry 2005). However, the design and analysis of these bridges have mainly relied on technical references and design and detail practices have varied from state to state.

In 2004, Federal Highway Administration (FHWA), in conjunction with the Constructed Facilities Center at West Virginia University, conducted a nationwide survey to obtain a status of usage and design for integral abutments and jointless bridges (Maruri and Petro 2005). Descriptions of integral and semi-integral abutments as well as figures depicting each type were provided for obtaining consistent replies. Another form of jointless bridges, 'deck extensions' was also described in the survey as the extension of the deck over the top of the backwall where joints are placed behind the backwall (i.e., on the approach side). According to the responses obtained from 39 states out of 53, the uses of jointless bridges are mostly encountered in the northern states such as Tennessee, Missouri, Illinois, Iowa, Kansas, and Michigan. Southern states like Florida, Alabama and Texas do not use integral bridges and reported to have one or less bridge with integral abutments. One of the noteworthy conclusions of the survey was regarding the states' future plans to utilize jointless bridges. According to the survey, 79% of the responding states are planning to design bridges as jointless whenever they meet the criteria for jointless bridges, and 54% percent of the responding states are planning to retrofit existing bridges and eliminate deck joints wherever possible. In response to the questions regarding the use of approach slabs, 31% use a sleeper slab at the end of approach slab, 26% float the slab on approach fills, and 30% use both designs.

The survey also revealed interesting issues regarding the integral and semi-integral abutment design. Forces and pressures accounted in the design of abutments and piles, pile orientation, and backfill material were the criteria used for integral abutment selection. Approach slab details vary significantly from one state to another. In summary, the general performance of jointless bridges was found satisfactory, and their implementation was described as the first option; however, there are still problems to be addressed. The most encountered problem is the settlement of approach slabs stated by 84 % of the responders. Other common problems encountered were cracking of approach slabs, cracking of the deck at integral abutment,

cracking of the integral abutment backwall, cracking of the wingwall, detailing, and excessive rotation of the backwall, respectively.

NYDOT evaluated 105 jointless bridge decks in 1996, through field inspections of specific bridge components for establishing the needed improvements (Alampalli and Yanotti 1998). Jointless bridge decks considered in this study were built by eliminating the joints and making the deck slab continuous over the abutment. The design included a bond-breaker installed between the top of the backwall and the bottom of the deck providing a sliding surface to accommodate longitudinal movements. The beams were not embedded but supported on conventional bearings independent of the backwall (Figure 2-4). As part of the field evaluation, engineers inspected several visible bridge components that are influenced by the deck design details at the abutment, approach slab, first five feet of the deck, and the wearing surface near the abutments. Settlement of the approach slab was commonly recorded. The study rated the performance of jointless decks as very good except for some minor deck cracking. The use of current jointless-deck details was recommended without significant design changes. The study also concluded that the integral bridges and jointless decks have been performing as designed and showed superior performance when compared to conventional bridges of similar age and exposure (Alampalli and Yanotti 1998). Minnesota uses a deck sliding over backwall configuration that is similar in detail with the NYDOT configuration (Figure 2-4). The approach slab width of the Minnesota bridge was reduced over the backwall and developed cracks that radiate from the edge of the top beam flange to the corner of the overhang sliding over the backwall (Figure 2-12) (Wetmore and Peterson 2005).

Figure 2-12. Cracking of Minnesota bridge deck at the reentrant corner

New Mexico has pursued semi-integral abutment types while retaining the bearings over pier caps. This resulted in some unexpected problems. In the rehabilitation of an existing four span bridge, joints were replaced with link slabs. The bridge deck, which had become continuous for four spans, was forced to move as a four-fold plate. The bearings failed to adequately accommodate for this four-fold movement, and, instead, transferred much of this movement into the pier cap. The substructure stiffness resisted the movement resulting in damage to the concrete pier caps. Pier cap repairs and bearing modifications have since addressed this problem. In the approach slab design, the use of sleeper support has reduced the approach slab settlement and associated problems, but poor compaction or deep sub-grade consolidation still lead to sleeper settlement. It is reported that there are issues to be resolved such as negative moment cracking in link slabs, construction sequence, abutment movement, and approach slab settlement (Maberry et al. 2005).

Virginia Department of Transportation (VDOT) has been promoting the use of jointless bridges for many years. VDOT currently implements three types of jointless construction: integral, semi-integral, and deck extension. VDOT also experienced problems associated with design and details. With the constant movement of the integral abutment, problems arose with the settlements of the approach backfill. Other problems were related to longitudinal superstructure movement, superstructure rotation, and staged constructions (Weakley 2005).

As part of the comprehensive study under the sponsorship of FHWA, field inspections of 15 Tennessee jointless bridges were carried out to evaluate the design details that may have worked well or those that may have not performed as anticipated (Tabatabai et al. 2005). The inspected bridges included different material and structure types, including steel, prestressed, and reinforced concrete; I-beams, box beams, and an arch. They also included straight, curved, and skewed bridges as well as new design and retrofitted jointless bridges. Some significant observations related to the performance of bridge components are as follows:

- *Very minor (hairline) transverse cracks were noted on the decks of two of the bridges retrofitted to be continuous deck on simply supported girders (decks with link slabs).*
- *Evidence of significant transverse movement of the abutments was observed in bridges with large skews and/or horizontal curves. U-type wingwalls on these abutments would be expected to be subjected to lateral resisting forces from soil passive pressure and from the piles. On the other hand the stub abutment wingwalls were performing well.*
- *Two of the bridges inspected did not have approach slabs. Some faulting, pavement settlement, and unraveling of deck concrete were observed at the interface of the asphalt pavement and backwall of the abutment in these two bridges.*
- *Three types of connections were documented between the reinforced concrete approach slab and the abutment backwall:*
    1. *In the first configuration, the end of the approach slab is supported on a haunched corbel or notch on the rear face of the abutment backwall, but without horizontal reinforcement tying the approach slab to the abutment. With this connection, cyclic expansion and contraction pushes the approach slab away from the abutment creating a gap. A large gap was observed between the approach slab and the abutment which was constructed without any horizontal reinforcement tying them together.*
    2. *The second configuration included top and bottom reinforcement extending from the deck concrete into the approach slab. This moment connection apparently resulted in a relatively minor crack located 18 to 36 inches (0.45 to 0.90 m) into the approach slab.*
    3. *The third configuration included reinforcement detailed for a pinned connection.*
- *Settlement of the far end of the approach slab (away from the bridge) was common. The settlement was partially associated with fill washout from insufficient drainage. It was also partially attributed to settlement of the backfill behind the abutment with cyclic contraction and expansion associated with creep, shrinkage, and thermal strains, combined with the use of relatively short approach spans such that the far*

ends of the approach slabs are within a zone of soil influenced by abutment movement.

- *Two bridges included in the inspection survey had concrete pavement outside the approach slab. In both cases, the approach slabs were in good condition, whereas the pavement showed significant faulting cracks. Typically, the ends of the approach slabs settle and concrete pavement cannot adequately accommodate this settlement thus cracks.*
- *The majority of the inspected bridges had asphalt pavement outside the approach slabs. Asphalt was patched for re-leveling the pavement to the approach slab interface region.*
- *Settlement of the approach slab can cause damage to attached barrier walls. Barrier walls should be jointed to the approach slabs to accommodate differential settlement.*
- *Two PC bridges were retrofitted with continuous decks, but without continuous beams (link slabs). Typically, at least one beam end was connected to each pier cap to generate a pinned connection between the superstructure and the pier so that the pier cap moves with the bridge superstructure. The other end of the beam (from the adjacent spans) was supported on expansion bearings. These two bridges exhibited minor (hairline) cracks on the decks at the piers.*
- *Transverse movement of integral abutments associated with large skews or horizontal curves should be anticipated in the details for the barrier walls, drainage structures, and ends of the approach slabs.*

Overall, the field performances of the bridges were indicated as satisfactory. For the most part, distress observed was related to details inadequate to accommodate the superstructure movement (Tabatabai et al. 2005).

Wing and Kowalsky (2005) monitored the first jointless link slab bridge constructed in North Carolina. The structure was monitored over a year for a full thermal cycle. Additionally, a load test was performed over the bridge to investigate demands under known loads. According to test results, under live load, the measured rotations were much lower than the design rotation. Before performing the load tests, a crack width of 0.063 in. (1.6 mm) was measured whereas the specified limit to the crack width was 0.013 in. (0.33 mm). This was attributed to debonding of the link slab. During the live load tests, no notable change in the width of the crack was measured. Thermal induced rotations were generally greater than those of the live load; however, measured rotations under thermal loads were also lower than the design rotations.

2.6.1.1 Performance of Michigan Link Slab Bridges

The Michigan Department of Transportation (MDOT) currently utilizes three approaches to eliminate the joints at the piers: continuous for dead and live load (steel girders), continuous for live load (prestressed concrete girders), and continuous deck only (link slabs). MDOT's Structural Research Unit has conducted a comprehensive study to investigate the feasibility of using link slabs in Michigan bridges (Gilani and Jansson 2004).

As part of the study, field inspections of eight bridges were carried out with link slab detail and constructed between 2001 and 2003. Performance of the link slabs was evaluated with respect to the observed cracking density and crack width. Of the eight bridges inspected, six were described to be performing satisfactorily or better. The typical cracking documented on the link slabs is assumed to be partial depth. This is because the deck strain near the bottom of the section must be compressive in order to develop the resisting moment couple with the top layer of reinforcement. Full depth cracks are indicated as a concern more than partial depth cracks as they allow more rapid infiltration of chlorides (Gilani and Jansson 2004). Brief descriptions of the inspected bridges and documented distress are given below.

2.6.1.1.1 S02 of 23081(WB I-496 over I-96)

This structure contains one link slab over the center pier constructed as part of a deck replacement project completed in 2002. It was reported that during construction, the longitudinal reinforcement within the link slab was incorrectly spaced. Transverse hairline cracks were documented which were less than 0.01 inches wide. One wide crack of 0.016 inches was documented along the saw cut. It was believed that crack formed either before the saw cut or longitudinal steel was insufficient.

2.6.1.1.2 S04-1, 2 of 63174 (NB and SB I-75 over 13 Mile Road)

Each of these three-span parallel structures contains two link slabs over the piers that were part of a deck replacement project completed in 2001. No visible cracking in the link slab regions was documented. Link slabs appeared to be performing very well although they were designed with a reinforcement ratio of 0.91%; that is less than recommended to meet the requirements for strength and crack control (Oesterle 1999).

2.6.1.1.3 S08 of 63101 (I-696 under Middlebelt Road)

This three-span steel bridge contains a link slab over the center pier that was constructed in 2001 as part of a deck replacement project. The bridge has a skew of 26 degrees. This is the second highest skew link slab bridge under MDOT jurisdiction. The beams (due to their relatively low stiffness and long span length) generate the largest design rotation accomodated by the link slab. Hairline cracks with widths between 0.002 and 0.004 inches were observed within 1-2 feet of the saw cut region with a similar pattern to that of S02 of 23081.

2.6.1.1.4 S02-3, 4 of 82062 (EB and WB US-12 over M-39)

Each of these four-span steel bridges contains a link slab that was constructed as a joint retrofit to remove the expansion joints in 2001. An additional layer of reinforcement was placed with the existing longitudinal steel. The existing bars weren't continuous through the link slab, reducing the effective area of longitudinal steel by half. Despite the detailing and reduced steel, the link slabs were performing considerably well. Only a few hairline cracks with widths less than 0.004 inches were observed. This bridge is also the only Department Bridge with a link slab and without stay-in-place metal forms.

2.6.1.1.5 S05 of 82025 (Connor Ave over I-94)

The link slab of this four-span steel structure was constructed over the center pier in 2001 as part of a deck replacement project. The link slab is documented to be in poor condition with extensive cracking. The cracking pattern is similar but more extensive to those of S02 of 23081 and S08 of 63101 as they are primarily parallel and within 2 feet from the sawcut. Some of the cracks also propagated in a longitudinal direction over beams. The crack widths ranged from 0.004 to 0.02 inches, with the majority being between 0.01 to 0.02 inches. Design details of inadequate reinforcement, incorrect bar spacing and construction issues specified as lack of a designated pour sequence were assumed to contribute to cracking. Maintenance recommendations included filling cracks with an epoxy sealer.

2.6.1.1.6 S15 of 82025 (Harper Ave over I-94)

The link slab of this four-span steel structure was constructed over the center pier in 2001 as part of a deck replacement project. This is the highest skew (45 degrees) link slab bridge under MDOT jurisdiction. Similar problems documented for S05 of 82025 were also evident for this bridge. The problems were again described to be due to inadequate reinforcement, the longitudinal reinforcement terminating at the same location on both sides of the saw cut, no specified pour sequence, and extra longitudinal reinforcement added under the transfer reinforcement.

Overall, link slab performance was described to vary widely from very good to poor. Cracking was considered to be the most important distress in evaluating the link slab performance. Consequently, a typical cracking pattern or failure mechanism was identified. The bearings of all eight-link slab bridges were assessed, and two bridges had expansion bearings at the link slab. These two were both performing very well whereas six bridges with fixed bearings under the link slab had varying degrees of performance issues. However, the investigators did not report that the support conditions of the beams at a link slab had any influence on link slab performance.

The MDOT study could not make a determination regarding the effect of skew on link slabs. Of the bridges with link slabs with subpar performance, it was either established or suspected that there were design or construction issues or both. The design issues were listed as inadequate longitudinal steel or spacing for crack control, longitudinal reinforcement that terminates in the middle of the link slab, not specifying a pour sequence that will limit the dead load moment induced to the link slab, and not providing a saw cut in a timely manner. This MDOT study made the following conclusions:

1. The link slab design was a practical and cost-effective detail for new bridges and retrofitting applications.
2. The link slab performance was related to the end rotations due to live load introduced negative flexure in the link slab.
3. The design of link slabs was conservative.
4. The link slab detail was not sensitive to fatigue failure.
5. Roofing paper for debonding was an effective solution.

2.7 MODELING AND ANALYSIS OF JOINTLESS BRIDGES

2.7.1 Link Slab

The original link slab study by Gastal and Zia (1989) included finite element analysis. The analysis accounted for the non-linear material properties, cracking of concrete, creep, shrinkage, thermal effects, and various load conditions. The study also included nonlinear finite element analyses of beams connected with link elements simulating the continuous deck over the piers. The analyses showed a range of behavior under various support conditions. Combined bending and horizontal movement of the beams at the beam joint depended on the horizontal fixity of the beam supports. In the case of the double-hinged condition at the center support (R-roller H-hinge H-hinge R-roller), the link was in tension and provided some degree of live load continuity. For the double-roller condition at the center support (HRRH), analyses showed that the deck link is under compression, and the beams act as simply supported.

Richardson (1989) introduced the concept of partially debonded continuous decks. His studies indicated that the support conditions influence deck stresses and potential deck cracking. Girder deflection is increased due to the reduced stiffness from debonding, and deck stresses increased with increasing girder deflection

El-Safty (1994) modified Gastal's finite element models by incorporating partial debonding of the deck from the supporting beams. El-Safty (1994) also introduced constant strain assumption through the depth of the link slab, whereas Gastal used a linearly varying strain in the analysis. El-Safty (1994) analyzed simply supported girders modeled using many isoparametric beam elements except for the link slab region. The link slab was modeled as a spring having only axial stiffness. According to his results, support conditions greatly influence the response of the jointless deck and beam system with partially debonded connections. In beams with two roller supports at each side of the link slab (HRRH), compressive force developed in the spring. In the case of hinge support at either side of the link slab (RHRH or HRHR), the spring was in tension, and one span acted stiffer than the other as measured by the slope of their respective load-deflection curve.

Zia, Caner and El-Safty (1995) conducted experiments on two, two-span jointless bridge decks with steel and prestressed concrete girders. For both steel and concrete girders with HRRH supports, tests showed that the link slab was in tension and bending with only the bottom layer of concrete under compressive stress. Whereas, El-Safty's analysis predicted compression in the link slab. Experiments also showed that the load-deflection behavior of the two spans was similar for both RHRH and HRHR support conditions.

Caner's (1996) main modification on El-Safty's computer model was the modeling of the link slab where spring elements were replaced with conventional beam elements. Caner's (1996) computer program was also capable of calculating the crack width if the analysis indicated cracking. Caner (1996) indicated that the stiffness of the link slab was much lower than the composite section, and thus, the continuity provided by the link slab was negligible. One other important conclusion that differed from other studies was that the behavior of the link slab is not affected by the support conditions.

Okeil and El-Safty (2005) indicated that, under live load, the link slab would be in tension regardless of the support conditions. Link slab design coefficients based on three-moment equations were derived and compared to FE analysis results where the link slab is defined using a spring element with axial stiffness only. The inconsistency with earlier tests results by Zia, Caner and El-Safty (1995) was explained in light of the fact that the slightest inward movement of the supports would relieve the tensile force in the link slab, and no data was provided on support movements.

There are additional recent studies carried out using FE analysis and other structural analysis techniques to investigate the component or full structural behavior of jointless bridges with various support conditions. Among these studies, Thippeswamy et al. (2002) modeled and analyzed five in-service jointless bridges composed of beam and column elements for different foundation systems under varying load conditions. Jointless bridges were modeled in a simplified fashion as 2D frame elements. Three of the models included spread footings (stiffer systems), whereas the remaining two models incorporated pile supports. Spread footing systems had compatible boundary conditions with themselves, such as fixed, hinged, and roller supports. Pile systems were analyzed according to their strong and weak bending

axis, respectively. Dead and live loads, creep, shrinkage, temperature gradient, settlement and earth pressure were considered in the analyses. Analyses results demonstrated that the major contributor to the total stress is the temperature gradient.

Furthermore, Nassif et al. (2002) conducted FE analyses and field inspections of approach and transition slabs in order to identify the probable cause of cracking, crack locations, and the factors that affect cracking. The primary concern of the study was non-integral abutment bridges with transition slabs, different from the bridge systems that are of interest in this project. However, it still holds value to briefly discuss the modeling techniques. ABAQUS was utilized to carry out the FE analyses. The approach and transition slab model for one lane width was modeled with reduced integration shell elements (S4R). Soil underneath the slabs was assumed as silty medium dense sand and modeled using one dimensional spring elements. The applied live loads were multiples of HS-20 design truck loading. The connection between the bridge abutment and approach slab was represented as a pinned connection whereas the soil support at the end of transition slab was again modeled with springs. A truck was positioned at various locations along the length and width. The minimum truck load to initiate first cracking was determined as 1.66 times HS-20 loading.

Thiagarajan and Roy (2005) carried out detailed finite element analysis of approach slab cracking due to void development underneath the slab. The cracking patterns for various void locations were investigated. A rectangular approach slab with dimensions of 142-in x 295-in was modeled and analyzed under truck and lane loads. Four-node reduced integration shell elements were used to model the slab. The connection between the slab and the soil was modeled with a series of spring elements. The connection between the approach slab and bridge abutment as well as the sleeper slab was represented by pin connections. AASHTO design truck and lane loadings were applied considering the tire contact area as per AASHTO LRFD Design Specifications. It was concluded that the approach slab is over-designed. The reinforcement yielded only when the live load reached twice the design loading and when the soil-slab interaction was removed by deactivating the spring element. As a part of the study, cracking of the approach slab under different slab thicknesses and different void locations was investigated. To model the void, springs were removed where voids were being considered. The analysis showed reduced rows of cracked elements when

the slab thickness was increased. As the void regions were enlarged, the intensity and extent of cracking increased. The slab deflections also increased with increased void area.

In addition, Cai et al. (2005) studied the structural performance of bridge approach slabs under embankment settlement. It was indicated that AASHTO code specifications do not provide guidelines regarding structural design of approach slabs inclusive of the effects of embankment settlement. A detailed FE analysis of a typical Louisiana approach slab with 40-ft length, 12-in thickness with a 4-ft sleeper slab for two lane widths was carried out using the ANSYS FE analysis program. Eight-noded hexahedron elements were used to model the approach slab. A 'contact and target pair' surface element was used to simulate the interaction between the soil and the slab. This contact element only provided compressive contact and accurately represented the contact and separation between the slab and the soil. Sensitivity analyses were carried out to determine the volume of soil underneath the slab that can be assumed as a semi-infinite medium. Live (HS-20 truck) and dead loads were considered. The deflections and internal moments of the approach slab were calculated under various settlement cases and dead and live loads. As expected, deflection magnitudes and moments increased with increasing settlement. Beyond 6-in of settlement the approach slab lost contact with soil. A parametric study was conducted to establish a design table by varying the slab thickness and length. From the parametric study results, exponential functions of slab thickness and length were derived with a regression analysis as an approach slab design chart.

Faraji et al. (2001) investigated the behavior of integral bridges under thermal expansion with nonlinear soil reaction behind abutment walls and around the foundation piles. Nonlinear soil behavior was modeled using nonlinear spring elements at the abutment and pile nodes. An equivalent 2D analysis was performed under linear soil pressure distribution. The average lateral earth pressure coefficient (K) was used for estimating the magnitude and location of the soil pressure. A deformation value is calculated from the average K value. K value is adjusted incrementally until the computed displacements matched assumed values. Later, a full 3D model of the bridge was developed. The nonlinear behavior of the springs, which were used to model the interaction between the abutment walls and soil, was defined from the force-deflection design curves recommended in the NCHRP design manual

("Manual for the Design of Bridge Foundation" 1991). Nonlinear force-deflection design curves recommended by American Petroleum Institute (API) ("Recommended practice for Planning, Designing, and Constructing Fixed Offshore Platforms" 1993) were also utilized to establish the spring properties for simulating the soil around the pile. The bridge model was subjected to a thermal loading increment (ΔT) of $112^{o}F$. While nonlinear springs were selected to represent the soil-substructure interaction, the linear elements were used to model the bridge structure. The deck slab was modeled using plate elements incorporating membrane action, while the stringers and diaphragms were modeled as beam elements. In the initial analyses, for simplicity, composite action was neglected. Further analyses included rigid links between the deck slab and stringers to ensure strain compatibility and shear transfer between the deck slab and girder elements. The pier caps and the piers were modeled as beam elements with intermediate nodes. Abutment walls were modeled as plate elements, which were connected to the bridge superstructure with fixed connections at the end of each girder. HP piles (H-shaped steel piles) were modeled with beam elements, which are connected to the abutment with fixed connections. Two different soil conditions and their combinations of loose and dense materials for the regions behind the abutment wall and next to the HP piles were considered. The analysis showed that the composite action of the slab and stringers must be accurately modeled. Otherwise, the relative stiffness of the deck compared to wall-pile-soil system will not be accurate, which will alter the structural response, especially in the composite bridge deck and the HP pile system moments. The results also showed that the level of compaction behind the wall greatly affects the axial forces and moments in the deck, increasing to more than twice from loose to dense soil. The level of compaction adjacent to HP piles did not significantly affect the abutment and superstructure moments and deflections. Analysis showed that a 148-ft long bridge subjected to a thermal load of $112^{o}F$, with loose soil behind both abutment and piles, resulted in 0.43-in displacement at each abutment at the deck level. However, at the deck level, soil condition did not significantly affect displacements. Hence, contrasting the study by Thippeswamy et al. (2002), this study shows that the lateral earth pressure is an important factor in the case of jointless bridge decks with integral abutments.

Mourad and Tabsh (1999) studied the stress distribution in concrete deck slabs in integral abutment bridges. The slabs were cast as composite decks with steel beams. Transverse and

longitudinal slab stresses in the deck slab were investigated in the positive and negative bending regions near and away from the integral abutment under one or more HS-20-44 standard truck loads. The slab stresses were compared to the corresponding stresses of an equivalent jointed bridge. The material behavior was assumed to be linearly elastic. The reinforced concrete deck was modeled using 4-node rectangular shell elements having three translational and two rotational degrees of freedom. The rotation normal to the shell plane was not defined. Top and bottom flanges of the steel girders were modeled using 2-node beam elements. Girder web was modeled with shell elements similar to those used for concrete slab. The beam element properties were lumped at the centroid of flanges. Intermediate diaphragms composed of X-braces were modeled using truss elements with three translational degrees of freedom. Rigid beams were used to connect slab and flanges in order to satisfy the compatibility of the composite behavior and account for the actual thickness of the haunch and deck slab. The reinforced concrete abutment wall and wing-walls were modeled using 8-node brick elements with three translational degrees of freedom at each node. Supporting H piles were modeled with 2-node beam element. Connectivity of piles to the abutment was assumed fixed since piles are embedded into the abutment or wing-wall. According to the results, under live load, maximum flexural stresses do not usually form at the same location of the slab in the integral abutment bridges as in the simply supported ones. This was mainly because the bending of slabs in simply supported bridges was due to one-way action, whereas the bending of slabs in integral abutment bridges was due to two-way action, particularly near the supports.

Moreover, Fennema et al. (2005) conducted field-monitoring and FE analysis of an integral bridge in order to examine the design variables. The first step of FE analysis was to develop the load-deflection curves of laterally loaded piles. The load-deflection curves established the behavior of springs that were used to model the piles. The second step consisted of a 2D analysis of the bridge composed of frame and spring elements. The third step of analysis was a complex 3D model consisting of frames, plates, and springs. In the 3D finite element model, beam elements were used to model prestressed concrete girders and diaphragms. The bridge deck, abutments and approach slabs were modeled with plate elements. Elastomeric bearings were modeled as stub-beam elements. Girders were supported on the stub-beam elements through a rigid link. Stub abutment support boundaries were restrained against

rotation and translation at each node of the plate elements. Standard abutments' (which included piles) support boundaries were fixed against translation. Standard abutment was not restrained against rotation due to a 0.01-in. thick piece of extruded polystyrene between the abutment and the backwall, designed to relieve passive pressure. Piers were fixed at the supports. The abutment-girder connection was assumed as rigid. A temperature increment of 112^{o}F was considered in the analysis. According to the results, establishing multi-linear soil spring properties from force-deflection curves to model soil-pile interaction was valid. Regarding pile response, 2D and 3D model results did not differ significantly. The primary mode of movement of the integral abutment was not the longitudinal displacement but through the rotation about the base of the abutment. Field data indicated that the girder-abutment connection is not rigid, and it is best to approximate it as hinged. This was determined by observing relative rotations of girders and abutments under bridge contraction and expansion. Girder axial forces were influenced by the stiffness of the backwall and girder spacing.

2.8 SUMMARY

This chapter summarized various link slab, sleeper slab, approach slab, and abutment details. Further, performance of the bridges that utilized various details was reviewed. Finally, bridge structural modeling concepts and procedures were reviewed. A summary of design details with recorded durability performance is provided below.

1. Continuous top and bottom rebar layers in the link slab (Figure 2-2) have been implemented in North Carolina.

2. NYDOT uses deck extension similar to MDOT's deck sliding over backwall configuration (Figure 2-4b) with the bottom rebar layer continuous through the construction joint.

3. MDOT has developed a specific dependent backwall configuration for retrofit applications (Figure 2-5).

4. ODOT, VDOT, and NYDOT use inclined reinforcements to connect the approach to the backwall, which acts as a perfect hinge joint (Figure 2-7 and Figure 2-8a).

5. NYDOT's semi-integral abutment detail (Figure 2-10) has recorded performance of preventing backfill washing into the sliding surfaces.

6. A sleeper slab is used to support approach slab as well as the pavement. Compressible material is used in between the pavement and sleeper slab stem to minimize pavement growth effects

7. Deck configurations with re-entrant corners create stress concentrations and should be avoided.

Intentionally left blank

3 FIELD INSPECTION

3.1 OVERVIEW

Five unique and three similar bridges with jointless features were identified and inspected. Field inspection was performed during fall 2006. The bridges were selected based on repair and design categories. First, two repair categories of deck replacement and deck overlay were considered. Second, three design categories of semi-integral with bearings redesigned, deck sliding over backwall with steel beams, and deck sliding over backwall with prestressed concrete beams were considered. These design categories were the most common retrofit applications. A list of bridges identified for inspection is given in Table 3-1. Figures A-1 - A-5 given in Appendix A illustrate bridge details: abutment type, bearing type, beam types and spacing, link slab location, and the approach as well as the sleeper slabs.

Table 3-1. Bridges Selected for Field Inspection

No	Bridge ID	Type	Work completed	Design Details	Skew	Width	No. of Beams	Beam Spacing	Abt. type	Link slabs
1	S04-1-63174	PC	Deck replacement, widening, substructure repair, and concrete beam end repair	Deck sliding over backwall, dependent backwall, sleeper slabs, modified fixed bearings at abutments, link slab over piers	0	60'	27	76"	DSB	2
2	S04-2-63174	PC	Deck replacement, widening, substructure repair, and concrete beam end repair	Deck sliding over backwall, dependent backwall, sleeper slabs, modified fixed bearings at abutments, link slab over piers	0	60'	27	76"	DSB	2
6	S08-41027	ST	Truss anchorage replacement, deck replacement, pin and hanger replacement, structure repair, painting, steel repairs, placing slope protection	Bearing and abutment details are available, conventional left abutment, semi-integral right abutment, dependent backwall, sleeper slabs, left abutment bearing fixed, right abt bearing is expansion, link slabs over pin and hangers	varies	58' varies	24	78"-102"-111"	CONV & SIA	2
9	S12-3-25042	PC	Deep resurfacing of the existing bridge deck, PCI beam end repair replacing joints over piers with link slab and superstructure repair.	Deck sliding over backwall, dependent backwall, link slab, sleeper slabs, modified fixed bearings at abutments	20	43'	22	76"-152"	DSB	3
10	S12-4-25042	PC	Deep resurfacing of the existing bridge deck, PCI beam end repair replacing joints over piers with link slab and superstructure repair.	Deck sliding over backwall, dependent backwall, link slab, sleeper slabs, modified fixed bearings at abutments	20	43'	22	76"-152"	DSB	3
11	B01-10042	ST	Deck replacement, substructure repair, structural steel repair, painting, approach work, and maintaining traffic	Deck sliding over backwall, backwall has a corbel as in detail 6.20.03, sleeper slab, dependent backwall, no bearing details, no link slab information, modified fixed bearings, flexible pier caps	20	40'	27	57.25"	DSB	2
12	S12-7-25042	PC	Deep resurfacing of the existing bridge deck, PCI beam end repair replacing joints over piers with link slab and superstructure repair.	Deck sliding over backwall, dependent backwall, link slab, sleeper slabs, modified fixed bearings at abutments	20	27’	16	66”-132”	DSB	3
13	S12-8-25042	PC	Deep resurfacing of the existing bridge deck, PCI beam end repair replacing joints over piers with link slab and superstructure repair.	Deck sliding over backwall, dependent backwall, link slab, sleeper slabs, modified fixed bearings at abutments	20	27’	16	66”-132”	DSB	3

Note: Highlighted Bridges are similar to 63174 and 25042.

ST: Steel PC: Precast prestressed concrete DSB: Deck sliding over backwall CONV: Conventional abutment SIA: Semi-Integral abutment

3.2 INSPECTION DATA

Inventory information of the bridges identified for field inspection is given in Table 3-2. The inspection dates and the level of inspection are given in Table 3-3. Three identical bridges were inspected along with the five unique bridges for identifying and documenting their performance. Digitized inspection templates with inspection data and photo log are included in Appendix B. This chapter discusses the observed link slab, approach slab, sleeper slab, backwall and abutment conditions. Selected photos are included in Appendix C.

Table 3-2. Inspected Bridges - Inventory Information

No	Bridge ID	Year Built	Region	County	Feature Intersected	Facility	Main Spans	Max Span (ft)	Length (ft)	Skew (Deg.)	Type
1	S04-1 of 63174+	2001	Metro	Oakland	13 Mile Road	I-75 NB	3	63	141	0	PC++
2	S04-2 of 63174+	2001	Metro	Oakland	13 Mile Road	I-75 SB	3	63	141	0	PC
3	S08 of 41027	1964	Grand	Kent	Monroe	I-196 EB M-21	3	72	179	variable	ST*
4	B01 of 10042	2003	North	Benzie	Betsie River	M-115	3	50	150	20	ST
5	S12-3 of 25042**	1969	Bay	Genesee	I-75	I-69 EB	4	70	210	20	PC
6	S12-4 of 25042**	1969	Bay	Genesee	I-75	I-69 WB	4	70	210	20	PC
7	S12-7 of 25042***	1969	Bay	Genesee	I-75	I-69 Ramp E	4	70	210	20	PC
8	S12-8 of 25042***	1960	Bay	Genesee	I-75	I-69 Ramp F	4	70	210	20	PC

+ Identical bridges; ++ Prestressed concrete girders; * Steel girders; ** Identical bridges; *** Identical bridges

Table 3-3. Dates of Inspection

No	Bridge ID	Description	Inspection Date	Inspection Level
1	S04-1-63174	I-75 NB over 13 Mile Rd	12/03/2006	Detailed Inspection
2	S04-2-63174	I-75 SB over 13 Mile Rd	12/03/2006	Details documented using digital images only
3	S08-41027	I-196 EB over Monroe Av	11/04/2006	Detailed Inspection
4	B01-10042	M115 over Betsie River	11/04/2006	Detailed Inspection
5	S12-3-25042	I-69 EB over I-75	11/05/2006	Detailed inspection (deck top surface not inspected)
6	S12-4-25042	I-69 WB over I-75	11/05/2006	Detailed Inspection
7	S12-7-25042	I-69 EB Ramp over I-75	11/05/2006	Detailed Inspection
8	S12-8-25042	I-69 WB Ramp over I-75	11/05/2006	Detailed Inspection

3.2.1 S04-1, 2 of 63174 (I-75 NB and SB over 13 Mile Road)

Each of these two identical three-span parallel structures contains two link slabs over the piers. Link slabs were incorporated during the deck replacement project completed in 2001 (Photo C-1). The total length of the bridge is 151 feet (two 5 ft. approach slabs, two 39 ft. end spans, and a 63 ft. middle span). The link slabs of these bridges are asymmetric with respect to the piers due to unequal adjacent spans. Debonded lengths of link slabs according to plans were 24 in. on span 1 and 3 and 36 in. on span 2.

No visible cracking was observed within the link slab regions. There is a transverse saw cut directly above the pier filled with joint sealant (Photo C-2). The bridge deck underside was not visible with the use of stay-in-place forms. However, inspection of the deck overhang revealed full-depth cracks directly above the piers (Photo C-2).

Longitudinal cracking was observed on approach slabs. The expansion joint between the approach slab and the sleeper slab was filled with debris (Photo C-3). However, the separation that was visible on the debris in the expansion joint is an indirect indication of a functioning joint (Photo C-3). Diagonal cracks radiating from the corner where the deck width is reduced were observed on both bridges (Photo C-4). Similar cracking has been observed on a Minnesota bridge, and it is recommended to avoid using re-entrant corners or provide detailing to control corner cracking.

The backwall, abutment wall, and bearings at the abutments were inspected. Vertical and D-cracking was documented on the abutment wall directly below the girders (Photo C-6 and Photo C-7).

3.2.2 S08 of 41027 (I-196 EB over Monroe Ave)

This steel girder bridge contains two link slabs over what were previously pin and hanger connections. The bridge deck, pin and hanger, and backwall were replaced in 2004 (Photo C-8). The total length of this three span bridge is 178.5 feet. Link slab details could not be identified in the bridge plans.

The inspection of the backwall, abutment wall, bearings, and deck underside was performed. Again, the use of stay-in-place forms prevented the inspection of the deck underside (Photo C-

9a). Only the overhang portion of the deck was visible and did not reveal any visible cracking (Photo C-9b). The top of the bridge deck could not be inspected due to high traffic volume as the bridge was on a detour with reduced shoulder width.

The overall abutment condition was good, except for a few cracks (Photo C-10). Also, the backwall was in excellent condition. Though the bridge coating is aesthetically pleasant, it hampers the inspection process.

Inspection of abutment bearings showed that the elastomeric bearings are in good condition, and deformations did not indicate damage to functional performance at the time of inspection (Photo C-11).

3.2.3 B01 of 10042 (M-115 over Betsie River)

This three-span structure contains two link slabs over the piers. Link slabs were cast during the deck replacement project completed in 2003 (Photo C-12). The total length of the bridge is 160 feet (two 5 ft. approach slabs and three 50 ft. spans). The link slabs of these bridges are symmetric about the piers since the adjacent span lengths are equal. The link slab length of each span is given as 4 ft., but the debonded lengths could not be identified in the plans.

Inspection of both link slabs from the top of the bridge and also from the underside revealed full-depth transverse cracks about the pier centerline (Photo C-13). Unlike S04-1, 2 of 63174, the link slabs of this bridge were not saw cut above the piers. Instead, construction joints between the deck and the link slab were filled with joint sealant. Construction joints were provided at a distance of 4 ft. on either side of the pier.

Approach slab inspection showed that a saw cut was provided aligned with the approach side backwall face and filled with joint sealant (Figure 3-1). Transverse cracking was documented within the vicinity of the saw cut (Photo C-14).

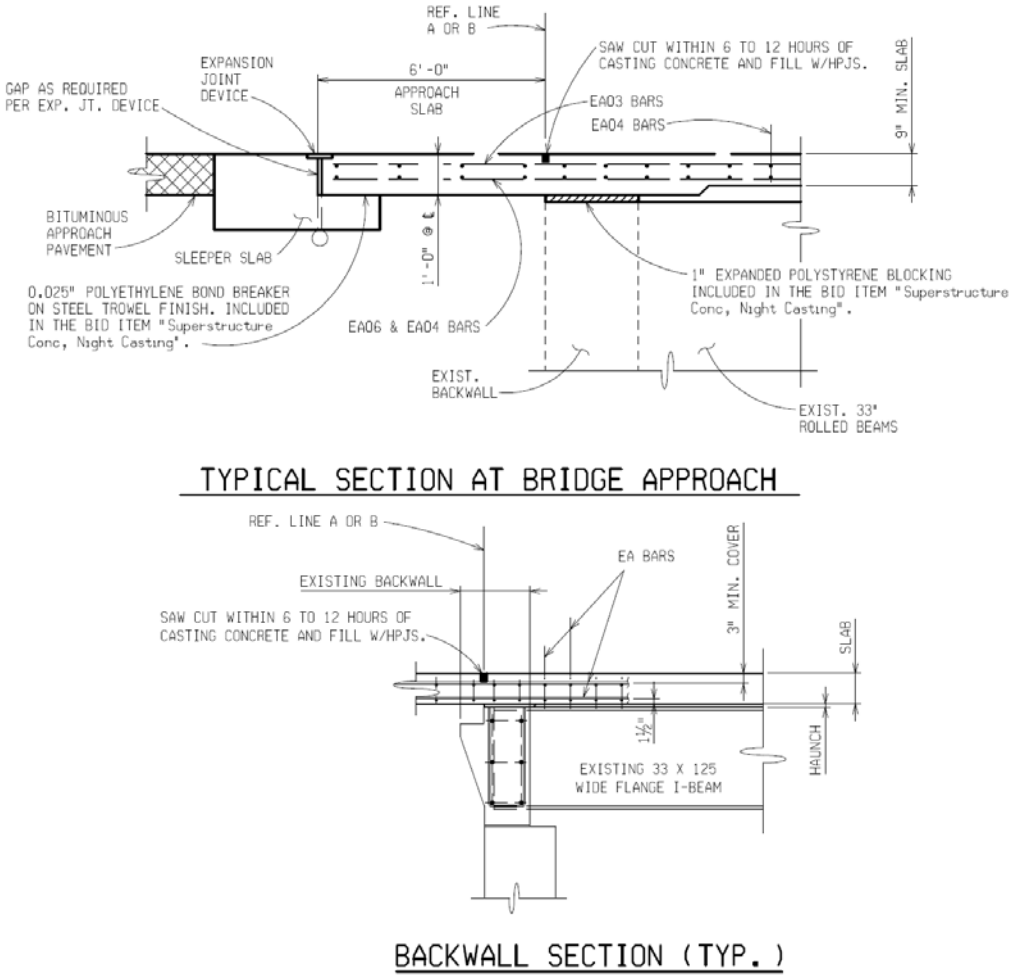

Figure 3-1. Abutment region details of B01-10042

Expansion joints provided at the sleeper slab were partially filled with debris. Due to rain on previous night, the debris was moist and perhaps concealed the separation along the dirt fill (Photo C-15).

Backwall and abutment wall inspection revealed vertical cracking of the abutment wall and diagonal cracking of the backwall (Photo C-16).

3.2.4 S12-3, 4 of 25042 (I-69 EB and WB over I-75)

Each of these two identical four-span parallel structures contains three link slabs over the piers. Link slabs were cast as a part of a repair project in 2003 that consisted of deep resurfacing of the existing deck, replacing of joints over the piers with link slabs, and replacing joints over the abutments with an approach slab and sleeper slab combination. These are the two middle bridges in Photo C-17 that shows four parallel bridges. Each of these two bridges includes two

traffic lanes. The total length of the bridge is 220 feet (two 5 ft. approach slabs, one 34.5 ft. end span, two 69.5 ft. middle spans, and a 36.5 ft. end span). The link slabs between spans one and two and three and four are asymmetric with respect to the piers due to unequal adjacent span lengths. The link slab over the middle pier or between span two and three is symmetric over the pier. Link slab topology is given in Table 3-4 and Table 3-5.

Table 3-4. Link Slab Lengths with Respect to Bridge Span

Link slab length	
2’ – 6” Span 1	3’ – 6” Span 2
3’ – 6” Span 2	3’ – 6” Span 3
3’ – 6” Span 3	2’ – 6” Span 4

Table 3-5. Link Slab Debonded Lengths with Respect to Bridge Span

Link slab debonded length	
1’ – 9” Span 1	2’ – 6” Span 2
2’ – 6” Span 2	2’ – 6” Span 3
2’ – 6” Span 3	1’ – 9” Span 4

Inspection documented that all link slabs have full-depth cracks over the piers (Photo C-18). Link slabs of I-69 EB were saw cut directly over the pier. Though saw cuts were provided, cracks were documented within their proximity (Photo C-19).

In the case of I-69 bridges, saw cuts were not seen on the approach slab over the abutments as in the case of B01 of 10042. Inspection revealed transverse cracking on the approach slab over the abutments (Photo C-20).

Expansion joints between the sleeper slab and the approach slab of I-69 EB bridge were filled with debris. Wide cracks formed through the joint debris are indications of functioning joint and contracting deck (Photo C-21).

Unrelated to the link-slab inspection, extensive transverse and diagonal deck cracking was observed on the bridge carrying I-69 EB (Photo C-22).

In the case of I-69 EB bridge, the backwall was sound, but vertical cracks were observed on the abutment wall. On the I-69 WB bridge, cracks were observed on the backwall alongside the bearings. Vertical cracking was also observed on the I-69 WB bridge abutment wall. Abutment

walls and pier caps of I-69 WB bridge showed more pronounced cracking than the I-69 EB bridge (Photo C-23).

3.2.5 S12-7, 8 of 25042 (I-69 EB and WB ramps over I-75)

Each of these two identical four-span parallel structures contains three link slabs over the piers. Link slabs were placed as a part of a project in 2003 that consisted of deep resurfacing of the existing deck, joint replacement over the piers with link slabs, and over the abutments with approach slab and sleeper slab combination. These are the two outside bridges in Photo C-17 that shows four parallel bridges. Each of these two bridges carries a single traffic lane. Total length of a bridge is 220 feet (two 5 ft. approach slabs, one 34.5 ft. end span, two 69.5 ft. middle spans, and a 36.5 ft. end span). The link slabs between spans one and two and three and four are asymmetric with respect to the piers due to unequal adjacent span lengths. Link slab over the middle pier or between span two and three is symmetric over the pier. Link slab topology is given in Table 3-4 and Table 3-5.

The deck underside, backwalls, and abutment walls of both bridges were inspected. Inspection revealed that link slabs have full-depth cracks over the piers (Photo C-24). Link slabs were saw cut directly over the pier (Photo C-25).

There was no saw cut provided on the approach slab over the abutment of both bridges. Inspection documented transverse cracking on the approach slabs over the abutment of I-69 EB ramp. However, there was no similar cracking on the I-69 WB ramp approach slabs over the abutments (Photo C-26). Approach slabs of both bridges showed diagonal cracks.

Expansion joints at the sleeper slabs and the approach slabs contained debris. Wide cracks visible through the debris filled joints are positive signs of joint performance (Photo C-27).

The abutment wall, backwall, and the pier cap conditions of I-69 ramps were similar to that of I-69 EB (Photo C-28). The abutment wall showed vertical cracks in the proximity of the girder ends. Backwalls had horizontal cracks aligned with the bearing edges with limited length.

3.3 INSPECTION DATA ANALYSIS

3.3.1 Jointless Bridge Performance

Full-depth transverse cracks were identified on links slabs directly over the piers (Table 3-6).

The approach slab conditions of S04-1-63174 and S04-2-63174 were identical. Diagonal cracks or transverse cracks over the abutments were not visible on the approach slabs of these two straight bridges. Though S12-3-25042 and S12-4-25042 are identical bridges, their performances were not identical. Diagonal cracks and transverse cracks over the abutments were documented only on the approach slabs of S12-3-25042. In the case of S12-4-25042, diagonal cracks were identified on both approach slabs, but no transverse cracks were documented over the abutment. S12-7-25042 and S12-8-25042 are also identical bridges, but approach slab conditions were not similar. The condition of the approach slab of S12-7-25042 was identical to that of S12-3-25042. Similarly, the conditions of S12-4-25042 and S12-8-25042 were identical. Though these bridges are not structurally identical, they carry traffic in the same direction and are adjacent to each other (Table 3-7).

Vertical cracks of the abutment wall were common to all inspected bridges. Abutment wall D-cracks were observed only on S04-1-63174 and S04-2-63174. However, the abutment wall of S04-2-63174 had multiple D-cracks, and the condition was not identical to that of S04-1-63174. Backwall cracks were observed only on B01-10042. Short horizontal backwall cracking near the bearings was documented in six out of eight inspected bridges. Distressed bearings were documented in five bridges (Table 3-8).

Table 3-6. Summary of Link Slab Inspection Data

Bridge ID	Description	Saw cut over pier	Full-depth crack	Bearing underneath link slab
S04-1-63174	I-75 NB over 13 Mile Rd	Yes	Yes	Exp – Exp+
S04-2-63174	I-75 SB over 13 Mile Rd	Yes	Yes	Exp - Exp
S08-41027	I-196 EB over Monroe Av	Deck top surface could not be inspected	Yes	P&H++
B01-10042	M115 over Betsie River	No	Yes	MF – MF*
S12-3-25042	I-69 EB over I-75	Yes	Yes	Exp - Exp
S12-4-25042	I-69 WB over I-75	Deck top surface could not be inspected	Yes	Exp - Exp
S12-7-25042	I-69 EB Ramp over I-75	Yes	Yes	Exp - Exp
S12-8-25042	I-69 WB Ramp over I-75	Yes	Yes	Exp - Exp

+ refer Figure 3-2 for details. It is considered expansion bearing when one-inch thick neoprene pad is used
++ Link slabs are placed over pin and hanger of the steel beam bridge
* refer Figure 3-2 for details. Lead papers are used at the abutment and at piers of certain bridges instead of the one-inch thick neoprene pad. This configuration is referred as the modified-fixed.

Table 3-7. Summary of Approach Slab Inspection Data

Bridge ID	Description	Saw cut over abutment	Cracks over abutment	Diagonal cracks	Expansion joint function	Skew (Deg.)
S04-1-63174	I-75 NB over 13 Mile Rd	No	No	No	Yes	0
S04-2-63174	I-75 SB over 13 Mile Rd	No	No	No	Yes	0
S08-41027	I-196 EB over Monroe Av	Deck top surface could not be inspected				variable
B01-10042	M115 over Betsie River	Yes	Yes	No	-+	20
S12-3-25042	I-69 EB over I-75	No	Yes*	Yes*	Yes	20
S12-4-25042	I-69 WB over I-75	No	No	Yes	Yes	20
S12-7-25042	I-69 EB Ramp over I-75	No	Yes*	Yes*	Yes	20
S12-8-25042	I-69 WB Ramp over I-75	No	No	Yes	Yes	20

* Only on one approach slab
+ Due to previous night rain cracks on dirt fill could not be seen

Table 3-8. Summary of Abutment and Backwall Inspection Data

Bridge ID	Description	Abutment wall cracks types		Backwall cracks		Distressed bearings	Bearing at abutment	Skew (Deg.)
		D	Vertical	General	Bearing vicinity			
S04-1-63174	I-75 NB over 13 Mile Rd	Yes	Yes	No	Yes	No	MF/MF+	0
S04-2-63174	I-75 SB over 13 Mile Rd	Yes	Yes	No	Yes	No	MF/MF	0
S08-41027	I-196 EB over Monroe Av	No	Yes	No	No	No	Fix/Exp++	variable
B01-10042	M115 over Betsie River	No	Yes	Yes	Yes	Yes	Exp/Exp	20
S12-3-25042	I-69 EB over I-75	No	Yes	No	No	Yes	MF/MF	20
S12-4-25042	I-69 WB over I-75	No	Yes	No	Yes	Yes	MF/MF	20
S12-7-25042	I-69 EB Ramp over I-75	No	Yes	No	Yes	Yes	MF/MF	20
S12-8-25042	I-69 WB Ramp over I-75	No	Yes	No	Yes	Yes	MF/MF	20

+ MF: Modified-fixed bearing (Figure 3-2); ++ Fix: Fixed-bearing and Exp: Expansion bearing

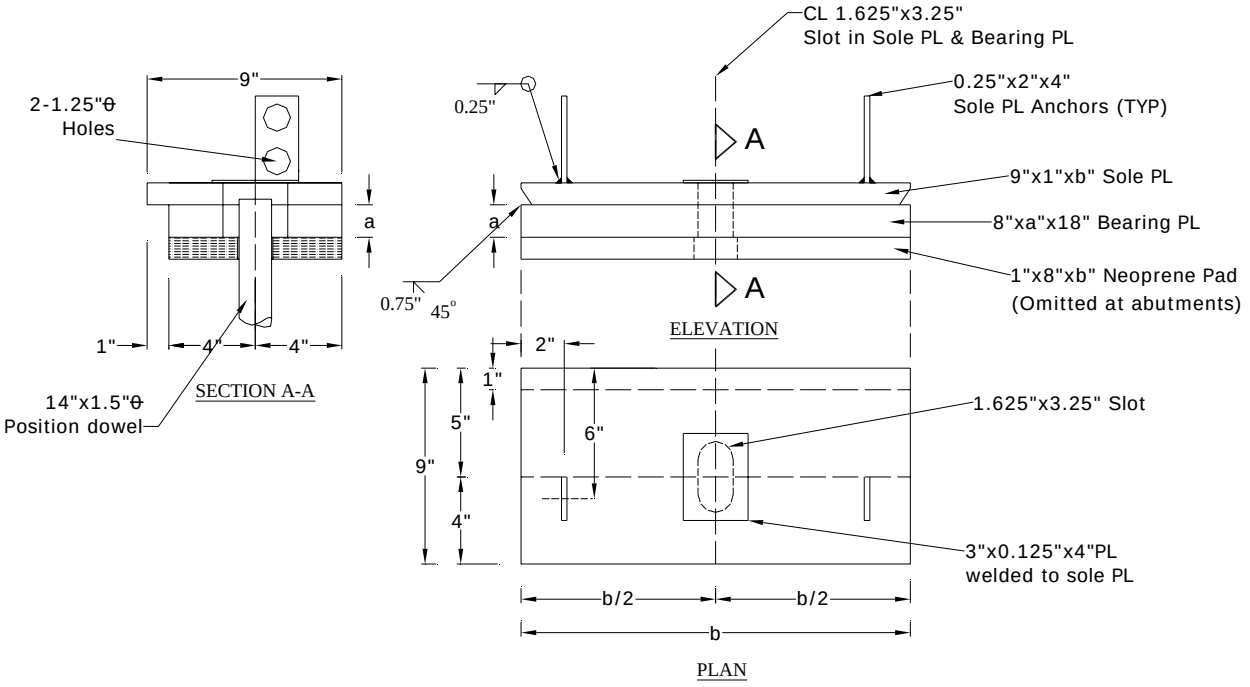

Figure 3-2. Configuration of the bearing used on inspected bridges

The bearing shown in Figure 3-2 provides limited translation of 0.875 inches for expansion or contraction. The bearing is considered as an expansion bearing with a one-inch thick neoprene pad. A one-inch neoprene pad is assumed to provide rotational degree of freedom in addition to the translational degrees of freedom. Most of the inspected bridges utilized this bearing at the abutments and, in certain cases, at the piers with lead paper between the bearing plate and the abutment replacing the neoprene pad. The bearing pad, with the removal of the neoprene, can only provide limited translational degree of freedom; thus it is somewhere between a pinned or a roller bearing. Further, with age there is the possibility of developing increased restraint to translation due to corrosion or damage to the lead. This bearing will be defined as the "modified-fixed bearing."

3.3.2 Summary of Inspectors' Comments - Abutment Condition

The repair project on bridges S04-1-63174 and S04-2-63174 consisted of deck replacement, widening, substructure repair, and concrete beam end repair (Table 3-1). Review of the S04-1-63174 inspectors' comments on the abutment conditions documented during field inspection prior to the repair project revealed that the observed abutment cracking predated the repair project (Table D-1 and Photo D-1). The same repair activity was performed on the S04-2-63174,

which is identical to S04-1-63174. Again, the review of the inspectors' comments on the abutment did not include the observed D-cracks under beam 6W on the north abutment and beam 9W on the south abutment (Table D-2 and Photo D-2). These cracks may be attributed to the forces developed from the restraining effects of the modified-fixed bearings.

The repair activity on the bridge S08-41027 consisted of truss anchorage replacement, deck replacement, pin and hanger replacement, substructure repair, painting, steel repairs, and placing slope protection (Table 3-1). Inspectors noted the presence of large vertical leaching cracks on the abutments. After the completion of repair work, only few typical vertical cracks were documented by the inspectors. During field inspection observations were similar to the documentation of the bridge inspectors' comments (Table D-3 and Photo D-3).

The repair activity on bridge B01-10042 consisted of deck replacement, substructure repair, structural steel repair, painting, and approach work (Table 3-1). Inspectors have noted only typical vertical abutment cracks in the inspection reports. Additional cracking observed included diagonal backwall cracks and several short, horizontal, backwall cracks that emanated from the bearings (Table D-4 and Photo D-4).

The repair activity on four bridges (S12 - 3/4/7/8 - 25042) consisted of deep resurfacing of the existing bridge deck, PCI beam end repair, replacing joints over piers with a link slab, and substructure repair (Table 3-1). Inspectors' comments included a few typical vertical cracks on the abutment walls. Observations were similar to those of the inspectors' comments, and the condition of the abutment walls and backwalls of these four bridges remained the same following the repair (Table D-5 to D-8 and Photo D-5 to D-8).

3.4 SUMMARY AND CONCLUSIONS

Based on the field inspection data and the inspectors' comments, the following conclusions have been made:

1. The causes of full depth link slab cracks need to be investigated, and design recommendations should be developed to abate cracking over the piers.

2. Saw cuts or construction joints on the deck directly over the abutment centerline need to be provided and sealed.

3. The causes of the diagonal backwall cracking of skew bridges need to be investigated to provide design recommendations to mitigate cracking.

4. Abutment wall D-cracks were only documented on S04-2-63174. However, the performance of this bridge is questionable as compared to S04-1-63174, in which the exposure conditions, design, and construction year are same as that of S04-2-63174.

5. Reentrant corners over the abutments should be avoided. When bridge configuration requires reduced approach slab width, alternate details should be developed to avoid load transfer between approach slab and the deck.

Intentionally left blank

4 FINITE ELEMENT MODELING AND ANALYSIS OF LINK SLAB REGION

4.1 OVERVIEW

The objective of finite element modeling and analysis is as follows: to evaluate the effects of various types and levels of loads on the design parameters of the jointless bridges with link slabs, to evaluate the impact of current design assumptions, and to provide fine-tuning of the current design for improved performance.

The bridge is divided into various components (Figure 1-1 and 1-2), and modeling techniques for each component and assemblages are discussed. Since contact action is expected between the link slab and girder within the debonded region, special modeling and analysis techniques are required. The FE analysis software ABAQUS is superior to other FE software in this respect since it includes a wide variety of contact and interaction modeling options.

Stress distribution within each bridge component is required in order to understand the behavior and interaction between various components of the system. For the representation of the 3-dimensional stress state, bridge components are modeled using C3D8 solid (brick) elements. Component interaction within the link slab debonded region was simulated using a surface-based contact method by defining two surfaces: the underside of the link slab and the top of the girders.

Analysis is performed on three dimensional single girder models with effective flange width and multi girder full width models. Two-span single girder assemblage models are developed for evaluating the effects of link slab design parameters in conjunction with live and thermal loads. Design parameters of the link slab are: link slab length with respect to adjacent span lengths, debonded length, girder height, and support conditions. The bearing stiffness effect is incorporated with the model using vertical and horizontal springs. The effects of varying debonded lengths on link slab stresses are investigated by using debonded lengths of 0%, 2.5%, 5.0%, and 7.5% of the span length. The effect of girder height is examined with two different (PCI Type III and PCI Type VI) standard PCI sections. Parametric analyses included the effect of adjacent span ratios. Deformation demand on bearings is investigated by analyzing single girder assemblage models under uniform thermal loads.

A total of 111 finite element analyses are conducted for the first part of the link slab region analysis. Additionally, link slab potential transverse crack width is calculated based on the deck casting sequence, debonded length of the link slab, and estimated concrete shrinkage. Finally, straight and 20^0 skew two-span, multi-girder full-width models, (referred to as full bridge models in this report), are developed for investigating load demand on link slabs and addressing additional issues from link slab torsion and twist that arise due to asymmetric loading of single and two lane bridges. A total of 88 finite element analyses are conducted on full bridge models.

4.2 ASSEMBLAGE MODELS OF LINK SLAB REGION

Single girder with an effective flange width is the simplest form of analysis model that is utilized for calculating axial force, moment, and shear demands on a girder of a straight or moderate skew bridge. The model is analyzed under various boundary conditions and the notional loads defined in AASHTO LRFD (2004). The single girder, two-span model is developed incorporating an effective flange width for selected support conditions. Beams are simply supported but the slab is made continuous over the middle supports linking the neighboring spans. This model is referred to as the "assemblage model of link slab region."

The objective is to investigate the influence of design parameters on link slab behavior and to calculate the moments and axial forces developed at the mid-section of the link slab. Additionally, the models are used to verify the design assumptions and potentially recommend fine-tuning to the design procedures.

The set of models developed for the analysis of the link slab region is based on the geometrical and material properties of S12-25042 (I-69 over I-75). The bridge has PCI Type III interior girders with a 9 in. concrete deck. The total length of the link slab between spans two and three is given as 84.4 in. (41.7 in. on each girder + 1 in. gap, span length is 69.5 ft = 834 in., 5% × 834 = 41.7 in.). The deck overhang is 30 in. on either side of the beam as shown in Figure 4-1. This overhang dimension is an average value taken from the plans according to the deck width and number of girders. (Center to center girder distance governs over 1/4 of span length and 12 times the deck thickness: AASHTO LRFD Section 4.6.2.6.) The haunch between the girder and deck is neglected as a means of simplifying the model. The models represent two 834 in. spans as shown in Figure 4-2.

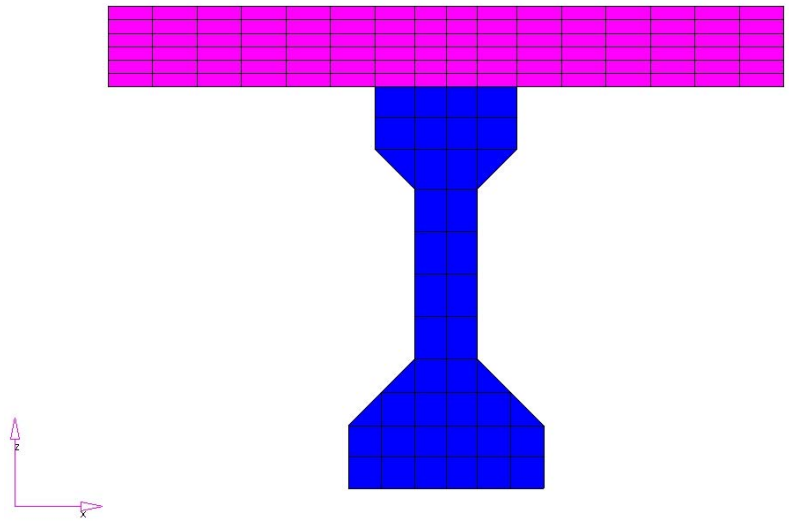

Figure 4-1. Front view of PCI Type III girder and the deck.

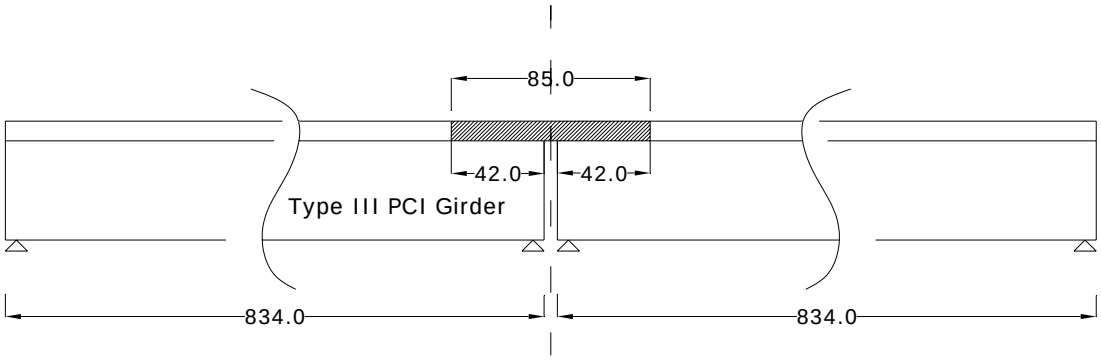

Figure 4-2. Side view of PCI Type III girder and the deck

The compressive strength of the girder and deck concrete is 5000 psi. The concrete modulus of elasticity calculated from $57000(f'_c)^{1/2}$ formula of AASHTO LRFD (2004) is 4031 ksi. Poisson's ratio of 0.2 is used for both deck and girder concrete. Live, thermal gradient, and uniform thermal loads are applied. Live load is applied symmetrically on both spans. Thermal gradient and uniform thermal loads are applied to the composite girder-deck cross-section.

The models have three basic support configurations: HRRR, RHHR, and RRHR (or similarly RHRR). The first model consists of a single hinge (H) support while rollers (R) are provided at the other supports (HRRR) allowing the bridge to expand or contract freely under uniform thermal loads. The second model consists of hinges underneath the link slab while rollers

support the far ends of the beams (RHHR). The third model consists of a hinge at either side of the link slab while the other beam ends are supported on rollers (RRHR or RHRR). HRRH and HRHR boundary conditions are not practical for use with link slabs. With such supports the bridge superstructure will develop restraining forces under volume change loads. A summary of load cases and boundary conditions is presented in Table 4-1.

Table 4-1. Load Cases and Support Conditions Utilized in Assemblage Models of Link Slab Region

Case	Support Conditions	Loading
L_1	HRRR	HL-93 **L**ive load on both spans to create maximum end rotation
L_2	RHHR	
L_3	RRHR	
TP_1	HRRR	**P**ositive **T**hermal gradient loading on both spans
TP_2	RHHR	
TP_3	RRHR	
TN_1	HRRR	**N**egative **T**hermal gradient loading on both spans
TN_2	RHHR	
TN_3	RRHR	
TC_1	HRRR	Uniform **T**hermal **C**ontraction loading on both spans
TC_2	RHHR	
TE_1	HRRR	Uniform **T**hermal **E**xpansion loading on both spans
TE_2	RHHR	

HL-93 (AASHTO LRFD 2004) loading is applied at a location to create maximum end rotation on the 69.5 ft spans of the bridge. The impact factor is taken as 1.33 from Section 3.6.2.1 of AASHTO LRFD (2004). As per Section 3.6.1.3 AASHTO LRFD (2004), a lane load of 0.64 k/ft is used in addition to the axle loads. Distribution factors are calculated assuming two or more lanes are loaded from the formulation in AASHTO LRFD (2004) (Table 4.6.2.2.2b-1). Distribution factors for interior girder moments are presented in Table 4-2 for different girder types and span lengths used throughout the study.

Table 4-2. Distribution Factors for Different Girder Types and Span Lengths

Girder type and length	Single lane loaded	Two or more lanes loaded	Front axle load with impact (kips)	Rear axle loads with impact (kips)
Type III, L = 69.5 ft	0.423	**0.571**	6.08	24.30
Type III, L = 91 ft	0.385	**0.532**	5.67	22.66
Type VI, L = 69.5 ft	0.478	**0.646**	6.88	27.50
Type VI, L = 150.3 ft	0.367	**0.528**	5.62	22.48

Thermal gradient loads are calculated from AASHTO LRFD (2004) Section 3.12.3 for Zone-3. A negative temperature gradient is obtained by multiplying the positive temperature values by -0.3. The height (*h*) in Figure 4-3 is the depth of full composite section. A uniform thermal expansion coefficient of 6.0 x 10^{-6} in./in./^{o}F is used for both deck and girder concrete.

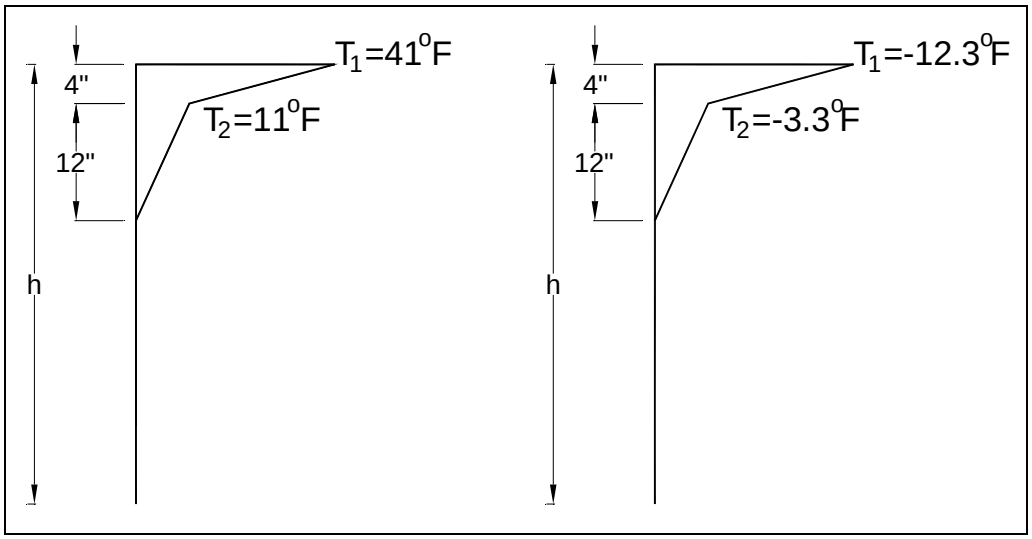

Figure 4-3. Positive and negative temperature gradient loads used in the analyses

The stresses are described on the coordinate convention of the 3-dimensional states of stress given in Figure 4-4(a). Sign convention for the description of resultant forces and moments calculated from stresses are shown in Figure 4-4(b).

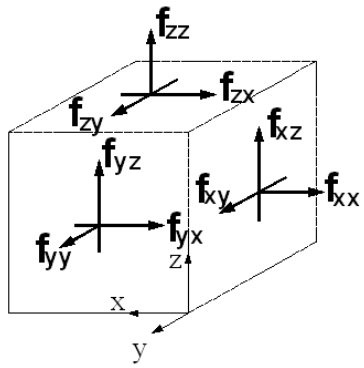

(a) sign convention for stress resultants

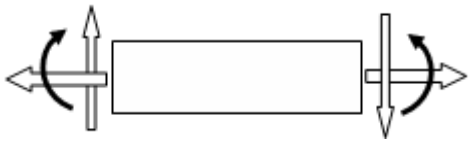

(b) sign convention for moment, shear, and axial force

Figure 4-4. Sign convention for finite element analysis results

4.2.1 Effect of Elastomeric Bearings

The support condition effects due to vertical and horizontal restraints caused by the elastomeric bearing stiffness are incorporated by a series of vertical and horizontal springs attached to the girder end footprint. The shear modulus (G) is the important design parameter of bearing pads as suggested by AASHTO LRFD (2004). According to MDOT Bridge Design Manual (2005) Section 7.02.05, plain bearings shall have a shear modulus of 0.20 ± 0.03 ksi, and laminated bearings shall have a shear modulus of 0.10 ± 0.015 ksi. Since the elastomer is specified explicitly by its shear modulus, these values should be used in design, and the other properties should be obtained from AASHTO LRFD (2004) Table 14.7.5.2-1.

Bearing dimensions obtained from S12 of 25042 bridge plans are 18 in. × 8 in. plain elastomers with 1.625 in. x 3.25 in. slots as shown in Figure 3-2. The bearing dimension of 18 inches is changed to 22 inches to match with the finite element mesh of the girder (Figure 4-5). This bearing type is described as modified-fixed when the neoprene pad is replaced with a lead paper. For assessing the bearing effects on link slab force resultants, lower and upper bound shear modulus (G) values of 0.170 ksi and 0.230 ksi for 50-durometer hardness elastomers are taken from the MDOT Bridge Design Manual (2005). The shape factor, S_i for each individual layer

and the effective compressive modulus (E_c) are calculated from Section C14.7.5.1-1 of AASHTO LRFD (2004) (Table 4-3).

The corresponding horizontal stiffness (k_x and k_y) and vertical stiffness (k_z) are calculated as shown below and tabulated in Table 4-3:

$$k_x = \frac{GA}{H} \text{ and } k_z = \frac{EA}{H} \quad (4\text{-}1)$$

Where, H is the elastomer total thickness.

Table 4-3. Geometric Properties and Stiffness of Neoprene Bearing Pads of S12-25042

Bearing Type over Piers	Modified-fixed	
Shear modulus, G (ksi)	0.17	0.23
Area (in^2)	170.70	170.70
S_i	2.90	2.90
Total elastomer thickness H (in)	1.00	1.00
Effective compressive modulus, E_c (ksi)	8.58	11.61
Total vertical stiffness, k_z (k/in)	1464.30	1981.11
Total transverse stiffness, k_x (k/in)	29.02	39.26
Total longitudinal stiffness, k_y (k/in)	29.02	39.26

Vertical and horizontal spring stiffness values given in Table 4-3 are distributed to girder end footprint nodes similar to the procedure utilized by Yazdani et al. (2000). Thirty-five horizontal and vertical springs are defined attached to the girder at the bearing location. Mesh dimensions and node labeling are depicted in Figure 4-5.

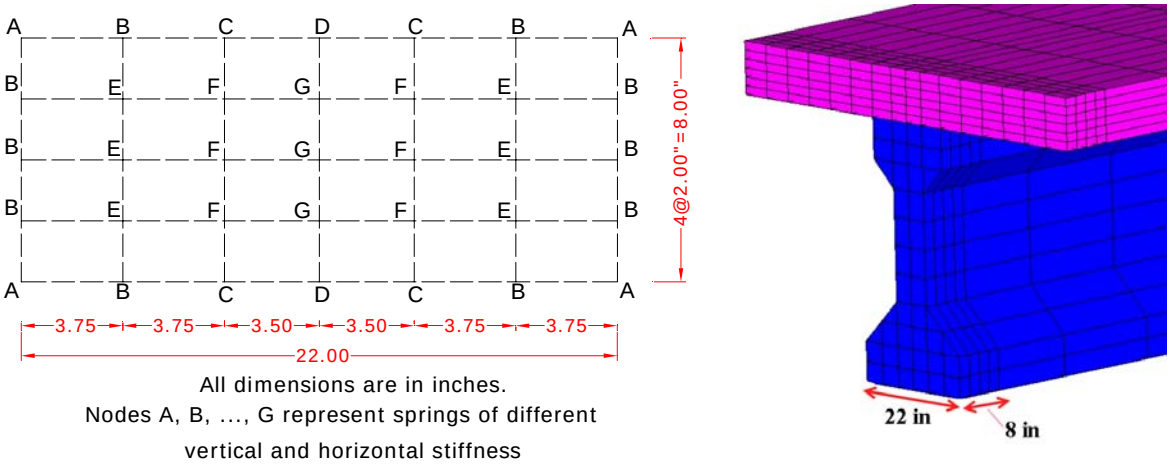

Figure 4-5. Spring locations at the girder end footprint

According to their corresponding tributary areas, the percentage of stiffness fraction that each node would take is shown in Table 4-4 below.

Table 4-4. Node Stiffness Fraction

Point	Stiffness fraction %
A @ 4	1.07
B @ 10	2.13
C @ 4	2.06
D @ 2	1.99
E @ 6	4.26
F @ 6	4.12
G @ 3	3.98

The analysis models incorporate the three fundamental support configurations (HRRR, RHHR, and RRHR/RHRR) given in Table 4-1 with lower and upper bound bearing stiffness values. The bearings in the actual bridge over the piers are expansion bearings shown in Figure 3-2. In addition to these three basic support configurations, a fourth case is developed using lower and upper bound bearing stiffness values representing expansion bearings at all the supports.

Boundary conditions and the net moment and axial forces are presented in Table 4-5 and Table 4-6 under live and thermal gradient loads, respectively.

Table 4-5. Moments and Axial Forces in the Link Slab for Various Support Conditions under Live Load

Case	1st support (Abutment)	2nd support (Pier)	3rd support (Pier)	4th support (Abutment)	Moment (ft-k)	Axial force (k)
L_1	H	R	R	R	-51	0
L_1^-	HR^-	$VS^- + HS^-$	$VS^- + HS^-$	$VS^- + HS^-$	-50	1
L_1^+	HR^+	$VS^+ + HS^+$	$VS^+ + HS^+$	$VS^+ + HS^+$	-50	2
L_2	R	H	H	R	-19	159
L_2^-	$VS^- + HS^-$	HR^-	HR^-	$VS^- + HS^-$	-19	160
L_2^+	$VS^+ + HS^+$	HR^+	HR^+	$VS^+ + HS^+$	-19	159
L_3	R	R (H)	H (R)	R	-51	0
L_3^-	$VS^- + HS^-$	$VS^- + HS^-$	HR^-	$VS^- + HS^-$	-50	6
L_3^+	$VS^+ + HS^+$	$VS^+ + HS^+$	HR^+	$VS^+ + HS^+$	-49	8
L_4^-	$VS^- + HS^-$	$VS^- + HS^-$	$VS^- + HS^-$	$VS^- + HS^-$	-50	1
L_4^+	$VS^+ + HS^+$	$VS^+ + HS^+$	$VS^+ + HS^+$	$VS^+ + HS^+$	-50	2

R: Roller, H: Hinge, VS: Vertical spring, HS: Horizontal spring, HR: Hinge + vertical spring, +/-: upper or lower bound bearing stiffness.
(Note: In HR conditions, restraints in all three directions are placed at a single node at the bearing centroid.)

Table 4-6. Moments and Axial Forces in the Link Slab for Various Support Conditions under Thermal Gradient Load

Case	1st support (Abutment)	2nd support (Pier)	3rd support (Pier)	4th support (Abutment)	Moment (ft-k)	Axial force (k)
TP_1	H	R	R	R	+61	0
TP_1^-	HR^-	$VS^- + HS^-$	$VS^- + HS^-$	$VS^- + HS^-$	+61	-4
TP_1^+	HR^+	$VS^+ + HS^+$	$VS^+ + HS^+$	$VS^+ + HS^+$	+61	-5
TP_2	R	H	H	R	+44	-84
TP_2^-	$VS^- + HS^-$	HR^-	HR^-	$VS^- + HS^-$	+44	-84
TP_2^+	$VS^+ + HS^+$	HR^+	HR^+	$VS^+ + HS^+$	+44	-85
TP_3	R	R (H)	H (R)	R	+61	0
TP_3^-	$VS^- + HS^-$	$VS^- + HS^-$	HR^-	$VS^- + HS^-$	+60	-5
TP_3^+	$VS^+ + HS^+$	$VS^+ + HS^+$	HR^+	$VS^+ + HS^+$	+60	-6
TP_4^-	$VS^- + HS^-$	$VS^- + HS^-$	$VS^- + HS^-$	$VS^- + HS^-$	+61	-2
TP_4^+	$VS^+ + HS^+$	$VS^+ + HS^+$	$VS^+ + HS^+$	$VS^+ + HS^+$	+61	-3
TN_1	H	R	R	R	-18	0
TN_1^-	HR^-	$VS^- + HS^-$	$VS^- + HS^-$	$VS^- + HS^-$	-18	1
TN_1^+	HR^+	$VS^+ + HS^+$	$VS^+ + HS^+$	$VS^+ + HS^+$	-18	1
TN_2	R	H	H	R	-13	25
TN_2^-	$VS^- + HS^-$	HR^-	HR^-	$VS^- + HS^-$	-13	25
TN_2^+	$VS^+ + HS^+$	HR^+	HR^+	$VS^+ + HS^+$	-13	26
TN_3	R	R (H)	H (R)	R	-18	0
TN_3^-	$VS^- + HS^-$	$VS^- + HS^-$	HR^-	$VS^- + HS^-$	-18	1
TN_3^+	$VS^+ + HS^+$	$VS^+ + HS^+$	HR^+	$VS^+ + HS^+$	-18	2
TN_4^-	$VS^- + HS^-$	$VS^- + HS^-$	$VS^- + HS^-$	$VS^- + HS^-$	-18	1
TN_4^+	$VS^+ + HS^+$	$VS^+ + HS^+$	$VS^+ + HS^+$	$VS^+ + HS^+$	-18	1

The analysis documented that the link slab is subjected to axial forces and flexure in the case of RHHR support conditions. The link slab moment under live loads is about 50 ft-kips for all the support configurations, except RHHR where it is reduced to 19 ft-kips. The link slab moment magnitude is not influenced by the position of H support with HRRR and RHRR support configurations except a minor change in axial load. Axial forces are only generated when horizontal bearing stiffness is included. Negative gradient load is additive to live load generating tensile stresses at the link slab top fiber for all boundary conditions investigated. Under positive thermal gradient loading in conjunction with RHHR, support configuration tensile stresses are at the link slab bottom fiber.

4.2.2 Effect of Link Slab Debonded Length

The debonded lengths on link slab stresses are investigated using four different debonded lengths of 0%, 2.5%, 5.0%, and 7.5% of the span length.

According to analysis results and as expected, link slab moments decrease with increasing debonded length. However, moment magnitudes are greatly influenced by the girder end support condition directly underneath the link slab (Figure 4-6 and Figure 4-7). The net link slab axial load is only slightly affected by debonded length. (Refer to Table E-1 given in Appendix E.) The change in moment decreases with increasing debonded length, remaining almost constant between 5% to 7.5% (Figure 4-6 and Figure 4-7).

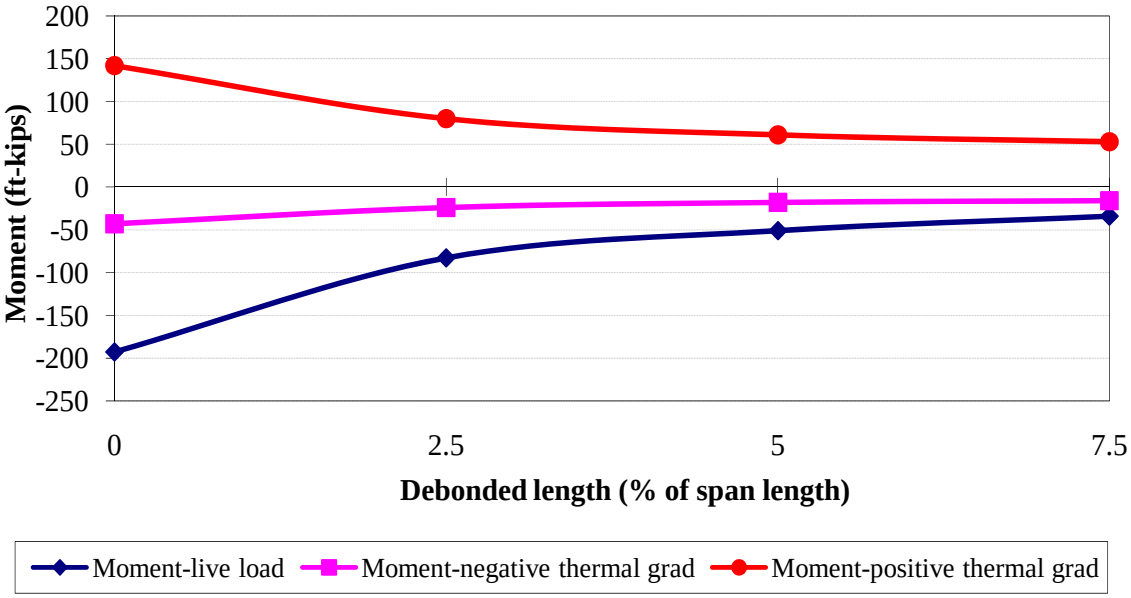

Figure 4-6. Moment against the debond length-HRRR and RRHR cases

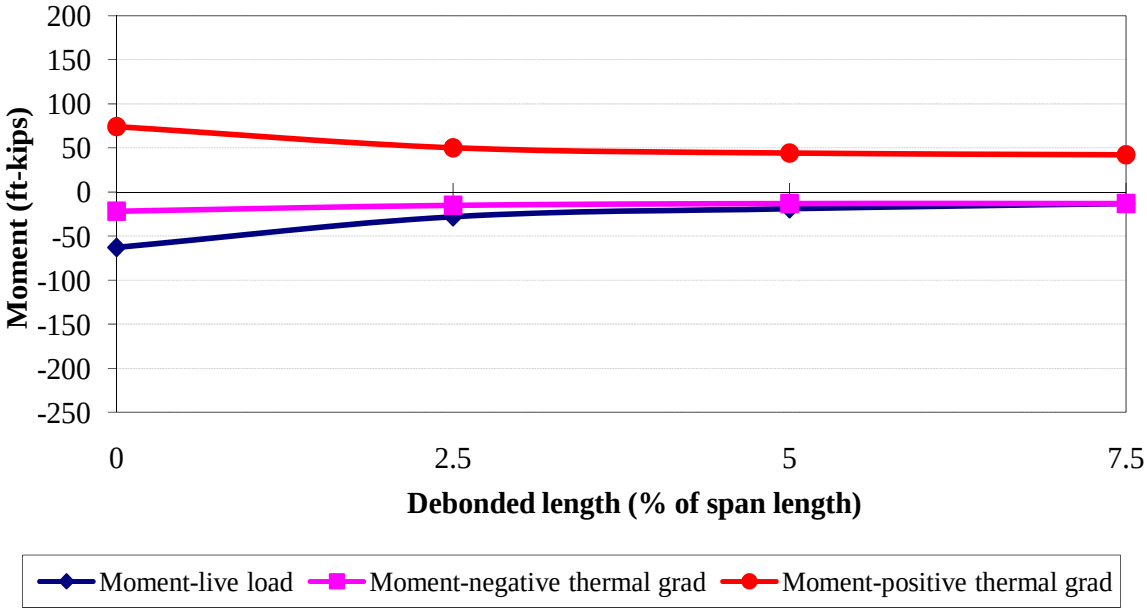

Figure 4-7. Moment against the debond length-RHHR case

4.2.3 Effect of Girder Depth

AASHTO PCI Type III girders in the base model are replaced with PCI Type VI girders to evaluate the effect of girder height on link slab stresses. Effective deck width is kept constant at 76 inches (Figure 4-8). Axle loads are increased based on the distribution factors. Thermal gradient loads are equal for both girder types since both are deeper than 12 inches. Moment and axial load under live and thermal gradient load cases are presented in Table 4-7.

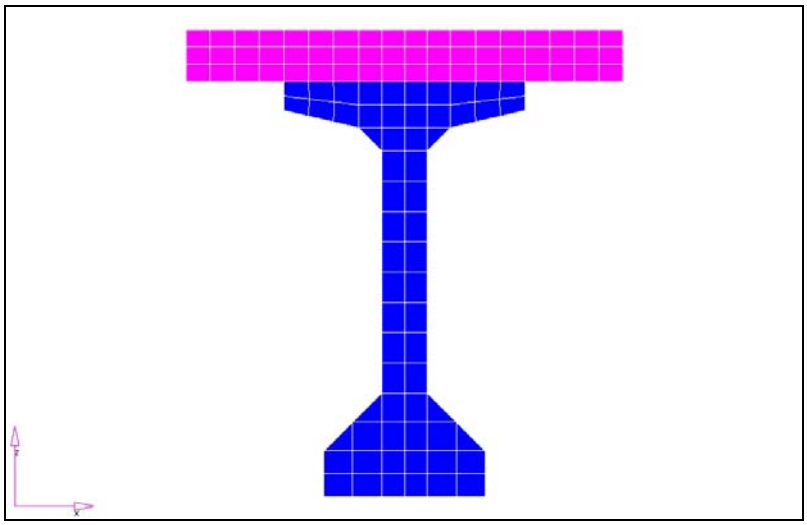

Figure 4-8. PCI Type VI girder and the deck

Table 4-7. Moments and Axial Forces Developed in the Link Slab for Different Girder Types

Case	Support	Moment (ft-k)		Axial force (kips)	
		Type III	Type VI	Type III	Type VI
L_1	HRRR	-51	-17	0	0
L_2	RHHR	-19	-6	159	104
L_3	RRHR	-51	-17	0	0
TP_1	HRRR	61	54	0	0
TP_2	RHHR	44	43	-84	-100
TP_3	RRHR	61	54	0	0
TN_1	HRRR	-18	-16	0	0
TN_2	RHHR	-13	-13	25	30
TN_3	RRHR	-18	-16	0	0

Although the live load acting on Type IV girders is higher than that of Type III girders, moment and axial forces decreased. This is due to the fact that girder end rotations are lower. Also, the link slab relative stiffness with respect to Type VI girders is lower compared to that of Type III girders. Hence, link slab moment and axial load are expected to increase with increasing span to depth ratio.

Moments due to positive and negative temperature gradient loading did not change appreciably, but a 20% increase in axial forces is calculated with increasing girder depth.

4.2.4 Effects of Adjacent Span Ratio

The effect of unequal span lengths is investigated by increasing the second span to 91 ft from 69.5 ft. A 100 ft span length is specified as the maximum for HS 25 truck loading and 7000 psi concrete in the PCI Bridge Design Manual (2003). Span length is reduced by about 10% in order to accommodate 5000 psi concrete strength and higher truck loading. The HL-93 loading on longer spans is increased since the distribution factors change with respect to length. The total link slab length is also increased to 98 inches from 85 inches. Moment and axial load for the case of different span lengths are compared in Table 4-8.

Table 4-8. Moment and Axial Forces in Link Slab for Different Span Ratios with Similar Girder Type

Case	Support	Moment (ft-k)		Axial force (kips)	
		Spans (ft) 69.5/69.5	Spans (ft) 69.5/91	Spans (ft) 69.5/69.5	Spans (ft) 69.5/91
L_1	HRRR	-51	-66	0	0
L_2	RHHR	-19	-22	159	200
L_3	RRHR	-51	-66	0	0
TP_1	HRRR	61	63	0	0
TP_2	RHHR	44	44	-84	-90
TP_3	RRHR	61	63	0	0
TN_1	HRRR	-18	-19	0	0
TN_2	RHHR	-13	-13	25	27
TN_3	RRHR	-18	-19	0	0

Moment and axial force increase under live load with increased span ratios. For the case of temperature gradient, moment and axial force changes are insignificant.

4.2.5 Effects of Adjacent Span Ratio with Different Girder Type

The effect of unequal span lengths with different girder types is investigated. The second span of the model is replaced with Type VI girders, and the length is increased to 150.3 ft. For Type VI girders, a 167 ft span length is specified as maximum for HS 25 truck loading and 7000 psi concrete in the PCI Bridge Design Manual (2003). Span length is reduced by about 10% in order to accommodate 5000 psi concrete strength and HL-93 loading. The HL-93 loading on the longer span is increased since the distribution factor changes with span and girder type. The total link slab length is also increased to 133 inches from 85 inches. Moment and axial load for different span lengths are tabulated in Table 4-9.

Table 4-9. Moment and Axial Forces Develop in Link Slab for Different Span Lengths with Different Girder Types (69.5 ft Type III and 150.3 ft Type VI)

Case	1st support (Abutment)	2nd support (Pier)	3rd support (Pier)	4th support (Abutment)	Moment (ft-k)	Axial force (k)
L_1	H	R	R	R	-62	0
L_2	R	H	H	R	-16	252
L_3	R	R (H)	H (R)	R	-62	0
TP_1	H	R	R	R	61	0
TP_2	R	H	H	R	42	-107
TP_3	R	R (H)	H (R)	R	61	0
TN_1	H	R	R	R	-18	0
TN_2	R	H	H	R	-13	32
TN_3	R	R (H)	H (R)	R	-18	0

Although the second span has a higher girder depth compared to the previous case where both spans had Type III girders (Table 4-8), moment values decrease slightly due to a lower link slab to composite girder (Type VI + deck) stiffness ratio. Moment changes are insignificant under temperature gradient loads. For all cases, an increase in axial force is observed (Table 4-8 and Table 4-9).

4.2.6 Effects of Uniform Temperature Loading

Uniform thermal load calculation is based on a base temperature – ambient temperature during construction. The base temperature is established by analyzing the daily maximum, daily minimum and mean temperature values between 1971 through 2000. The data is obtained from the National Climatic Data Center (2004) for the Dearborn and Detroit Metro Airport locations as presented in Table 4-10.

Table 4-10. Daily Maximum, Minimum, and Mean Temperatures for Dearborn and Detroit Metro Airport Locations for Years 1971 through 2000 (^{o}F)

Location	Month	Daily Max	Daily Min	Mean	Monthly Mean
Dearborn	Apr	59.6	36.8	48.2	62.8
	May	72.3	47.3	59.8	
	Jun	81.3	56.9	69.1	
	Jul	85.7	61.6	73.7	
	Aug	84	60.2	72.1	
	Sep	76.6	52.1	64.4	
	Oct	64	40.7	52.4	
Detroit Metro Airport	Apr	57.8	38.4	48.1	62.6
	May	70.2	49.4	59.8	
	Jun	79	58.9	69	
	Jul	83.4	63.6	73.5	
	Aug	81.4	62.2	71.8	
	Sep	73.7	54.1	63.9	
	Oct	61.2	42.5	51.9	

Based on the monthly mean in Table 4-10, a base temperature of 62.7 ^{o}F is defined averaging the Dearborn and Detroit Metro Airport measurement locations. Section 3.12.2 of AASHTO LRFD (2004) states that design thermal movement associated with a uniform temperature change may be calculated using either Procedure A or Procedure B. Procedure A thermal load is based on the difference between the lower or upper bound temperature values given in AASHTO LRFD (2004) and the base temperature. In Procedure B, the difference between the maximum or

minimum design temperature and the base temperature is used to calculate the total design thermal load for joints and bearings. Procedures A and B temperature ranges, and positive and negative uniform temperature load used in finite element analysis are given in Table 4-11.

Table 4-11. Procedures A and B Temperature Ranges, Base Temperature, and Temperature Differences to be Applied for Expansion and Contraction Cases

Procedure	A	B
Minimum Temperature (^{o}F)	0	-10
Maximum Temperature (^{o}F)	80	105
Base Temperature (^{o}F)	62.7	62.7
Expansion (^{o}F)	17.3	42.3
Contraction (^{o}F)	-62.7	-72.7

A uniform thermal expansion coefficient of 6.0 x 10^{-6} /^{o}F is used for both deck and girder concrete. Support configurations HRRR and RHHR are the only cases considered for analysis. The RRHR case is not considered since the results would be similar to RHHR support configuration. Under HRRR conditions the structure is allowed to expand from or contract towards the hinged support. Ideal support conditions, as well as the effects of lower and upper bound bearing stiffness, are also investigated. The respective vertical and horizontal bearing stiffness range was between 1464.30 k/in. - 1981.11 k/in. and 29.02 k/in. - 39.26 k/in. (Table 4-3).

The main objective in uniform thermal analysis is to calculate the range of bridge elongation and contraction. However, moment and axial load will also develop from bearing restraints. Displacements achieved under uniform thermal load are required for evaluating modified-fixed bearing performance. In defining a notation for the thermal loads, '*E*' designates expansion and '*C*' contraction, '*A*' designates thermal loads calculated using AASHTO Procedure A and '*B*' for procedure B. Moment and axial load are presented in Table 4-12 for different support conditions and Procedure A and Procedure B uniform thermal loads. Table 4-13 shows the displacements attained under uniform thermal load.

Table 4-12. Link Slab Moments and Axial Forces - Various Support Conditions and Uniform Thermal Loads

Case	1st support (Abutment)	2nd support (Pier)	3rd support (Pier)	4th support (Abutment)	Moment (ft-k)		Axial force (kips)	
					A	B	A	B
TC_1	H	R	R	R	0	0	0	0
TC_1^-	HR^-	$VS^- + HS^-$	$VS^- + HS^-$	$VS^- + HS^-$	0	0	18	21
TC_1^+	HR^+	$VS^+ + HS^+$	$VS^+ + HS^+$	$VS^+ + HS^+$	0	0	24	28
TC_2	R	H	H	R	-1	-1	4	5
TC_2^-	$VS^- + HS^-$	HR^-	HR^-	$VS^- + HS^-$	-1	-1	8	10
TC_2^+	$VS^+ + HS^+$	HR^+	HR^+	$VS^+ + HS^+$	-1	-1	10	12
TE_1	H	R	R	R	0	0	0	0
TE_1^-	HR^-	$VS^- + HS^-$	$VS^- + HS^-$	$VS^- + HS^-$	0	0	-5	-12
TE_1^+	HR^+	$VS^+ + HS^+$	$VS^+ + HS^+$	$VS^+ + HS^+$	0	0	-7	-16
TE_2	R	H	H	R	0	-1	-2	-3
TE_2^-	$VS^- + HS^-$	HR^-	HR^-	$VS^- + HS^-$	0	0	-2	-6
TE_2^+	$VS^+ + HS^+$	HR^+	HR^+	$VS^+ + HS^+$	0	0	-3	-7

R: Roller, H: Hinge, VS: Vertical spring, HS: Horizontal spring, HR: Hinge + vertical spring, +/-: upper or lower bound bearing stiffness.

Table 4-13. Displacements under Uniform Thermal Loads

Case	Displacement, Proc. A (in)			Displacement, Proc. B (in)		
	1st support	Center	4th support	1st support	Center	4th support
TC_1	0	-0.31	-0.63	0	-0.36	-0.73
TC_1^-	0	-0.30	-0.61	0	-0.35	-0.71
TC_1^+	0	-0.29	-0.60	0	-0.34	-0.70
TC_2	0.32	0	-0.32	0.37	0	-0.37
TC_2^-	0.31	0	-0.31	0.36	0	-0.36
TC_2^+	0.31	0	-0.31	0.36	0	-0.36
TE_1	0	0.09	0.17	0	0.21	0.42
TE_1^-	0	0.08	0.17	0	0.20	0.41
TE_1^+	0	0.08	0.17	0	0.20	0.41
TE_2	-0.09	0	0.09	-0.22	0	0.22
TE_2^-	-0.09	0	0.09	-0.21	0	0.21
TE_2^+	-0.09	0	0.09	-0.21	0	0.21

Link slab moments under uniform thermal loads are negligible, but axial forces develop with increasing bearing stiffness. Girder end displacements under uniform thermal loads are within the tolerable limits of the bearings.

4.2.7 Effects of Bridge Deck Casting Sequence and Drying and Hydration Thermal Loads

The link slab is placed, in most cases, over the piers where negative moments develop under live and negative thermal loads. The link slab is placed last to avoid the development of a negative moment due to the self weight of the deck. Due to restraint ends of the link slab, under hydration

thermal loads and drying shrinkage, there is a potential for cracking. Considering a thermal expansion coefficient of 6×10^{-6} /^{0}F and a uniform strain distribution through a cast-in-place concrete deck, Aktan et al. (2003) showed that temperature differentials around 20 – 22 ^{0}F is adequate for initiating cracking of a standard 9-in. deck. As recommended by Aktan et al. (2003), CEB-FIP Model Code (1990) and ACI 209 prediction models are utilized to determine the upper and lower bound values of shrinkage strains. Early-age concrete mechanical properties required for the formulation are estimated and shown in Table 4-14. Shrinkage calculations assume a 28-day concrete strength of 5000 psi with Type 1 cement and wet curing periods of 2, or 7, or 14 days (Table 4-15). MDOT structural concrete design requires a 7 day wet cure (MDOT 2003b). Also, ambient relative humidity of 60 % is assumed.

Table 4-14. Early Age Concrete Properties

Model	ACI 209	CEB-FIP 90
Compressive Strength (psi)	565	989
Tensile Strength (psi)	178	236
Elasticity Modulus (ksi)	1441	1758
Cracking strain (10^{-6})	123	134

Table 4-15. Predicted Drying Shrinkage for Various Wet Curing Durations

ACI 209 (Microstrain)	**CEB-FIP 90** (Microstrain)	**Curing duration** (days)
266	32	2
234	29	7
178	23	14

Aktan et al. (2003) showed that the hydration thermal load alone is sufficient for initiating deck cracks. Once the deck is cracked under hydration thermal loads, crack widths are increased under drying shrinkage. In this project the same methodology is used to calculate link slab crack width. Lower and upper bound cracking strains are estimated using ACI 209 and CEB-FIP 90 as 123 and 134 microstrains (Table 4-14). Lower and upper bound drying shrinkage of 7-day wet cure concrete are estimated to be 29 and 234 microstrains. It is assumed that the total length change in the link slab due to hydration thermal loads and shrinkage represents the crack width. Lower and upper bound total shrinkage values are calculated combining CEB-FIP Model Code (1990) and ACI 209 (1992) estimations as 152 (i.e., 123+29) and 368 (i.e., 134+234)

microstrains. Crack widths are estimated by multiplying the link slab length by the calculated total shrinkage strains (Table 4-16). Creep effects and reinforcement effects are not taken into account, and both effects will reduce the crack width.

Table 4-16. Lower and Upper Bound Link Slab Crack Widths for Inspected Bridges

No.	Bridge ID	Main Spans	Max. Span (ft)	Bridge Length (ft)	Link slab length (in)	Link slab cast last?	Crack width (in)	
							Lower bound	Upper bound
1	S04-1 of 63174	3	63	141	60	Yes	0.009	0.022
2	S04-2 of 63174	3	63	141	60	Yes	0.009	0.022
3	S08 of 41027	3	72	179	68-78	Yes	0.010	0.029
4	B01 of 10042	3	50	150	61	Yes	0.009	0.022
5	S12-3 of 25042	4	70	210	52-61	Yes	0.008	0.022
6	S12-4 of 25042	4	70	210	52-61	Yes	0.008	0.022
7	S12-7 of 25042	4	70	210	52-61	Yes	0.008	0.022
8	S12-8 of 25042	4	70	210	52-61	Yes	0.008	0.022

Link slab cracking under live load effects are also evaluated. The reinforcement details of the S12-7/8-25042 top (main) reinforcement layer consist of #7 (new) and #4 (existing) bars both placed at 12 inches. In S04-63174 bridges, #6 and #3 bars are placed at 9.5 inches. Main (longitudinal) reinforcement is placed over the #6 transverse bars resulting in a clear cover of 2.28 and 2.34 inches for 25042 and 63174 bridges, respectively. The crack widths are calculated using the Gergely-Lutz equation. Live load moments (M_n) are calculated using the Caner-Zia design procedure based on HS-25 truck loading. Calculations for B01 of 10042 and S08 of 41027 are not performed since exact cross-sections of the composite girder-deck could not be identified.

Table 4-17 shows the calculated 'z' values and corresponding crack width under live load. The minimum link slab length that would prevent cracking is also determined for the two rebar orientations and cross-section properties by using reinforcement stress and z value as the limiting criteria.

Crack width calculated by the Gergely-Lutz equation:

$$\omega = 0.076\beta f_s (d_C A)^{\frac{1}{3}} = 0.076\beta \cdot z \qquad (4\text{-}2)$$

where,

$$z = f_s (d_c A)^{\frac{1}{3}} \quad (4\text{-}3)$$

and,

ω: surface crack width in units of 0.001 in.

β: ratio of distances to neutral axis from extreme tension fiber and from the centroid of main reinforcement

ρ: reinforcement ratio

f_s: reinforcement stress in ksi

d_c: concrete cover measured from extreme tension fiber to the centroid of nearest reinforcement level in inches (limited to 2 inches as per AASHTO LRFD 5.7.3.4)

A: Effective area per bar in in^2 (while calculating A, d_c should be limited to 2 inches as per AASHTO LRFD 5.7.3.4)

Section 5.7.3.4 of the AASHTO LRFD (2004) limits 'z' calculated from Eq. 4-3 to 130 k/in for severe exposure conditions and 170 k/in for moderate exposure conditions. If the resulting 'z' is above the limits, a relief cut is to be provided and sealed prior to service (Needham and Juntunen 2000).

Table 4-17. Calculated Link Slab Crack Widths under Live Load

No	Bridge ID	Link slab length (in)	Reinforcement	I_{comp} (in^4)	M_n (kips-in /ft)	f_s (ksi)	Z	Crack width (in)	Min. link slab length* (in)
1	S04-1 of 63174	60	#6 @9.5 #3 @9.5	392,892	165.2	38.2	179	0.018	83
2	S04-2 of 63174	60	#6 @9.5 #3 @9.5	392,892	165.2	38.2	179	0.018	83
3	S08 of 41027	68-78	N/A	N/A	N/A	N/A	N/A	N/A	N/A
4	B01 of 10042	61	N/A	N/A	N/A	N/A	N/A	N/A	N/A
5	S12-3 of 25042	52-61	#7 @12 #4 @12	392,892	190.6	38.6	198	0.020	80
6	S12-4 of 25042	52-61	#7 @12 #4 @12	392,892	190.6	38.6	198	0.020	80
7	S12-7 of 25042	52-61	#7 @12 #4 @12	392,892	190.6	38.6	198	0.020	80
8	S12-8 of 25042	52-61	#7 @12 #4 @12	392,892	190.6	38.6	198	0.020	80

f'_c = 5000 psi, longitudinal bars are placed on top over #6 transverse bars

* Based on z <= 130 and allowable stress limit in the reinforcement per AASHTO LRFD 5.7.3.4

The ‘z’ values are greater than the allowable limits for severe exposure conditions given by AASHTO LRFD (2004). In crack width calculations, β factors are calculated by assuming concrete cover measured from extreme tension fiber to the centroid of the nearest reinforcement level (d_c) as 2 inches. Crack widths calculated using the upper bound total predicted that shrinkages values are greater than those developed by live load.

4.2.8 Moment Curvature Relation for Link Slab Design

According to the current link slab design, bottom reinforcements are discontinued over the pier. Section properties and reinforcement orientation of S07-8 of 25042 bridges show the top reinforcement layer consisting of 6 - #7 and 6 - #4 bars within effective flange width of 76 inches. The bottom rebar layer consists of 6 - #6 and 6 - #5 bars. The top clear cover is 2.2 inches, whereas the cover is reduced to 1.9 inches at the bottom layer.

Although current link slab design considers service loads with crack width criteria, the strength limit state response is presented for comparison purposes. AASHTO LRFD (2004) Strength I limit state uses a null factor for thermal gradient and 1.75 for live load. The load factor for uniform thermal load is 1.2 for deformations and 0.5 for all other effects. In Service I limit state, which is used for crack control, live load factors for live and thermal gradient loads are 1.0 and 0.5, respectively. The load factor for thermal gradient can be taken as 1.0 when live load is not considered. The load factor for uniform thermal load is 1.2 for deformations and 1.0 for all other effects.

Utilizing analysis results under live (LL), negative thermal gradient (NTG), and Procedure B uniform thermal contraction (UTC) loads in conjunction with different support configurations, moment and axial force for Strength I and Service I limit states are calculated (Table 4-18).

Combined effects of negative thermal gradient and uniform thermal contraction resultants are used in Service 1-C case and positive thermal gradient, and uniform thermal expansion resultants are used in Service 1-E case. The cracking moment of the link slab section considered in this analysis is calculated as 40.5 ft-kips. Service I-C and Service I-E limit state moments developed under HRRR support configurations, with ideal boundary conditions and with upper and lower bearing stiffness, are greater than the cracking moment capacity of the link slab.

The link slab is subjected to a combined effect of moments and axial forces; hence the moment interaction diagram should also be used in the analysis and design. The moment interaction diagram developed for ultimate loads is shown in Figure 4-9. AASHTO LRFD (2004) Strength I limit state moments and axial forces, as depicted in Figure 4-9, exceed the singly reinforced section capacity. AASHTO LRFD (2004) Service I limit state moments and axial forces, as shown in a moment-interaction diagram (Figure 4-9), indicate that the current link slab details are not adequate to satisfy the service load demands. Service I limit state moment and axial force values are taken from fundamental load cases in Table 4-18 where bearing stiffness is not incorporated. Note that uniform thermal loads contribute only to the axial forces. Under HRRR support configurations, positive moments developed solely under positive thermal gradient loads exceed the capacity of singly reinforced cross-section. This may be resolved by continuing bottom rebar layers as shown in Figure 4-9 for comparison.

Table 4-18. Link Slab Moments, Axial Forces, and Stresses under Combined Loading

Limit state	Cases	Moment (ft-kips)	Axial force (kips)
Strength I 1.75 LL+0.50 UTC	HRRR	-89	0
	HRRR$^-$	-88	11
	HRRR$^+$	-88	15
	RHHR	-34	281
	RHHR$^-$	-34	285
	RHHR$^+$	-34	284
Service I-C 1.0 LL+0.5 NTG+1.0 UTC	HRRR	-60	0
	HRRR$^-$	-59	23
	HRRR$^+$	-59	31
	RHHR	-27	177
	RHHR$^-$	-29	183
	RHHR$^+$	-27	184
Service I-E 1.0 PTG+1.0 UTE	HRRR	61	0
	HRRR-	61	-16
	HRRR+	61	-21
	RHHR	44	-87
	RHHR-	44	-90
	RHHR+	44	-92

LL: Live load, UTC: Uniform thermal contraction, NTG: Negative thermal gradient, PTG: Positive thermal gradient, UTE: Uniform thermal expansion

Current link slab design is based on girder end rotations under live load. AASHTO LRFD (2004) Service I limit state requires the combined effect of live and thermal loads. Appendix F presents a detailed calculation procedure for moment and axial load demand under thermal gradient loading that can be incorporated into current link slab analysis procedure.

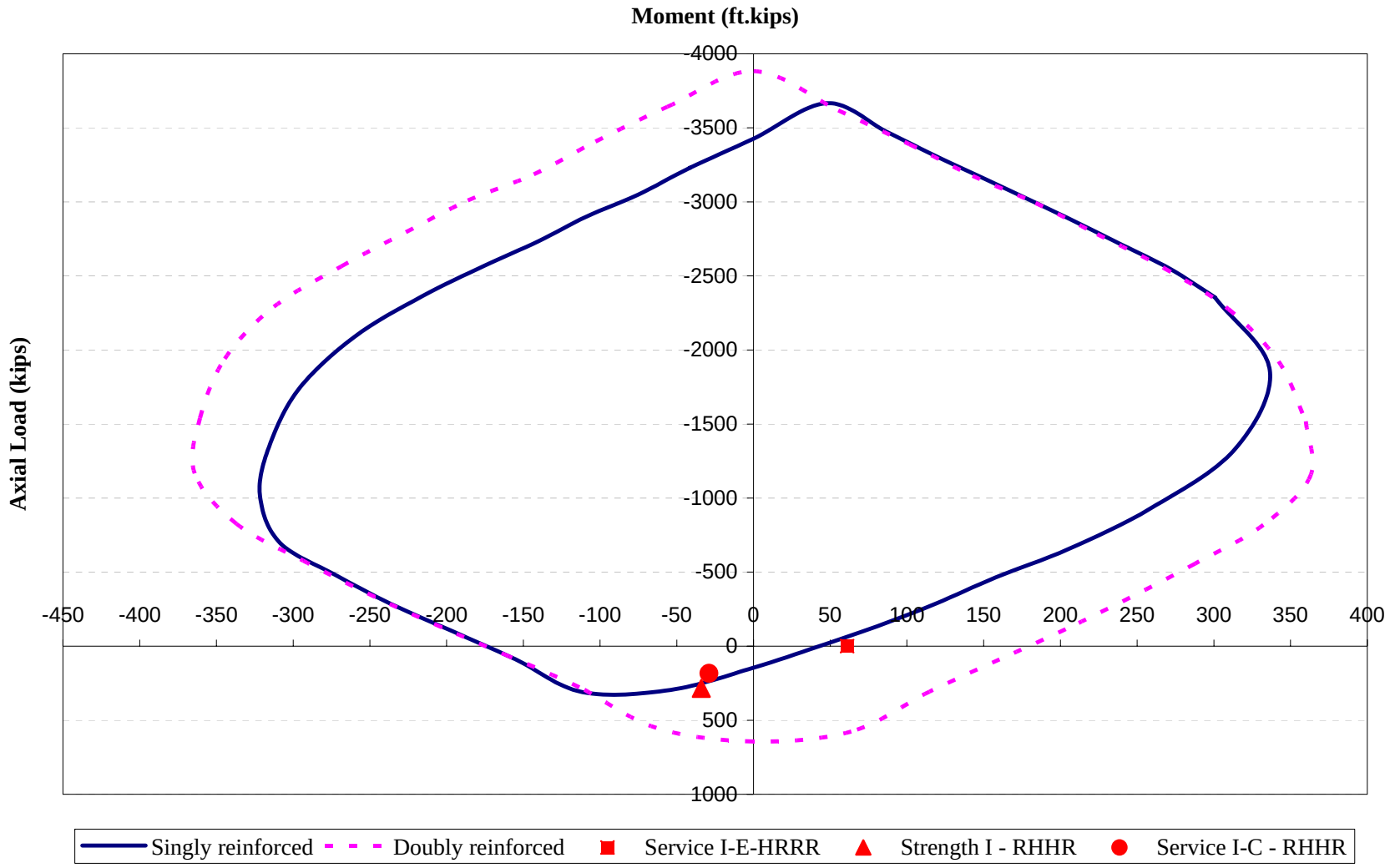

Figure 4-9. Moment interaction diagram for singly and doubly reinforced sections and load demand on the link slab under various load combinations.

4.2.9 Summary and Conclusions of Link Slab Assemblage Analysis

FE Analyses is carried out using a single girder analysis model to evaluate the effects of types and levels of loads on the link slab design parameters. Design parameters are: link slab length with respect to adjacent span lengths, debonded length, girder height, adjacent span length ratios, and support conditions. Summarized results of single girder assemblage models of the link slab region are presented in Table 4-19.

Table 4-19. Analysis Results Summary – Single Girder Model of Link Slab Bridge

Design Parameters	Effect on	Support Conditions		
		RHHR	RHRR / RRHR	HRRR
Live load	Top layer	T	T	T
	Bottom layer	T	C	C
Neg. thermal gradient	Top layer	T	T	T
	Bottom layer	C	C	C
Debond length ↑	Live/Neg. Thermal	M ↓	M ↓	M ↓
Girder size ↑	Live load	M↓ F↓	M↓ F~	M↓ F~
	Neg. gradient	M~ F↑	M~ F~	M~ F~
Adjacent span ratio ↑	Live load	M↑ F↑	M↑ F~	M↑ F~
	Neg. gradient	M~ F~	M~ F~	M~ F~

T: Tension, C: Compression, M: Moment, F: Axial force, ~: Minimal effect, ↑: increase, ↓: decrease.

The literature is inconsistent on the impact of different support configurations on the link slab moments and forces generated under various types and levels of loads. Current design is solely based on the girder end rotation without any regard to supports under the link slab. Based on the analysis performed on single girder models, the following conclusions are drawn.

1. Under live load, the link slab is under combined bending and tension for the RHHR cases whereas only bending is critical for HRRR and RRHR support configurations.

2. Girder end support conditions under the link slab greatly influence the moment and axial force developed within the link slab.

3. Moments developed at the link slab decrease with increasing debonded length. Using 5% of the span length as the debonded length is recommended. However, when girder end supports are fixed (hinge), debonded length can be reduced.

4. Link slab moments and axial forces increase with increasing span to depth ratio.

5. Link slab moments decrease with increasing beam depth. This is due to reduction in relative link slab-girder stiffness. However, axial forces increase with deeper sections as a result of greater top fiber translation even under small beam end rotations.

6. Axial force developed in the link slab under uniform thermal load in conjunction with bearing stiffness is not large enough to cause link slab cracking.

7. Girder end displacements under uniform thermal loads are within the tolerable limits of the existing bearings.

8. Full depth cracking potential increases under combined effects of live and negative thermal gradient loads when the link slab is over two hinge supports. Under a full thermal cycle with positive and negative gradients, there is potential for full depth cracking.

9. Moments generated under positive thermal gradient alone may exceed the singly reinforced link slab section capacity for cases without compressive force (i.e. HRRR or RRHR)

10. The link slab is subjected to combined flexural and axial loads under specific support configurations. In these cases a moment interaction diagram should be used for link slab design. Further, continuous bottom reinforcements are recommended.

11. Current link slab design is based on the moment demand due to live load. AASHTO LRFD (2004) Service I limit state requires the combined effect of live and thermal load. The analysis procedure developed for calculating moment and axial load demand due to thermal gradient load is presented in Appendix F. Link slab design should include the thermal load effects calculated using the procedure given in Appendix F.

12. Crack width calculated from the predicted total shrinkage strains exceed the crack widths caused by live loads. Full-depth cracking is attributed to thermal hydration and drying shrinkage stresses developed in the link slab. Use of minimum possible debonded length is encouraged to avoid cracking. Providing a saw cut directly over the pier center line is advised for crack management.

4.3 FULL BRIDGE MODELS OF LINK SLAB REGION

Full bridge models are developed with the objective of evaluating the moment and force demand in the link slab under symmetric and asymmetric live loads and negative thermal gradient loads on single and two lane bridges Analysis cases are defined based on the support conditions and the load types (Table 4-20 - Table 4-21). The effect of uniform thermal load is excluded since similar bearing demands calculated from single girder models are expected in the longitudinal direction.

Table 4-20. Live Load Analysis Cases

Case	1st support (Abutment)	2nd support (Pier)	3rd support (Pier)	4th support (Abutment)
L_1	H	R	R	R
L_1^-	HR^-	$VS^- + HS^-$	$VS^- + HS^-$	$VS^- + HS^-$
L_1^+	HR^+	$VS^+ + HS^+$	$VS^+ + HS^+$	$VS^+ + HS^+$
L_2	R	H	H	R
L_2^-	$VS^- + HS^-$	HR^-	HR^-	$VS^- + HS^-$
L_2^+	$VS^+ + HS^+$	HR^+	HR^+	$VS^+ + HS^+$
L_3	R	R (H)	H (R)	R
L_3^-	$VS^- + HS^-$	$VS^- + HS^-$	HR^-	$VS^- + HS^-$
L_3^+	$VS^+ + HS^+$	$VS^+ + HS^+$	HR^+	$VS^+ + HS^+$
L_4^-	$VS^- + HS^-$	$VS^- + HS^-$	$VS^- + HS^-$	$VS^- + HS^-$
L_4^+	$VS^+ + HS^+$	$VS^+ + HS^+$	$VS^+ + HS^+$	$VS^+ + HS^+$

R: Roller, H: Hinge, VS: Vertical spring, HS: Horizontal spring, HR: Hinge + vertical spring, +/-: upper or lower bound bearing stiffness.

Table 4-21. Negative Thermal Gradient Analysis Cases

Case	1st support (Abutment)	2nd support (Pier)	3rd support (Pier)	4th support (Abutment)
TN_1	H	R	R	R
TN_1^-	HR^-	$VS^- + HS^-$	$VS^- + HS^-$	$VS^- + HS^-$
TN_1^+	HR^+	$VS^+ + HS^+$	$VS^+ + HS^+$	$VS^+ + HS^+$
TN_2	R	H	H	R
TN_2^-	$VS^- + HS^-$	HR^-	HR^-	$VS^- + HS^-$
TN_2^+	$VS^+ + HS^+$	HR^+	HR^+	$VS^+ + HS^+$
TN_3	R	R (H)	H (R)	R
TN_3^-	$VS^- + HS^-$	$VS^- + HS^-$	HR^-	$VS^- + HS^-$
TN_3^+	$VS^+ + HS^+$	$VS^+ + HS^+$	HR^+	$VS^+ + HS^+$
TN_4^-	$VS^- + HS^-$	$VS^- + HS^-$	$VS^- + HS^-$	$VS^- + HS^-$
TN_4^+	$VS^+ + HS^+$	$VS^+ + HS^+$	$VS^+ + HS^+$	$VS^+ + HS^+$

R: Roller, H: Hinge, VS: Vertical spring, HS: Horizontal spring, HR: Hinge + vertical spring, +/-: upper or lower bound bearing stiffness.

Two bridges selected for modeling are S12-3&4 of 25042 (two lanes) and S12-7&8 of 25042 (a single lane). Two identical spans of 69.5 ft. and a link slab are included in the model. The models are analyzed under live and negative thermal gradient load cases. The two bridges have Type III PCI interior girders with a 9 in. concrete deck. The total length of the link slab between span two and three is 84.4 in. Material properties and boundary conditions are the same as the single girder assemblage models. Diaphragms are modeled using rigid link elements between girders at girder ends, quarter points, and mid-span. Each bridge is also re-modeled incorporating a 20 degree skew in order to investigate the impact of skew.

Normal stress distributions along the width for all fundamental support conditions are presented in Appendix E.

4.3.1 Straight Bridge

4.3.1.1 Single Lane Straight Full Bridge Model

A single-lane straight full bridge model is established from the plans of S12-7 & 8 of 25042 (Figure 4-10). These bridges have five PCI Type III girders spaced at 66 in. on spans two and three.

Wheel loads are placed so as to create maximum torsion (M_{yy}) at the center of link slab considering AASHTO LRFD restrictions. The actual loading in the FE models slightly deviated from that given in Figure 4-11 because of mesh limitations. Moment and force demands are calculated for the full bridge width as well as five effective girder-deck segments at the centerline of the link slab (Figure 4-11).

Moments (M_{xx}, M_{yy}, and M_{zz}) and axial force (N) are obtained directly over the pier acting on the link slab transverse cross-section for the full bridge width. Notations are shown in Figure 4-12. The bending moments and axial force are evaluated for the effective link slab width of 66 inches (M_{eff} and N_{eff}) and presented in Table 4-22 and Table 4-23.

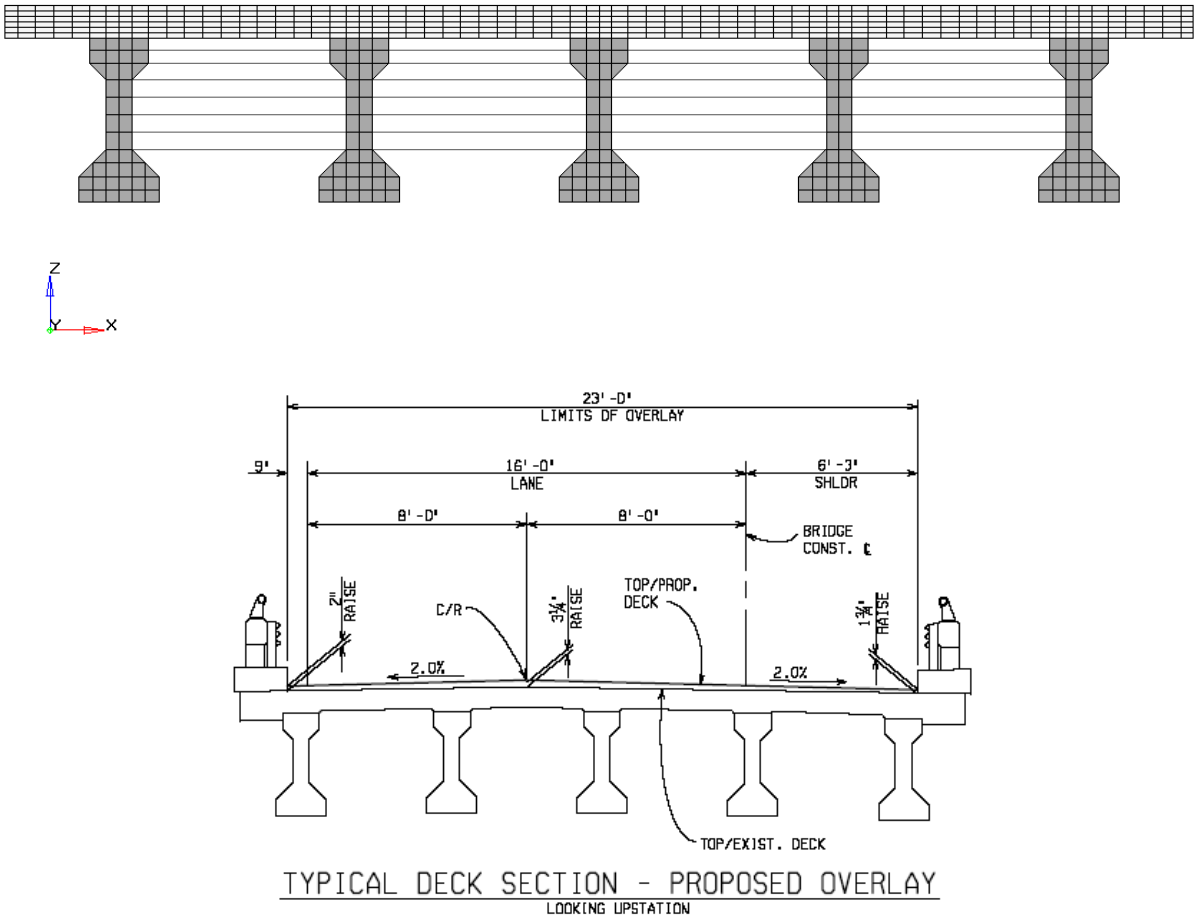

Figure 4-10. Cross-section of S12-7& 8 of 25042: FE model and actual section

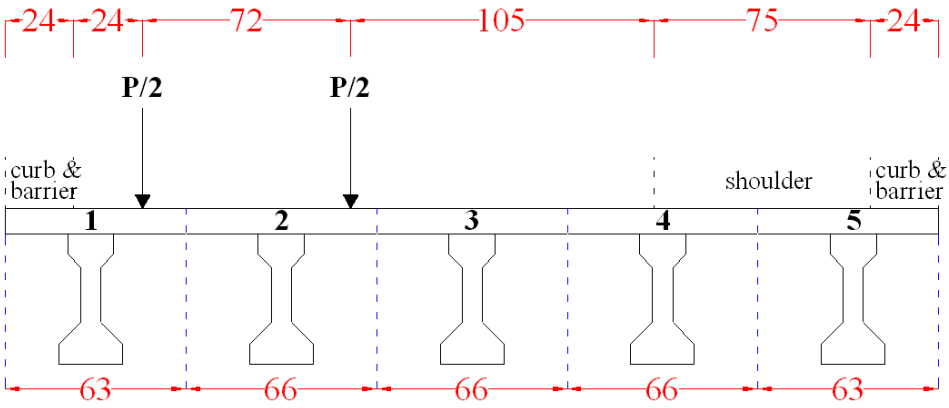

Note: all units are in inches

Figure 4-11. Transverse position of a single truck and effective slab segments

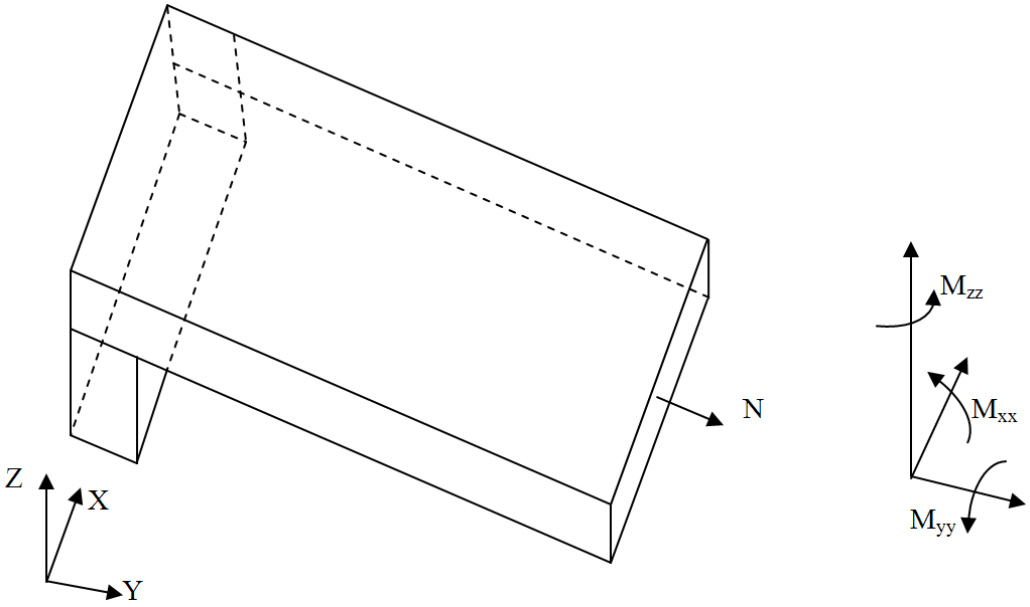

Figure 4-12. Notations for moments and axial forces

Table 4-22. Live Load Moments and Axial Force at Link Slab Cross-Section and within Effective Width under Various Support Conditions for Straight Single Lane Bridge

Case	Full Width				Effective Width	
	M_{xx} (Bending) ft-kips	M_{yy} (Torsion) ft-kips	M_{zz} (Twist) ft-kips	N (Axial load) kips	M_{eff}* ft-kips	N_{eff}* kips
L_1	-81	-2	0	0	-32	2
L_1^-	-79	-14	12	2	-30	2
L_1^+	-79	-12	56	2	-30	0
L_2	-29	-3	1541	275	-12	109
L_2^-	-29	-2	1614	276	-12	112
L_2^+	-29	-2	1620	275	-12	112
L_3	-81	-15	0	0	-32	2
L_3^-	-79	-62	779	11	-28	29
L_3^+	-78	-51	863	15	-28	32
L_4^-	-80	-6	225	2	-31	7
L_4^+	-80	-5	286	3	-30	11

Table 4-23. Negative Temperature Gradient Moments and Axial Forces at Link Slab Cross-Section and within Effective Width under Various Support Conditions for Straight Single Lane Bridge

Case	Full Width				Effective Width	
	M_{xx} (Bending) ft-kips	M_{yy} (Torsion) ft-kips	M_{zz} (Twist) ft-kips	N (Axial load) kips	M_{eff}* ft-kips	N_{eff}* kips
TN_1	-87	0	0	0	-21	3
TN_1^-	-86	0	0	5	-21	4
TN_1^+	-86	0	0	7	-21	4
TN_2	-64	0	0	121	-16	31
TN_2^-	-64	0	0	121	-16	31
TN_2^+	-64	0	0	122	-16	31
TN_3	-87	0	0	0	-21	4
TN_3^-	-85	0	0	7	-21	5
TN_3^+	-85	0	0	9	-21	5
TN_4^-	-86	0	0	3	-21	3
TN_4^+	-86	0	0	4	-21	4

Under live load, link slab twist is small with ideal support conditions corresponding to HRRR and RRHR cases. With the introduction of bearing stiffness, the twisting moment increases for all the boundary conditions, except for HRRR. The largest twisting moment occurs under RHHR support configuration. Twisting moments on the link slab increase with increasing girder end restraints underneath the link slab (i.e., RHHR > RRHR > HRRR). This is due to large longitudinal reactions that develop asymmetrically beneath the link slab. Maximum effective flange bending (M_{eff}) and axial force (N_{eff}) are obtained for segment 1 designated in Figure 4-11.

Under negative thermal gradient, torsion or twisting of the deck diminishes because the load is symmetric. The maximum bending moment is developed within the effective flange of the center segment, (segment 3 in Figure 4-11), as expected.

Under live load, for some cases axial load resultants for effective width (N_{eff}) are greater than those obtained for the full bridge width (N). This is due to the tensile and compressive stress distribution along the link slab transverse cross-section while the effective width forces are calculated for the segment with the greatest longitudinal stress. Normal stress distribution along the full bridge width is included in Appendix E.

4.3.1.2 Two Lane Straight Full Bridge Model

A two-lane straight full bridge model is developed from the plans of S12-3 & 4 of 25042. These bridges have seven Type III PCI girders on spans two and three spaced at 76 in (Figure 4-13).

Wheel loads are placed to generate maximum torsion (M_{yy}) at the center of the link slab following the restrictions given in AASHTO LRFD. Actual loading defined in the FE models deviates slightly from what is presented in Figure 4-14 because of mesh limitations. Note that load eccentricity may be further increased by loading the shoulders; however, in this analysis trucks are positioned on design lanes (Figure 4-14).

Moments (M_{xx}, M_{yy}, and M_{zz}) and axial force (N) are obtained directly over the pier acting on the link slab transverse cross-section for the full bridge width. Notations are shown in Figure 4-12. The bending moments and axial force are evaluated for the effective link slab width of 76 inches (M_{eff} and N_{eff}) and presented in Table 4-24 and Table 4-25.

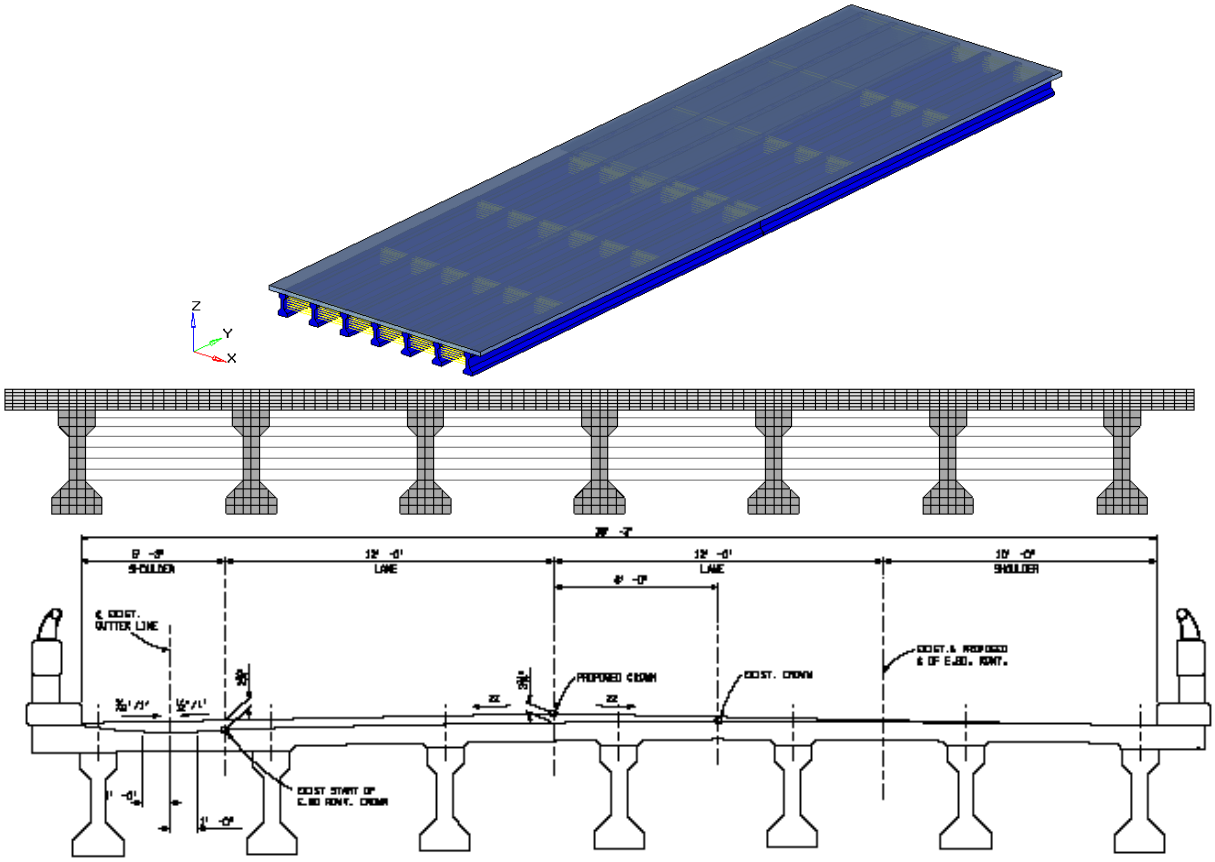

Figure 4-13. Isometric and cross-section views of S12-3&4 of 25042

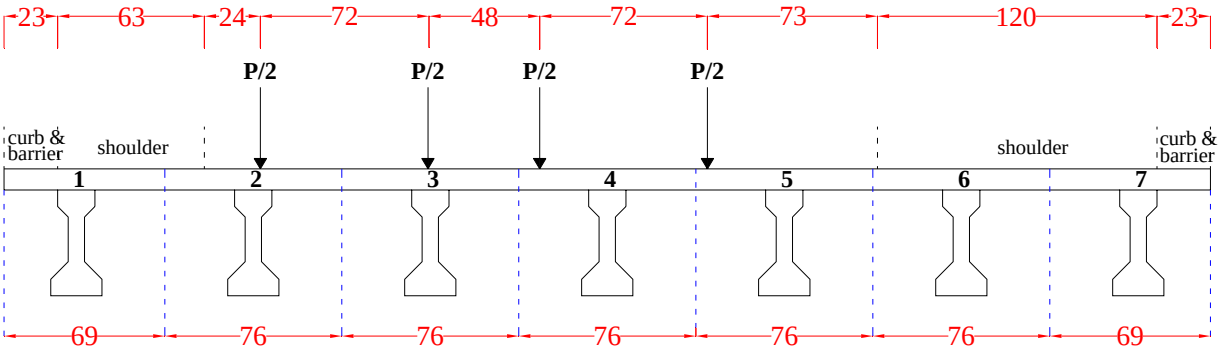

Note: All units are in inches.

Figure 4-14. Transverse position of two trucks and effective link slab segments

Table 4-24. Live Load Moments and Axial Forces at Link Slab Cross-Section and within Effective Width under Various Support Conditions for Straight Two Lane Bridge

Case	Full Width				Effective Width	
	M_{xx} (Bending) ft-kips	M_{yy} (Torsion) ft-kips	M_{zz} (Twist) ft-kips	N (Axial load) Kips	M_{eff}* ft-kips	N_{eff}* kips
L_1	-172	-2	0	0	-36	7
L_1^-	-168	-14	186	4	-35	9
L_1^+	-167	-12	161	5	-35	9
L_2	-63	-3	2203	536	-13	101
L_2^-	-64	-3	2254	540	-14	102
L_2^+	-63	-3	2250	536	-13	101
L_3	-172	-16	0	0	-37	10
L_3^-	-168	-71	704	21	-35	8
L_3^+	-165	-56	814	27	-34	10
L_4^-	-169	-7	138	4	-36	-4
L_4^+	-169	-6	179	6	-36	-4

Table 4-25. Negative Temperature Gradient Moments and Axial Forces at Link Slab Cross-Section and within Effective Width under Various Support Conditions for Straight Two Lane Bridge

Case	Full Width				Effective Width	
	M_{xx} (Bending) ft-kips	M_{yy} (Torsion) ft-kips	M_{zz} (Twist) ft-kips	N (Axial load) kips	M_{eff}* ft-kips	N_{eff}* kips
TN_1	-140	0	0	0	-25	7
TN_1^-	-139	0	0	7	-25	8
TN_1^+	-139	0	0	10	-25	8
TN_2	-104	0	0	179	-19	38
TN_2^-	-104	0	0	180	-19	37
TN_2^+	-104	0	0	181	-19	38
TN_3	-140	0	0	0	-25	8
TN_3^-	-138	0	0	10	-24	9
TN_3^+	-137	0	0	13	-24	10
TN_4^-	-139	0	0	4	-25	7
TN_4^+	-139	0	0	6	-25	7

The bending moment and axial load correlate well with the results of single girder analysis. A comparison in the moments and axial forces are presented in the summary and conclusions part of this section. Under live loads, link slab torsion (M_{yy}) increases under asymmetric boundary conditions underneath the link slab (e.g., RRHR). Twisting moments (M_{zz}) increase with the restraint underneath the link slab (e.g., M_{zz} for RHHR is greater than that of RRHR). This is due to longitudinal reactions generated asymmetrically underneath the link slab. Twisting moments of analysis cases L_4^+ and L_4^- are also of significant range. Under live load, the maximum effective flange bending (M_{eff}) and axial force (N_{eff}) are developed in segment 2 defined in Figure 4-14. For thermal load, only bending moments (M_{xx}) are present, and as expected maximum bending occurs at the center segment (segment 4 in Figure 4-14).

4.3.2 Skew Bridge

4.3.2.1 Single Lane Skew Full Bridge Model

Bridge plans of S12-7 & 8 of 25042 are used to develop the 20^o skew bridge model. These bridges have five Type III PCI girders on span two and three spaced at 66 in. (Figure 4-10 and Figure 4-11). Moments and axial force are obtained at the centerline of the link slab directly over the pier centerline parallel to the skew angle (Section A-A of Figure 4-15).

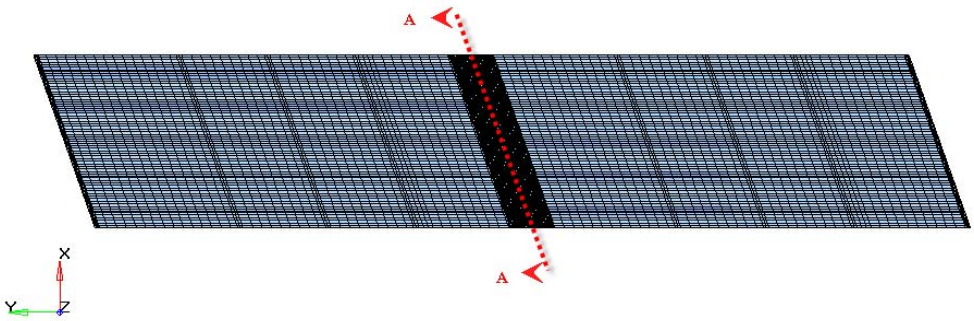

Figure 4-15. Top view of the 20° skew single lane bridge model and output section A-A

Moments about each coordinate axis (M_{xx}, M_{yy}, and M_{zz}) and axial force (N) in longitudinal (YY) direction are obtained at the link slab cross-section directly over the pier for full bridge width. Bending moments and axial force for the effective link slab width of 66 in. (M_{eff} and N_{eff}) are calculated. Analysis results are presented in Table 4-26 and Table 4-27, respectively.

Table 4-26. Live Load Moments and Axial Forces at Link Slab Cross-Section and within Effective Width under Various Support Conditions for 20° Skew Single Lane Bridge

Case	Full Width				Effective Width	
	M_{xx} (Bending) ft-kips	M_{yy} (Torsion) ft-kips	M_{zz} (Twist) ft-kips	N (Axial load) kips	M_{eff}* ft-kips	N_{eff}* kips
L_1	-77	-51	0	0	-32	4
L_1^-	-81	-19	57	1	-30	6
L_1^+	-80	-24	7	2	-30	3
L_2	-29	-10	1507	269	-12	110
L_2^-	-29	-12	1579	271	-12	113
L_2^+	-29	-13	1584	269	-12	113
L_3	-81	-35	0	0	-32	4
L_3^-	-95	26	740	11	-28	24
L_3^+	-90	14	823	14	-27	28
L_4^-	-76	-49	214	2	-32	5
L_4^+	-80	-33	275	3	-31	7

Table 4-27. Negative Temperature Gradient Moments and Axial Forces at Link Slab Cross-Section and Effective Width under Various Support Conditions for 20° Skew Single Lane Bridge

Case	Full Width				Effective Width	
	M_{xx} (Bending) ft-kips	M_{yy} (Torsion) ft-kips	M_{zz} (Twist) ft-kips	N (Axial load) kips	M_{eff}* ft-kips	N_{eff}* kips
TN_1	-79	-49	0	0	-23	7
TN_1^-	-81	-37	33	5	-23	8
TN_1^+	-80	-39	33	7	-23	9
TN_2	-58	-33	0	119	-17	37
TN_2^-	-57	-35	0	120	-17	37
TN_2^+	-57	-36	0	120	-17	37
TN_3	-79	-47	0	0	-23	8
TN_3^-	-79	-42	35	7	-22	10
TN_3^+	-78	-44	35	9	-22	10
TN_4^-	-80	-37	0	3	-23	8
TN_4^+	-80	-40	0	4	-23	8

Under live load, bending and axial force are close to the results of the single-lane straight bridge. In straight bridges, under asymmetric loading, the asymmetric boundary conditions underneath the link slab increased the link slab torsion (M_{yy}). However, in skew bridges, under asymmetric loading, torsion develops irrespective of the support conditions. Under negative thermal gradient, bending and axial force are close to that of the straight bridge. Link slab torsion increases due to skew geometry irrespective of the support conditions. The twist of the link slab (M_{zz}) is obtained for only the lower and upper bounds of T_1 and T_3 cases where at least one support is restrained for translation while the bearing stiffness of other supports provides partial restraint. Under live load, maximum bending (M_{eff}) and axial force (F_{eff}) are calculated at segment 1 shown in Figure 4-11. Under negative thermal gradient, maximum bending (M_{eff}) is at the center segment (segment 3 in Figure 4-11).

4.3.2.2 Two Lane Skew Full Bridge Model

Bridge plans of S12-3 & 4 of 25042 are used to develop the 20° skew two-lane full bridge model. These bridges have seven Type III PCI girders on span two and three spaced at 76 in. (Figure 4-13 and Figure 4-14). Moment and axial forces are obtained at the centerline of the link slab directly over the pier centerline (section A-A of Figure 4-16).

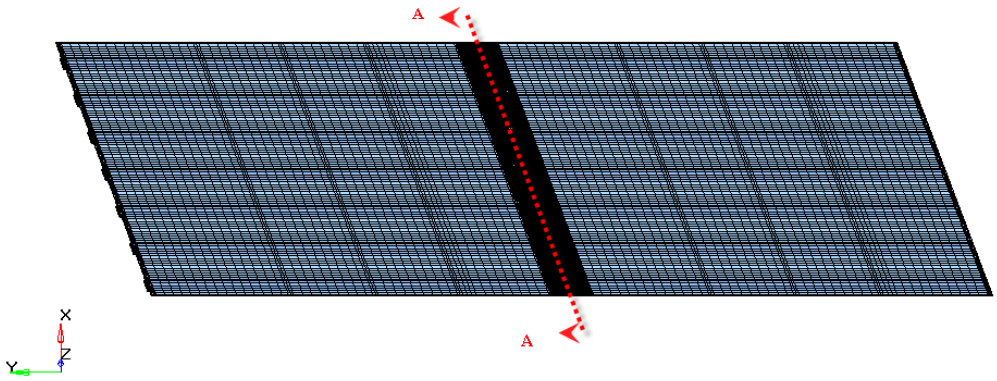

Figure 4-16. Top view of the 20° skew two lane bridge model and output section A-A

Moments about each coordinate axis (M_{xx}, M_{yy}, and M_{zz}) and axial force (N) in longitudinal (YY) direction are obtained at the link slab cross-section directly over the pier for full bridge width. Bending moments and axial force for the effective link slab width of 76 in. (M_{eff} and N_{eff}) are calculated. Analysis results are presented in presented in Table 4-28 and Table 4-29.

Table 4-28. Live Load Moments and Axial Forces at Link Slab Cross-Section and within Effective Width under Various Support Conditions for 20° Skew Two Lane Bridge

Case	Full Width				Effective Width	
	M_{xx} (Bending) ft-kips	M_{yy} (Torsion) ft-kips	M_{zz} (Twist) ft-kips	N (Axial load) Kips	M_{eff}* ft-kips	N_{eff}* kips
L_1	-148	-172	3	0	-42	-31
L_1^-	-167	-88	370	10	-40	-27
L_1^+	-162	-102	359	10	-40	-27
L_2	-30	-128	2220	534	-17	144
L_2^-	-29	-137	2272	537	-18	144
L_2^+	-28	-138	2269	533	-18	144
L_3	-156	-143	2	0	-41	35
L_3^-	-176	-68	594	21	-39	43
L_3^+	-164	-92	691	27	-39	45
L_4^-	-160	-118	135	4	-42	34
L_4^+	-155	-131	175	6	-42	34

Table 4-29. Negative Temperature Gradient Moments and Axial Forces at Link Slab Cross-Section and within Effective Width under Various Support Conditions for 20° Skew Two Lane Bridge

Case	Full Width				Effective Width	
	M_{xx} (Bending) ft-kips	M_{yy} (Torsion) ft-kips	M_{zz} (Twist) ft-kips	N (Axial load) kips	M_{eff}* ft-kips	N_{eff}* kips
TN_1	-125	-93	1	0	-26	7
TN_1^-	-129	-73	97	7	-26	8
TN_1^+	-128	-77	104	9	-26	9
TN_2	-91	-68	1	175	-20	37
TN_2^-	-90	-71	1	176	-20	38
TN_2^+	-90	-71	1	177	-20	38
TN_3	-125	-92	1	0	-26	8
TN_3^-	-125	-82	79	9	-26	10
TN_3^+	-124	-84	89	13	-26	10
TN_4^-	-127	-79	1	4	-26	2
TN_4^+	-126	-82	1	6	-26	9

Under live load, the maximum bending moment (M_{eff}) for segment 3 shows about a 5 kip-ft increase compared to that of the straight bridge. Axial force (N_{eff}) also increased from about 40 kips to 45 kips. The torsion of the link slab (M_{yy}) increased irrespective of the boundary conditions. Under negative thermal gradient loading, the bending moment and axial force are close to that of the straight bridge. The torsion of the link slab increased under negative thermal gradient load irrespective of the boundary conditions. Significant twist (M_{zz}) is calculated for the lower and upper bounds of T_1 and T_3 cases where at least one support is restrained for translation while the bearing stiffness of other supports provide partial restraint. Under negative thermal gradient, maximum bending moment and axial force occur at the center segment (segment 4 in Figure 4-14). Under live load, maximum bending occurs in segment 3 shown in Figure 4-14 whereas the highest axial load occurs in segment 1 for all the cases except L_2. Moment and axial force couples presented for effective width in Table 4-28 are for segment 3.

4.3.3 Summary and Conclusion of Full Bridge Analyses

FE analyses is carried out to evaluate the moment and force demand in the link slab due to longitudinally symmetric and transversely asymmetric live loads and negative thermal gradient acting on both straight and 20° skew single and two lane bridges. Results of moment and axial

force for live and negative thermal gradient loads calculated for effective flange width (M_{eff} and N_{eff}) of one and two-lane straight full bridge models are summarized in Table 4-30 and Table 4-31 respectively. Moment and axial force on effective width cross-sections (M_{eff} and N_{eff}) obtained from all the models (single girder, single lane straight, single lane skew, two lane straight, and two lane skew) are compared in Table 4-32 through Table 4-35.

Table 4-30. Moments and Axial Forces for Single Girder and Straight Full Bridge Models under Live Load

Case	Single girder		Single lane-straight		Two lane-straight	
	M(ft-k)	N(k)	M_{eff} (ft-k)	N_{eff} (k)	M_{eff} (ft-k)	N_{eff} (k)
L_1	-51	0	-32	2	-36	7
L_1^-	-50	1	-30	2	-35	9
L_1^+	-50	2	-30	0	-35	9
L_2	-19	159	-12	109	-13	101
L_2^-	-19	160	-12	112	-14	102
L_2^+	-19	159	-12	112	-13	101
L_3	-51	0	-32	2	-37	10
L_3^-	-50	6	-28	29	-35	8
L_3^+	-49	8	-28	32	-34	10
L_4^-	-50	1	-31	7	-36	-4
L_4^+	-50	2	-30	11	-36	-4

Table 4-31. Moments and Axial Forces for Single Girder and Straight Full Bridge Models under Negative Thermal Gradient Load

Case	Single girder		Single lane-straight		Two lane-straight	
	M(ft-k)	N(k)	M_{eff} (ft-k)	N_{eff} (k)	M_{eff} (ft-k)	N_{eff} (k)
TN_1	-18	0	-21	3	-25	7
TN_1^-	-18	1	-21	4	-25	8
TN_1^+	-18	1	-21	4	-25	8
TN_2	-13	25	-16	31	-19	38
TN_2^-	-13	25	-16	31	-19	37
TN_2^+	-13	26	-16	31	-19	38
TN_3	-18	0	-21	4	-25	8
TN_3^-	-18	1	-21	5	-25	9
TN_3^+	-18	2	-21	5	-24	10
TN_4^-	-18	1	-21	3	-25	7
TN_4^+	-18	1	-21	4	-25	7

Table 4-32. Moments and Axial Forces for Single Girder and Single Lane Straight and 20° Skew Full Bridge Models under Live Load

Case	Single girder		Single lane-straight		Single lane-skew	
	M(ft-k)	N(k)	M_{eff} (ft-k)	N_{eff} (k)	M_{eff} (ft-k)	N_{eff} (k)
L_1	-51	0	-32	2	-32	4
L_1^-	-50	1	-30	2	-30	6
L_1^+	-50	2	-30	0	-30	3
L_2	-19	159	-12	109	-12	110
L_2^-	-19	160	-12	112	-12	113
L_2^+	-19	159	-12	112	-12	113
L_3	-51	0	-32	2	-32	4
L_3^-	-50	6	-29	29	-28	24
L_3^+	-49	8	-28	32	-27	28
L_4^-	-50	1	-31	7	-32	5
L_4^+	-50	2	-31	11	-31	7

Table 4-33. Moments and Axial Forces for Single Girder and Single Lane Straight and 20° Skew Full Bridge Models under Negative Thermal Gradient Load

Case	Single girder		Single lane-straight		Single lane -skew	
	M(ft-k)	N(k)	M_{eff} (ft-k)	N_{eff} (k)	M_{eff} (ft-k)	N_{eff} (k)
TN_1	-18	0	-21	3	-23	7
TN_1^-	-18	1	-21	4	-23	8
TN_1^+	-18	1	-21	4	-23	9
TN_2	-13	25	-16	31	-17	37
TN_2^-	-13	25	-16	31	-17	37
TN_2^+	-13	26	-16	31	-17	37
TN_3	-18	0	-21	4	-23	8
TN_3^-	-18	1	-21	5	-22	10
TN_3^+	-18	2	-21	5	-22	10
TN_4^-	-18	1	-21	3	-23	8
TN_4^+	-18	1	-21	4	-23	8

Table 4-34. Moments and Axial Forces for Single Girder and Two Lane Straight and 20° Skew Full Bridge Models under Live Load

Case	Single girder		Two lane-straight		Two lane-skew	
	M(ft-k)	N(k)	M_{eff} (ft-k)	N_{eff} (k)	M_{eff} (ft-k)	N_{eff} (k)
L_1	-51	0	-36	7	-42	-31
L_1^-	-50	1	-35	9	-40	-27
L_1^+	-50	2	-35	9	-40	-27
L_2	-19	159	-13	101	-17	144
L_2^-	-19	160	-14	102	-18	144
L_2^+	-19	159	-14	101	-18	144
L_3	-51	0	-37	10	-41	35
L_3^-	-50	6	-35	8	-39	43
L_3^+	-49	8	-34	10	-39	45
L_4^-	-50	1	-36	-4	-42	34
L_4^+	-50	2	-36	-4	-42	34

Table 4-35. Moments and Axial Forces for Single Girder and Two Lane Straight and 20° Skew Full Bridge Models under Negative Thermal Gradient Load

Case	Single girder		Two lane-straight		Two lane - skew	
	M(ft-k)	N(k)	M_{eff} (ft-k)	N_{eff} (k)	M_{eff} (ft-k)	N_{eff} (k)
TN_1	-18	0	-25	7	-26	7
TN_1^-	-18	1	-25	8	-26	8
TN_1^+	-18	1	-25	8	-26	9
TN_2	-13	25	-19	38	-20	37
TN_2^-	-13	25	-19	37	-20	38
TN_2^+	-13	26	-19	38	-20	38
TN_3	-18	0	-25	8	-26	8
TN_3^-	-18	1	-25	9	-26	10
TN_3^+	-18	2	-24	10	-26	10
TN_4^-	-18	1	25	7	27	2
TN_4^+	-18	1	25	7	26	9

The full bridge link slab analysis results can be summarized as follows:

1. Under transversely asymmetric live load,
   (a) In straight bridges, link slab torsion (M_{yy}) increased when asymmetric boundary conditions exist underneath the link slab (e.g., RRHR).
   (b) In straight bridges, twisting moments (M_{zz}) increased as the restraint underneath the link slab increases (e.g., M_{zz} for RHHR is greater than that of RRHR).
   (d) In straight bridges, twisting moments of analysis cases L_4^+ and L_4^- (all expansion bearings with upper and lower bound stiffness) are of significant magnitude.
   (c) In skew bridges, link slab torsion increased irrespective of the support conditions.

2. Under negative thermal gradient loading, only link slab torsion increased irrespective of support conditions due to skew geometry. Twist occurred only with the lower and upper bounds of T_1 and T_3 load cases where at least one support of the bridge is restrained for translation and the bearing stiffness of other supports provide partial restraints.

3. Upper and lower bound bearing stiffness provided at the supports influenced link slab twist and torsion.

4. Link slab bending moments obtained from the single girder model are 26 – 32% greater than the effective width moments obtained from the two lane straight full bridge model (Table 4-30). The moment variation is due to two main factors. First, live load is not placed directly over a girder of the multi girder model. Second, the applied live loads per unit width are lower in the full bridge model due to application of uniform load only over the traffic lanes. Whereas, in the single girder model the effective flange width of 76 inches is fully loaded with the lane load.

5. Under negative thermal gradient, link slab bending moments of a single girder model are 33 – 46% less than the effective width moments of a two-lane straight full bridge model (Table 4-31).

6. Under live load, the link slab bending moment obtained from the single girder model is 5 – 22% less than the effective width moments obtained from the two-lane 20^0 skew full bridge model (Table 4-34).

7. Under negative thermal gradient, the link slab bending moment obtained from the single girder model is 44 – 54% less than the effective width moment obtained from the two-lane 20^0 skew full bridge model (Table 4-35).

8. Bending moments and axial forces obtained from skew full bridge models are generally greater than those obtained from straight full bridge models. Further investigation of skew bridges under uniform thermal loads is required.

9. Under negative thermal gradient, bending moment and axial force both increase with increased bridge width. This may be attributed to the presence of diaphragms plus the Poisson's effect in conjunction with bearing restraints.

5 FINITE ELEMENT MODELING AND ANALYSIS OF APPROACH SLAB AND ABUTMENT REGION

5.1 OVERVIEW

The objective of the analysis is for the realistic simulation of the structural system behavior under load at the approach slab and abutment region where the deck sliding over backwall (independent backwall) or backwall sliding over abutment (dependent backwall) design is implemented eliminating expansion joint over the abutment. The objective is also to evaluate the critical stress levels and locations with respect to the deck, backwall, abutment, approach slab, and sleeper slab. The overall goal is the development of new and verification of existing design details. The FE models are analyzed under live and thermal loads. Furthermore, moment and axial force demands at the critical sections as well as the bearing deformations under uniform thermal loads are presented.

Three dimensional single girder and multi-girder FE models are developed representing two major design categories: independent and dependent backwalls. As a first step, single girder assemblage models are developed. Two independent and four dependent backwall configurations are developed evaluating their comparative response under live and thermal loads. Differences in the FE models are: (1) location of the hinge connection between the deck and approach slab and (2) inclusion of an expanded polystyrene (EPS) layer over the backwall. The analytical model incorporates sliding surfaces with friction coefficients defined at contact interfaces where sliding would occur. The deformation demand on the bearings is calculated under uniform thermal loads. The backfill effect and sleeper slab rocking are incorporated into selected models. The effects of frozen bearing restraint and approach slab restraint due to frozen subgrade on structural system behavior are investigated. Multi-girder straight and 20^0 skew models are developed for three different backwall configurations. The objective of these models is to assess if single girder analysis provides sufficient accuracy for use in calculating design demands. Another important consideration included in the analysis is the approach slab torsion and twist due to asymmetric loading and skew.

The data extracted from the FE analyses of the approach slab region models include the nominal axial force and moments obtained for critical regions, as well as stresses, under various

combinations of dead, live, and thermal loading. Approach slab and deck section capacity is calculated for comparison purposes.

5.1.1 Moment and Axial Capacity of Approach Slab and Deck

Analysis results need to be assessed against capacities. For this purpose moment capacities of the deck and approach slab of a 9 in. thick 5000 psi concrete section with various rebar arrangements and a clear cover of 3 inches are calculated as shown in Table 5-1. The cracking moment (M_r) of the cross-section is calculated as 7.2 ft-kips/ft (assuming f_r =530 psi and $M_r = f_r.I_g/y$). Axial load capacity of the cross-section at the joint with continuous bottom reinforcement with various rebar arrangements using f_a =36 ksi, is shown in Table 5-2.

Table 5-1. Moment Capacity of Deck and Approach Slab for Unit Width

Bar spacing (both top and bottom)	Area of each layer (in^2)	Moment capacity (ft-kips/ft)
#6 @ 6 inches	0.88	30.5
#6 @ 8 inches	0.66	25.6
#6 @ 10 inches	0.53	21.9
#6 @ 12 inches	0.44	19.2

Table 5-2. Axial Load Capacity of Deck and Approach Slab for Unit Width

Bar spacing (bottom only)	Area of each layer (in^2)	Axial load capacity (kips/ft)
#6 @ 6 inches	0.88	31.7
#6 @ 8 inches	0.66	23.8
#6 @ 10 inches	0.53	19.1
#6 @ 12 inches	0.44	15.8

5.2 ASSEMBLAGE MODELS OF APPROACH SLAB AND ABUTMENT REGION

A single girder model that spans between the abutment and the first pier is developed for the effective flange width of the deck. Components incorporated into the model are approach slab, sleeper slab, and backwall. The width of the approach, sleeper, and backwall is equal to the effective flange width. The model is referred to as the "assemblage model of approach slab region" and represents the simplest analysis model of a straight or moderately skewed abutment region of a jointless bridge system.

One full span length is modeled for realistic representation of live load application and the restraints. PCI Type III girders with effective flange widths of 76 in. are used for both abutment

types using the geometrical properties of S12 of 25042 bridge with a girder span length of 69.5 ft (834 in.) (Figure 5-1). The compressive strength ($f_c^{'}$) of 5000 psi, modulus of elasticity of 4031 ksi, and Poisson's ratio of 0.2 are assumed for both deck and girder concrete. Elasticity modulus and Poisson's ratio of expanded polystyrene (EPS) are identified to be 0.2 ksi and 0.09 (Chun et al. 2003 and Gnip et al. 2007).

Independent and dependent backwall models are analyzed under live and uniform thermal loads. The MDOT Bridge Design Manual (2005) Section 7.01.07 provides a temperature range for determining the thermal forces and movements in conformance with AASHTO "cold climate" range. Uniform thermal load is calculated from AASHTO LRFD (2004) for both Procedures A and B and is applied to the composite girder-deck cross-section. Further details on this issue were described in the FE modeling and analysis of link slab region (Chapter 4). Procedures A and B temperature ranges, and positive and negative uniform temperature differences used in the finite element analysis were given in Table 4-10.

Independent backwall models include two sliding surfaces: (1) at the sleeper slab and approach slab interface and (2) at the expanded polystyrene and deck interface (Regions 1 and 2 in Figure 5-1a). Dependent backwall configurations include one additional sliding surface at the backwall and abutment interface (Region 5 in Figure 5-1b). In the dependent backwall model where deck and backwall are monolithic, expanded polystyrene between the backwall and deck is removed. Both configurations include a one-inch gap between the stub of sleeper slab and the end of approach slab to allow for expansion. The effect of various friction coefficients at sliding surfaces is analyzed under uniform thermal loads in conjunction with live and dead loads (Table 5-3).

Table 5-3. Friction Coefficients Utilized in Models under Uniform Thermal Load

Case	Independent backwall interfaces		Dependent backwall interfaces		
	Sleeper - Approach	Deck - EPS	Sleeper - Approach	Deck - EPS	Abutment – Steel plate
A_1	0	0	0	0	0
A_2	0	0.5	0	0.5	0.5
A_3	0	1	0	1	1
A_4	1	0	1	0	0
A_5	1	1	1	1	1

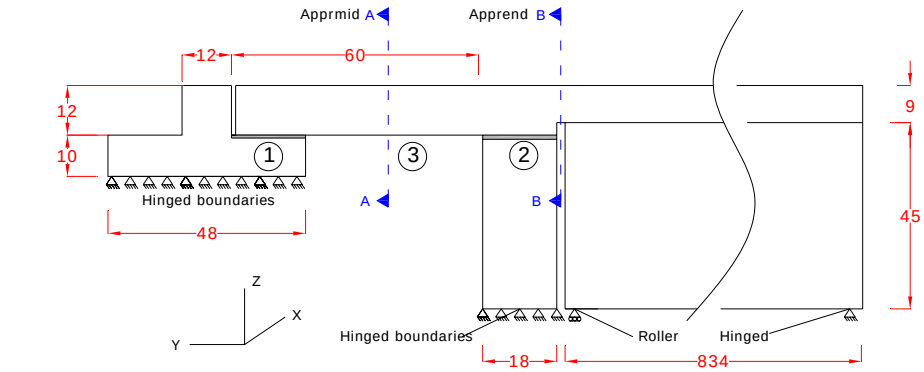

Note: all units are in inches

(a)

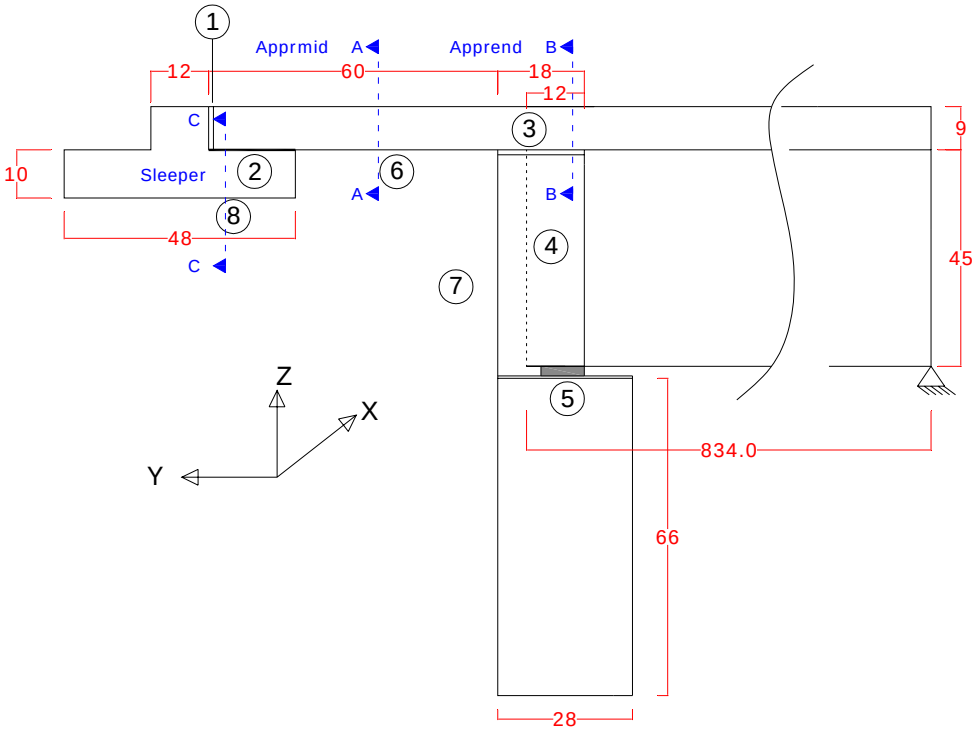

Note: all units are in inches

(b)

Figure 5-1. Elevations of assemblage model of approach slab region (a) independent backwall and (b) dependent backwall (not drawn to scale)

Section 3.6.1.3.3 of AASHTO LRFD (2004) requires using axle loads instead of wheel loads for slab design. According to Section 4.6.2.1 of AASHTO (2004), approximate methods of analysis in which the approach slab is subdivided into strips perpendicular to the supporting components

are considered acceptable when the slab span is less than 15 ft. Section 3.6.1.3.3 of AASHTO (2004) states that longitudinal primary strips should be designed for all loads specified including lane load. The total load on one design traffic lane is divided by the calculated strip width to obtain the load per unit width of the equivalent strip. In Table 4.6.2.1.3-1 of AASHTO (2004), the width of primary strip for a cast-in-place concrete slab is defined as;

$26.0 + 6.6S$ *(for positive moment)* (5-1)

$48.0 + 3.0S$ *(for negative moment)* (5-2)

Where, S is the spacing of supporting component in feet.

For both independent and dependent backwall configurations, the clear distance between the edge of the sleeper slab and backwall (S) is 43 inches (3.58 ft). The corresponding equivalent longitudinal strip width is calculated as 50 and 59 inches for the positive moment and negative moment, respectively.

The single girder analysis models were developed for the effective flange width of 76 inches. Changing the effective flange width from 76 inches to 50 or 59 inches for modeling the approach slab region is not practical due to three-dimensional effects. For this reason, the effective width of the approach slab is also kept at 76 inches. The truck and lane loads acting on the approach slab are prorated to account for the increase in effective width by a ratio of 76/50 (i.e., 1.52). The prorated lane load and truck (axle) loads are 0.97 k/ft and 48.64 kips (i.e., 1.52×0.64 k/ft and 1.52×32 kips), respectively. An impact factor of 1.33 is used in conjunction with wheel load as per AASHTO (2004) Section 3.6.1.2.3 and 3.6.2. Section 3.6.1.2.5 of AASHTO (2004) requires distributing wheel load over an area of 10×20 inches^2. In the model, wheel load is distributed over a 9 in. x 21 in. area considering FE mesh limitations. For cases where live load is acting on the approach slab and span, the middle axle of the HL-93 loading is placed on the approach slab so that the rear axle load could be placed 14 ft apart towards the span side to create maximum negative deck moment over the backwall.

The approach slab is supported by a compacted fill subgrade as well as the sleeper slab and the backwall. The worst case scenario is to assume that the subgrade backfill was settled such that the approach slab is only supported by the backwall and sleeper slab.

The MDOT Bridge Design Manual (2005) Section 7.03.01 specifies that abutment is designed for multiple load configurations. For the independent and dependent backwall assemblage models discussed in this report, the following load cases are considered:

CASE II: Bridge open to traffic with truck loading on the approach only.
CASE III: Bridge with traffic on it and no load on approach.
CASE IV: Contraction – Case II loading plus the effects of uniform negative thermal in the deck transmitted to the abutment. Expansion – for integral abutments Case IV instead assumes the Case III loading plus the effect of uniform positive thermal transmitted from the deck.

Two additional load cases other than those listed above are considered to investigate the critical load demands. The first load case is similar to Case II given in MDOT manual, and it considers truck loading on both the approach slab and adjacent span, referred to as Case II-B. The second load case is similar to Case IV in MDOT manual, and it includes negative thermal gradient instead of uniform thermal. This case is referred as Case IV-NG.

For all load combinations, except Case IV-NG, a load factor of 1.0 is used following AASHTO LRFD (2004) Service I criterion. Load Case IV-NG, where live load is applied in conjunction with the negative thermal gradient, a load factor of 0.5 is used for the negative thermal gradient load following AASHTO LRFD (2004) guidelines.

5.2.1 Single Girder Analysis Model for Independent Backwall Configuration

The independent backwall assemblage model shown in Figure 5-1a consists of deck, girder, approach slab, sleeper slab, backwall, EPS, and polyethylene components. Two different independent backwall details are investigated. The first detail is the current MDOT detail (MDOT Bridge Design Guide, 6.20.03.A) where deck and approach slab continuity is provided by the top continuous rebars. In the second detail, the deck and approach slab are detached, and continuity is provided with a hinge at a section aligned with the span side backwall face. The second detail prevents moment transfer from the span to approach slab, but shear and axial force are transferred (i.e. continuous bottom layer rebars). These two details will be referred to as "*continuous*" and "*detached*" independent backwall models, respectively.

A 1.5 in. gap is incorporated between the girder end and backwall. Girder end bearings over the abutment are modified-fixed (Figure 3-2), and far end support bearings are fixed. Modified-fixed bearings allow 0.875 inch displacement in either direction for expansion or contraction. The bottoms of the sleeper slab and backwall are modeled as fixed (Figure 5-1a).

Regions 1 (polyethylene) and 2 (EPS) in Figure 5-1a designate the two contact interfaces of the model. Different friction coefficients are specified to define the contact properties of the regions. Region 3 designates the aggregate base interface. The subgrade effect is neglected assuming no contact between the approach slab and backfill. Due to assumed subgrade settlements, the dead load of the approach slab is also incorporated into the analysis. If subgrade effects are considered, vertical and horizontal springs (friction between approach slab and aggregate base) can be incorporated restraining the movement. The approach slab with horizontal restraint due to subgrade friction is also analyzed and will be presented later in the report. However, analyses conducted by Oesterle et al. (2005) indicated that the horizontal forces in the approach slab from soil friction are minimal. Nominal moments and axial forces are calculated at two different sections (section A-A and B-B) for the case of '*continuous*' independent backwall configurations as shown in Figure 5-1a. For the case of '*detached*' configuration, no moment is requested at section B-B since hinges are assigned at that section.

The stresses and their variations are described within the components based on the coordinate convention of the 3-dimensional states of stress given in Figure 4-4(a). The sign convention for the description of resultant forces and moments are shown in Figure 4-4(b).

5.2.1.1 Approach Slab and Deck Region

The approach slab and approach slab-deck interface stresses and nominal moments and axial forces are calculated for the aforementioned load combinations.

Prior to analysis of Case II and IV load configurations, the maximum displacement demand at the bearings was calculated for positive and negative uniform thermal loads of Procedure B by analyzing the assemblage model with zero friction on all the sliding surfaces. The purpose of this analysis is to determine if the displacement reaches the bearing limitation of 0.875 inches. The analysis results indicated that the maximum displacement of the bearing under uniform thermal load of procedure B with minimum restraints at the interfaces is only 0.360 inches under

contraction and 0.211 inches under expansion. The total displacements are below 0.875 inches; hence, bearing is modeled as a roller for further analysis.

5.2.1.1.1 Case II: Live load on approach slab + dead load of approach slab

Under the combined effects of live load and dead load of the approach slab, localized stresses are expected at the approach slab mid-span. For the '*continuous*' configuration, the maximum compressive and the tensile stresses (stress YY) at the approach slab's mid span top and bottom fibers are 980 psi and 990 psi, respectively. These stresses increased to 1045 and 1052 psi when a deck-approach slab interface is hinged (Figure 5-2). The maximum nominal moment obtained at the mid-span of approach slab (apprmid) is 10.2 and 11.2 ft-kips/ft for '*continuous*' and '*detached*' independent backwall configurations, respectively. Under Case II loading changing friction coefficient effects of sliding surfaces is minimal. Nominal moment and axial force are presented in Table 5-4 and Table 5-5 for '*continuous*' and '*detached*' independent backwall configurations, respectively.

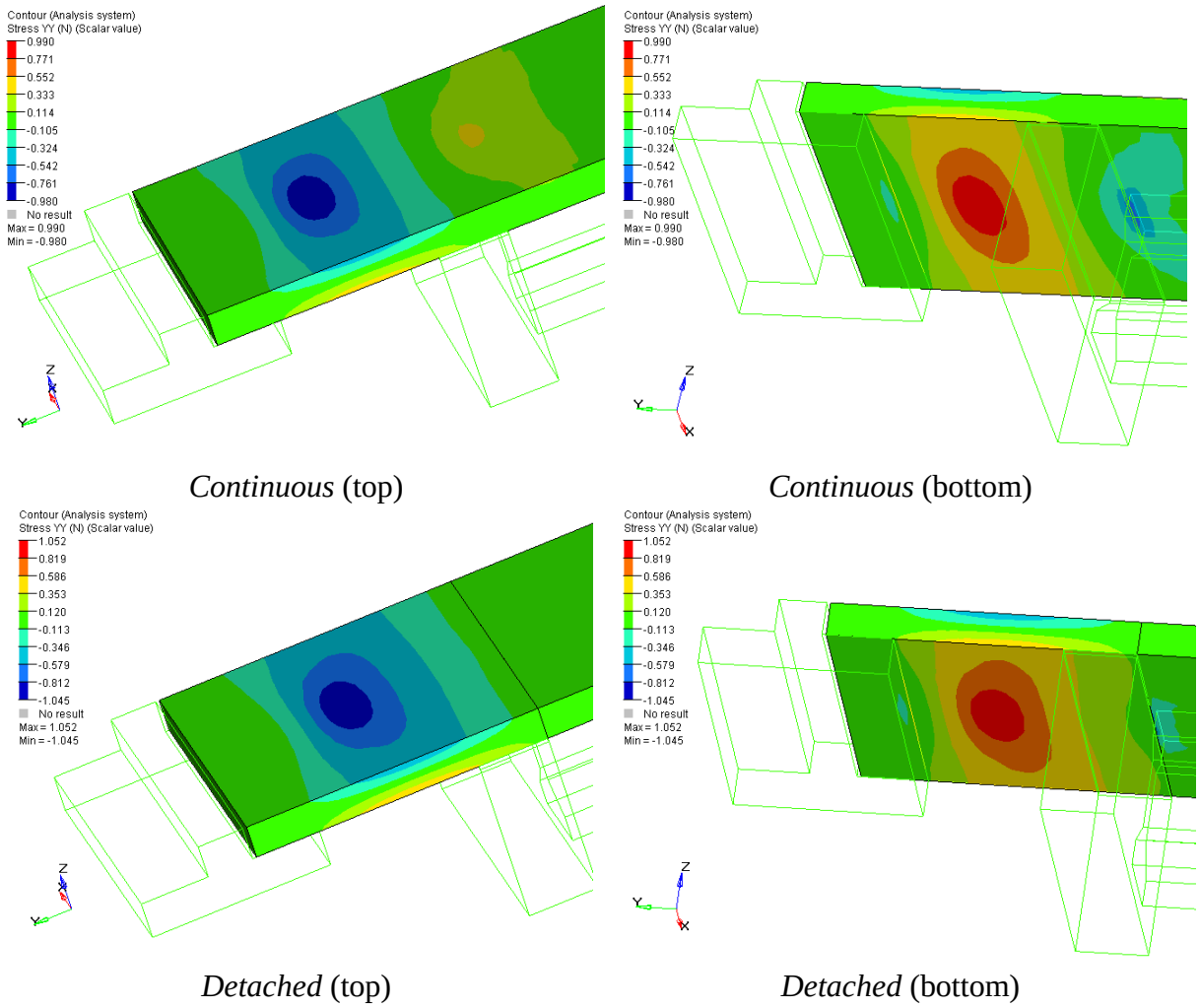

Continuous (top) *Continuous* (bottom)

Detached (top) *Detached* (bottom)

Figure 5-2. Stress YY under Case II loading (ksi)

5.2.1.1.2 Case II-B: Live load on approach slab and span + dead load of approach slab

This load case is investigated for the '*continuous*' configuration only since hinge connection will not allow moment transfer between the deck and approach slab. Under a live load acting on the approach slab and adjacent span plus a dead load on the approach slab, localized stresses occur at the deck near the backwall. With zero friction on the sliding surfaces, maximum tensile and compressive stresses at the top and bottom fibers of the approach slab's mid section are 905 psi and 1540 psi, respectively (Figure 5-3). The maximum nominal moment at the approach slab's mid-span, "apprmid" (section A-A), is 8.1 ft-kips/ft. A nominal moment of -8.8 ft-kips/ft is obtained at the deck section over the backwall (section B-B: "apprend"). Under Case II-B loading, the impact of changing friction at the interfaces is minimal. Nominal moment and axial force are presented in Table 5-4.

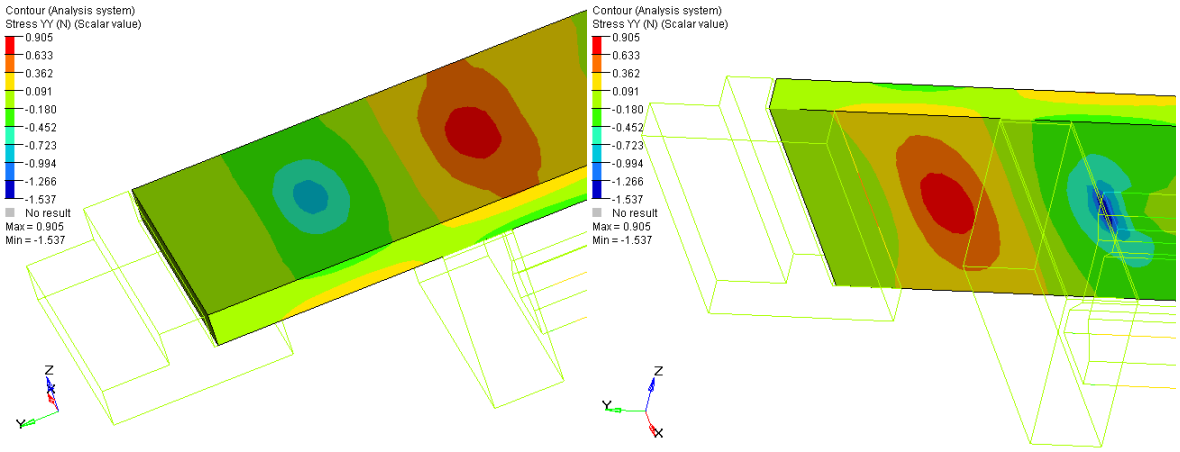

Figure 5-3. Stress YY under Case II-B loading (ksi)

5.2.1.1.3 Case IV-A and Case IV-B: Live load on approach slab + dead load of approach slab + Procedure A or Procedure B negative uniform thermal load

Under combined live, dead, and Procedure A negative uniform thermal loading with zero interface friction (A_1), normal stress (YY) contours are shown in Figure 5-4. Nominal moment and axial force under various friction interfaces are presented in Table 5-4 and Table 5-5. Stresses and moment resultants at "apprmid" (section A-A) increased in the '*detached*' configuration compared to that of '*continuous*' configuration.

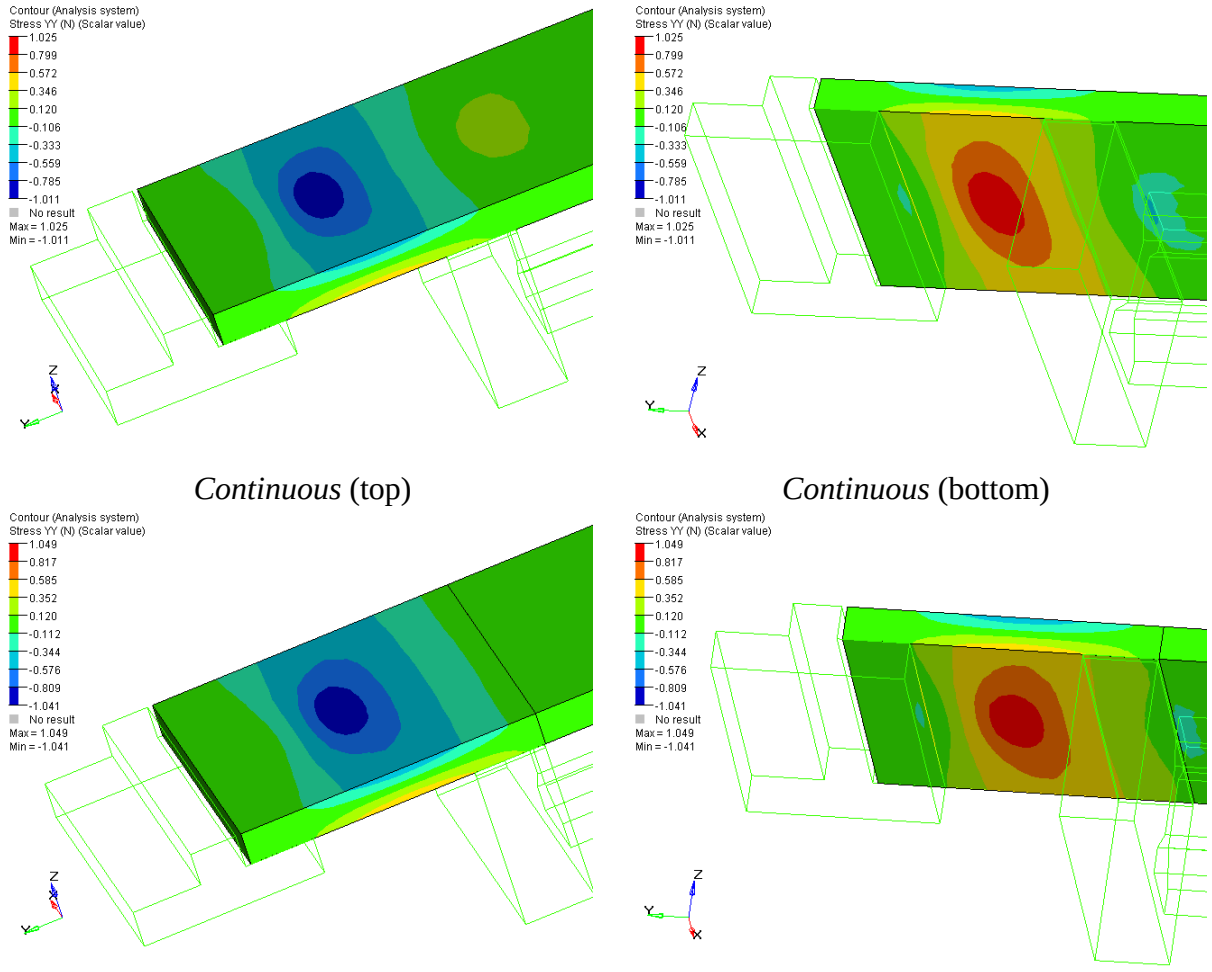

Continuous (top) *Continuous* (bottom)

Detached (top) *Detached* (bottom)

Figure 5-4. Stress YY developed under Case IV-A loading (ksi)

5.2.1.1.4 Case IV-NG: Live load on approach slab + dead load of approach slab + negative thermal gradient load

Under combined live, dead, and negative thermal gradient loading with zero interface friction, stresses at the approach slab-deck interface over the backwall are between 925 psi and 550 psi. Normal stress (YY) contours for the zero interface friction (A_1) are presented in Figure 5-5. Nominal moment and axial force under various friction interfaces are presented in Table 5-4.

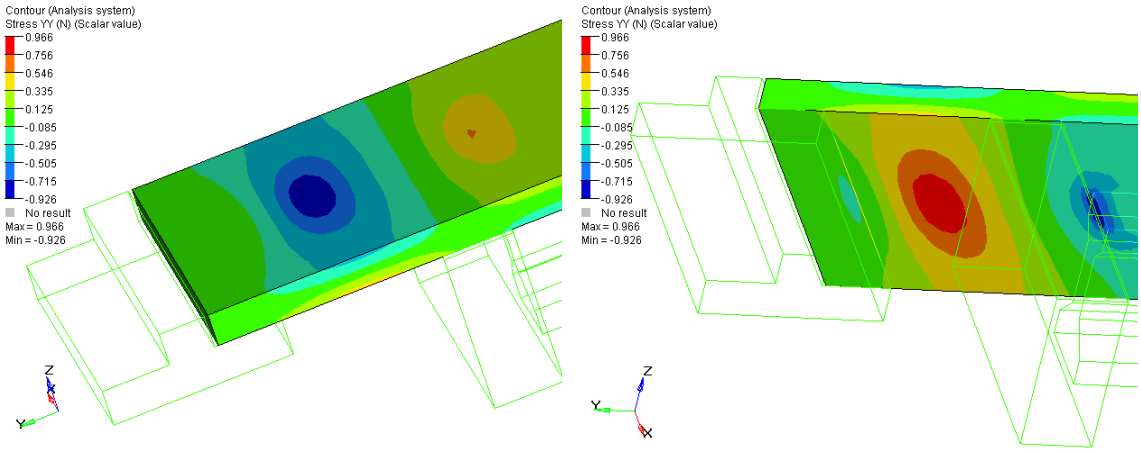

Figure 5-5. Stress YY developed under Case IV-NG loading, top and bottom views respectively (ksi)

Table 5-4. Nominal Moment and Axial Force for '*Continuous*' Independent Backwall Configuration under Various Loading with Different Friction Coefficient at Interfaces

Section	Analysis Case	Case II Loading		Case II-B Loading	
		M (ft-k/ft)	N (k/ft)	M (ft-k/ft)	N (k/ft)
Apprmid	A_1	10.2	0.0	8.1	0.0
	A_2	10.2	0.0	8.1	0.0
	A_3	10.2	0.0	8.1	0.0
	A_4	10.0	-0.7	7.4	3.1
	A_5	10.0	-0.7	7.5	3.0
Apprend	A_1	-2.8	0.0	-8.8	0.0
	A_2	-2.8	0.0	-8.8	0.0
	A_3	-2.8	0.0	-8.8	0.1
	A_4	-2.7	-0.7	-8.5	3.1
	A_5	-2.7	-0.7	-8.6	3.1

Section	Analysis Case	Case IV-A Loading		Case IV-B Loading		Case IV-NG Loading	
		M (ft-k/ft)	N (k/ft)	M (ft-k/ft)	N (k/ft)	M (ft-k/ft)	N (k/ft)
Apprmid	A_1	10.7	0.0	10.8	0.0	9.5	0.0
	A_2	10.6	0.0	10.7	0.0	9.5	0.0
	A_3	10.6	0.0	10.6	0.0	9.5	0.0
	A_4	12.0	6.6	12.1	6.7	9.5	0.0
	A_5	11.9	6.6	12.0	6.6	9.5	0.0
Apprend	A_1	-1.2	0.0	-0.9	0.0	-4.8	0.0
	A_2	-1.1	0.5	-0.9	0.6	-4.8	0.0
	A_3	-1.1	1.0	-0.8	1.1	-4.8	0.0
	A_4	-1.8	6.6	-1.5	6.7	-4.8	0.0
	A_5	-1.7	7.7	-1.4	7.8	-4.8	0.1

Table 5-5. Nominal Moment and Axial Force for '*Detached*' Independent Backwall Configuration under Various Loading with Different Friction Coefficient at Interfaces

Section	Analysis Case	Case II Loading		Case IV-A Loading		Case IV-B Loading	
		M (ft-k/ft)	N (k/ft)	M (ft-k/ft)	N (k/ft)	M (ft-k/ft)	N (k/ft)
Apprmid	A_1	11.2	0.0	11.1	0.0	11.1	0.0
	A_2	11.2	0.0	11.1	0.0	11.1	0.0
	A_3	11.2	0.0	11.1	0.0	11.1	0.0
	A_4	10.8	-1.1	13.6	7.3	13.6	7.3
	A_5	10.8	-1.1	13.5	7.3	13.5	7.3

When Case II loading is applied on the '*continuous*' system, the changing friction coefficient at the interface did not affect deck and approach slab stresses. There is slight influence of friction coefficient under Case II-B loading due to a minute interface slip under span loading. Under Case II-B loading of the approach slab mid-span moments decreased by around 20% due to continuity of the deck over the backwall; however, approach slab end moments ('*apprend*') increased from -2.8 ft-kips/ft to -8.8 ft-kips/ft.

Under Case IV-A loading, approach slab mid section moments of the '*continuous*' system are increased for all analysis cases while approach end moments are decreased compared to Case II loading. Axial forces are increased due to interface friction. When negative thermal gradient loading (Case IV-NG) is applied, approach slab mid-span moments are decreased while end moments are increased. The behavior is similar to that of Case II-B loading since negative thermal gradient generates stresses similar to live load.

In the '*detached*' independent backwall configuration, approach slab mid-span moments and stresses increase, but the stresses at the deck over the backwall are eliminated. Thus, the '*detached*' configuration is preferred over the '*continuous*' detail. The hinge detail can be obtained by providing continuous rebars at the bottom layer in conjunction with a construction joint.

5.2.1.1.5 Approach Slab Subgrade and Bearing Restraints

Restraint effects that may stem from frozen approach slab subgrade or bearings are incorporated by modifying existing models. The models are modified by placing a link between the approach slab and aggregate base or bearing and abutment contact surfaces with a threshold limit so that

their relative motion is prevented until the threshold value was reached. Once the threshold limit is achieved, the approach slab and backwall will now slide with regular tangential contact interactions with or without friction. The ultimate response of the assemblage with or without threshold limit will be the same unless failure initiates while the restrains are active. While the approach slab and subgrade are tied together, displacement against the time plot of an approach slab node coinciding with the subgrade node is represented by the solid curve in Figure 5-6. Once the threshold is achieved at time t, the approach slab is no longer tied to the subgrade and will resume response with diminished restraint forces (dashed curve in Figure 5-6).

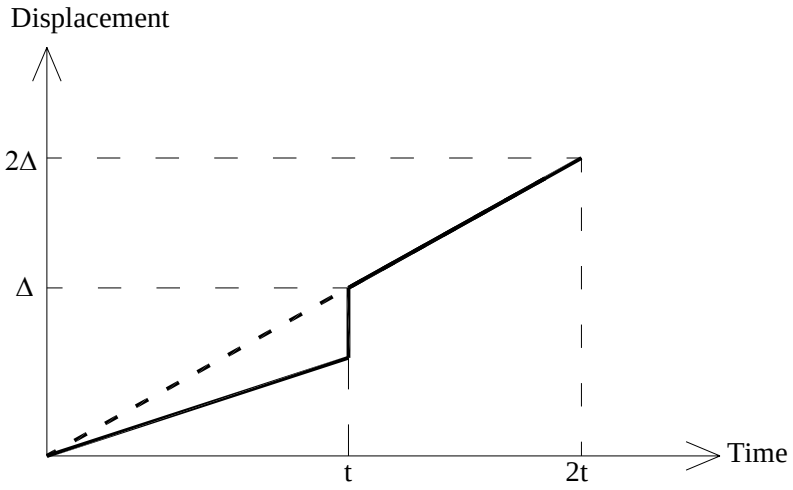

Figure 5-6. Displacement vs time plot of an approach slab node coinciding with a subgrade node

The level of restraint, either by approach slab subgrade or by bearings, may generate critical load demands within the approach slab that may exceed section capacity. Documentation of such failures was not found in the literature.

5.2.2 Single Girder Analysis Model for Dependent Backwall Configurations

The dependent backwall assemblage model includes the abutment, sleeper slab, approach slab, backwall, deck, and the girder (Figure 5-1b). Four different dependent backwall configurations are investigated. All four configurations have similar details as shown in Figure 5-1b. The differences are within the monolithic deck-backwall connection at region 3. In all configurations, the girder is embedded 12 inches into the backwall (Figure 5-1b). Interface regions (2, 3, and 5) utilize contact elements for sliding surfaces. Nominal moments and axial

force are obtained at three different sections: Section A-A *(Apprmid)*, B-B *(Apprend)*, and C-C *(Sleeper)* (Figure 5-1b), where applicable.

Other common features of each configuration are as follows: in region 1, a one-inch gap is left for expansion; in region 2, contact elements are placed to model the movement of the approach slab over the sleeper slab (polyethylene layer). According to the plans, there is no detail incorporated to prevent the uplift of the approach slab over the sleeper slab. Hence, in the model, the approach slab is allowed to separate from the sleeper slab. Region 3 modeling depends on the specific configuration being investigated.

In practice, girders are tied to the backwall by means of a series of 0.5-inch diameter bars in one-inch diameter holes (MDOT 2003a 6.20.01). In integral and semi-integral abutment details, according to MDOT Bridge Design Guide 6.20.04A (2003a), dowel bars are grouted prior to casting the backwall. Effectively, in region 4, the girder and backwall are pinned, and any relative motion between the girder and backwall is prevented. With the bars placed at the web, girder rotation with respect to the backwall is allowed.

Region 5 modeling does not necessitate using special elements to describe modified-fixed bearings. Plans of S12 of 25042 show modified-fixed bearings provide 0.875-inch translation (Figure 3-2). Preliminary analyses showed that, with the specified geometrical and material properties, critical expansion length to exceed the bearing displacement limit would be 167 ft. In the current model, with only single spans of 69.5 ft, the allowable translation limit will not be exceeded. The girder-backwall combined system and the abutment interface, which is region 5, was represented by contact interfaces. Two different contact interfaces are defined within region 5 (Figure 5-1b), between: (1) the bearing plate and abutment and (2) the backwall and abutment. Different friction coefficients are applied only for the bearing plate and abutment region; the backwall-abutment interface is always assumed to slide freely.

Region 6 denotes the approach slab subgrade area. Subgrade support of the approach slab is neglected in order to simulate the worst-case scenario as was discussed in the case of the independent backwall model. If subgrade effects are incorporated, vertical springs will reduce approach slab stresses under live load, but horizontal springs (threshold friction between approach slab and aggregate base) can restrain the translations. However, analyses conducted by

Oesterle et al. (2005) indicated that the horizontal forces in the approach slab from soil friction are minimal. Aggregate base restraints are not investigated for the dependent backwall configuration since results would be similar to that of independent backwall configurations, where horizontal restraints did not cause any distress.

Region 7 represents the backfill. Although the upper (12 in. high) portion behind the backwall is backfilled with different grading, this effect is neglected, and the backfill is modeled assuming uniform backfill properties throughout. Springs are assigned representing the stiffness properties of the backfill. Stiffness values can be modified, if needed, to represent the effect of different backfill grading.

Hinge supports are placed underneath the sleeper slab (region 8); hence the sleeper slab will not be allowed to rock. The effects of sleeper slab rocking on approach slab stresses are investigated separately.

Four different dependent backwall configurations are investigated. The first dependent backwall configuration represents currently utilized retrofit detail. This detail was utilized in all the inspected retrofitted bridges, but was not found in the MDOT bridge design guides. In this detail, the deck and approach slab are continuous and slide over the backwall. The backwall is isolated from the deck by an inch thick EPS layer (Figure 5-7a). In region 3 of Figure 5-1b, an inch thick EPS layer is added between the backwall and deck to provide the sliding surface between the deck and the backwall. As discussed earlier, expanded polystyrene in the model is assigned a modulus of elasticity of 0.2 ksi and a Poisson's ratio of 0.09 (Chun et al. 2003; Gnip et al. 2007). This configuration is referred to as "*EPS 1*" in analysis cases. The second dependent backwall configuration utilizes a construction joint on the approach slab beyond the projection of the span side backwall face. To model this configuration, the deck and approach slab are detached, and continuity is provided by a hinge connection between the deck and the approach slab and aligned with span side backwall face. This configuration is referred as "*EPS 2*" in analysis cases (Figure 5-7b).

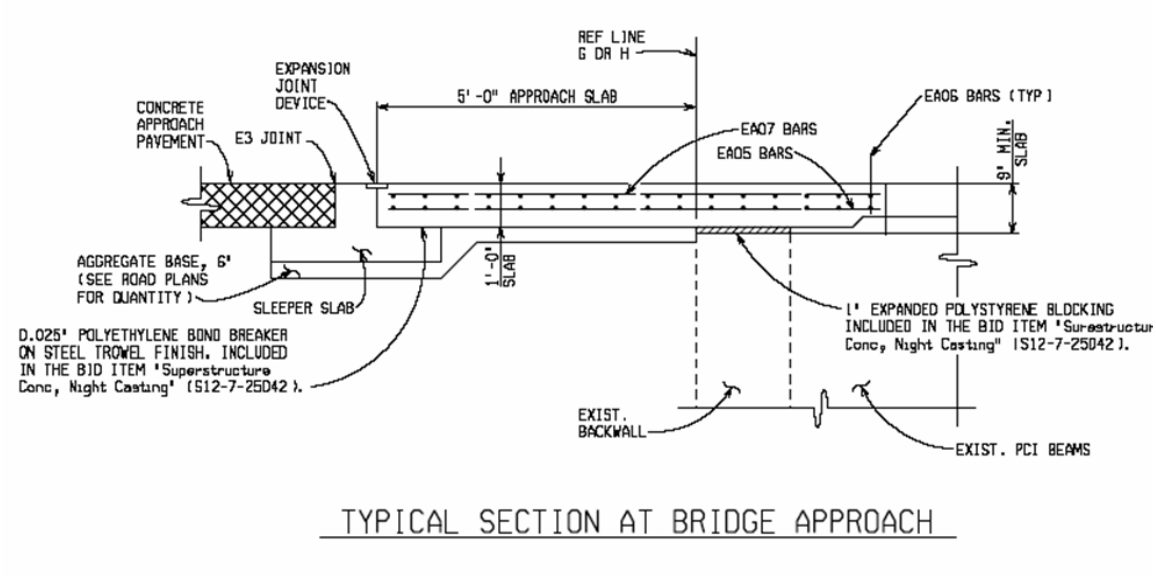

(a)

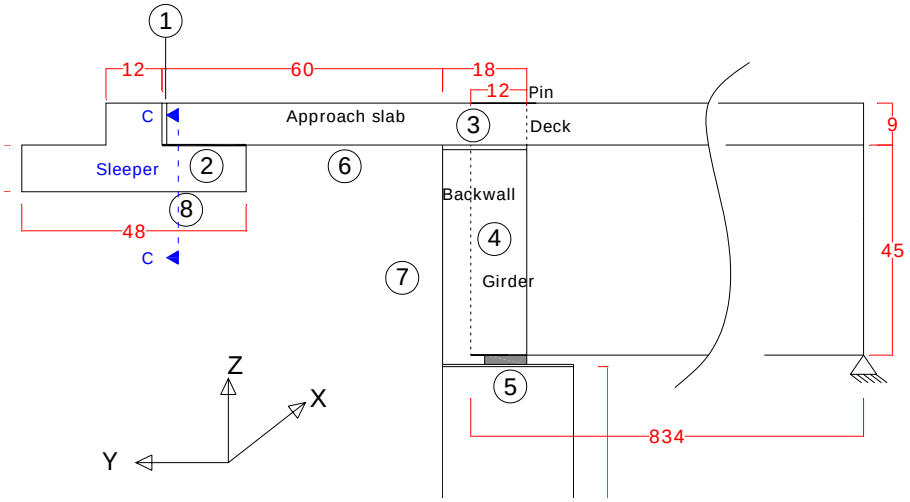

(b)

Figure 5-7. (a) *EPS 1* and (b) *EPS 2* dependent backwall configurations

The third dependent backwall configuration is similar to the current MDOT new construction detail included in the guide. In this configuration, the EPS layer is removed, and the deck and backwall components are monolithic; continuity between the deck and the approach slab is provided by a hinge connection aligned with the approach side backwall face (Figure 5-8-a). This configuration is referred as "*monolithic 1*". In the fourth configuration, the approach slab and backwall components are monolithic without the EPS layer, and the continuity between the deck and the approach slab is provided through a hinge at a cross-section aligned with the span side backwall face (Figure 5-8-b). This configuration is referred as "*monolithic 2*".

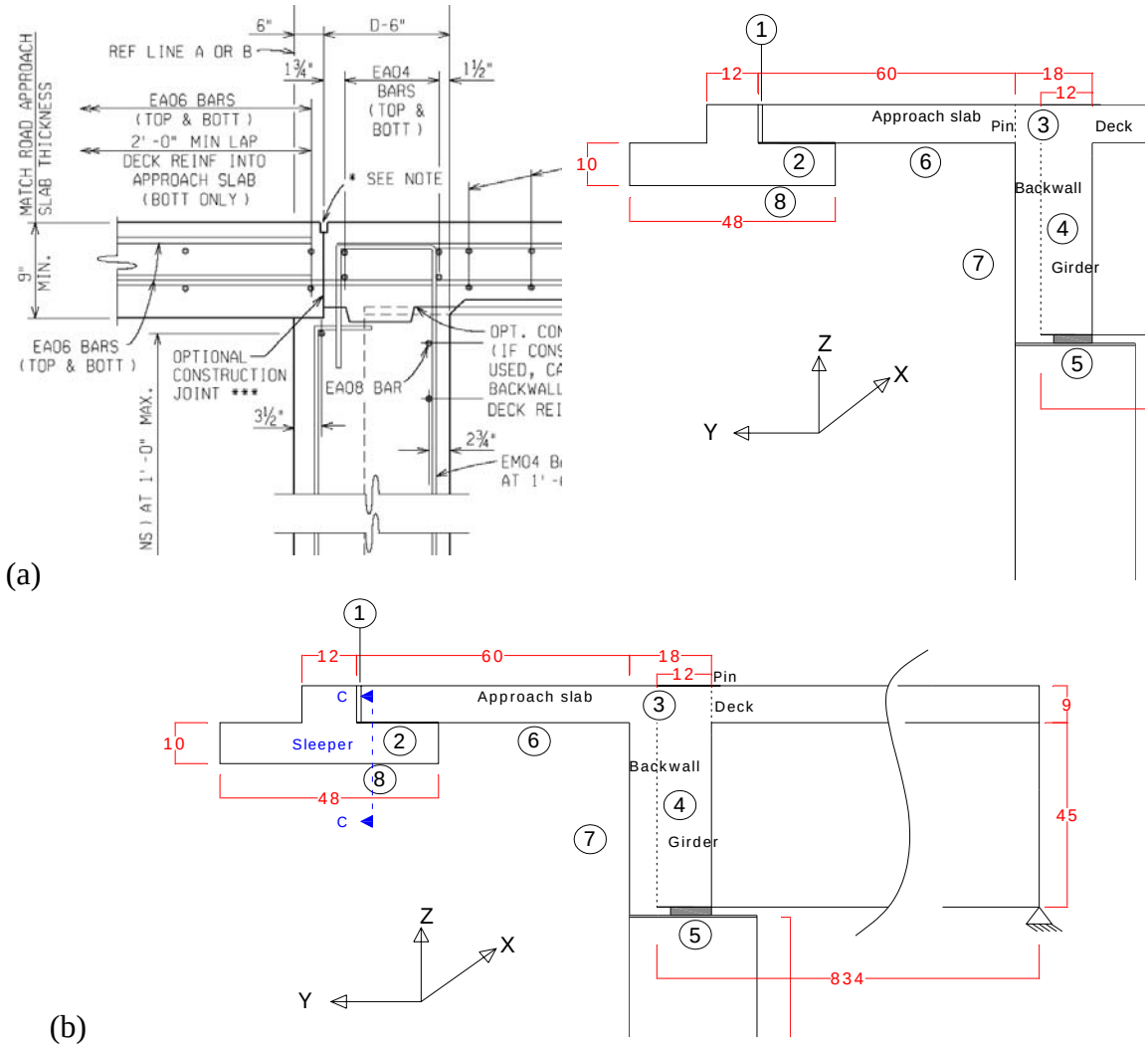

Figure 5-8. (a) *Monolithic 1* (b) *Monolithic 2* dependent backwall configurations

5.2.2.1 Approach Slab and Deck Region

Moments and axial force developed in the approach slab and the deck are investigated with and without backfill effects under the aforementioned load combinations. Backfill is incorporated into the models using springs. The lateral earth pressure distribution and the calculation of spring stiffness using available data from literature are presented in the following section.

5.2.2.1.1 Modeling of backfill effects

The ratio of effective horizontal normal stress (σ'_x) to effective vertical normal stress (σ'_z) of a soil mass is presented as;

$$K=\sigma'_x / \sigma'_z \qquad (5\text{-}3)$$

Where, K is the coefficient of lateral earth pressure and may be selected depending on the degree of wall movement. Horizontal earth pressure distribution is triangular when lateral earth pressure coefficient (K) is a constant. The resultant force of the earth pressure distribution is at H/3 above the base of the wall and magnitude is expressed as:

$$F = \frac{1}{2} K\gamma H^2 \qquad (5\text{-}4)$$

Where, γ is the unit weight of the soil, and H is the abutment height.

The lateral earth pressure variation will be nonlinear if there is wall rotation about the base and cannot be represented with a triangular distribution (Faraji et al. 2001). In order to estimate these nonlinear force-deformation effects behind the abutment and backwall, a chart developed by Clough and Duncan (1971) is utilized as shown in Figure 5-9. This chart was developed for loose, medium-dense, and dense-cohesionless granular materials and available through Clough and Duncan (1991) and NCHRP 343 (1991).

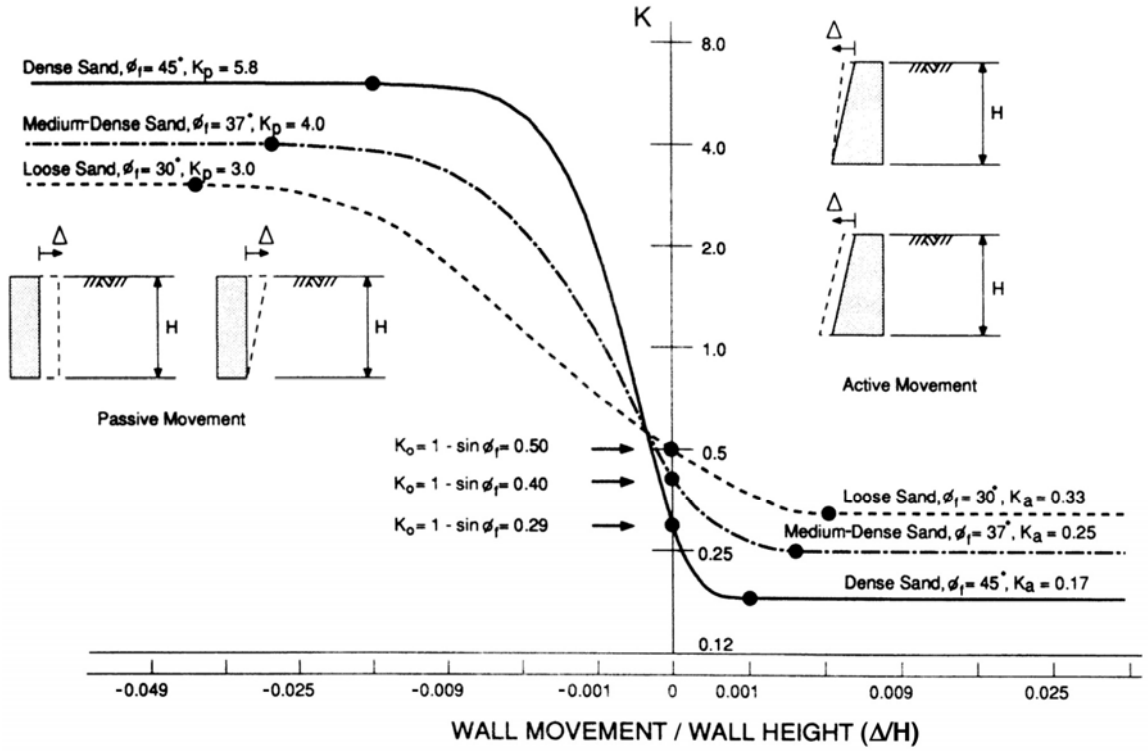

Figure 5-9. Relationship between wall movement and earth pressure (Clough and Duncan 1991)

For uniform density dry soil, vertical effective normal stress (σ'_z) is calculated from:

$$\sigma'_z = \gamma z \qquad (5\text{-}5)$$

Where, γ is the dry density of soil (90 lb/ft^3 (NCHRP-343 1991), and z is the depth from ground surface.

By using Eq. 5-3 and Eq. 5-5, effective horizontal normal stress (σ'_x) can be written as,

$$\sigma'_x = K\gamma z \qquad (5\text{-}6)$$

The effective soil stiffness behind the abutment wall is calculated by multiplying the tributary area of each node with the lateral earth pressure. Multiple force-deflection curves are calculated for elements at different heights, since each node line will have a different height along the axis (z). The Δ/H values are multiplied with the wall height to obtain the specific non-linear force-deflection curve for that node level. Considering backwall rocking, backfill earth pressure distribution along the height of the backwall and abutment wall is represented with a second order shape of which the magnitude varies with deflection (Figure 5-10).

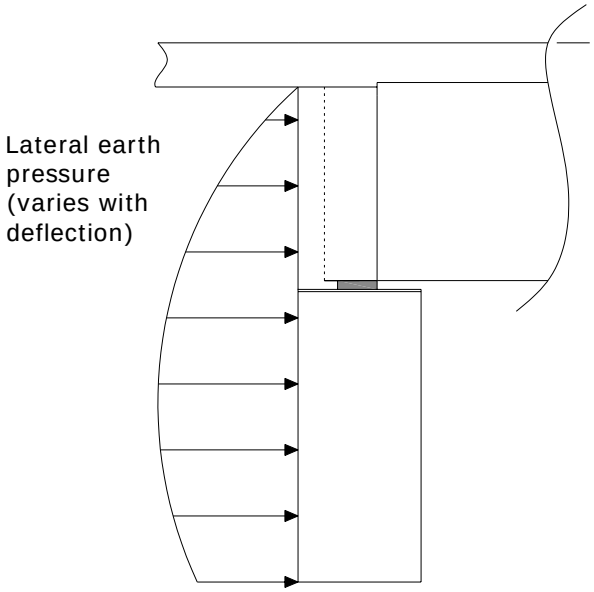

Figure 5-10. Lateral soil pressure distribution along the height of backwall and abutment wall

Under positive uniform thermal load, backfill resistance on the backwall increases with increasing displacement until backfill stiffness reaches a specified value. Beyond the specified value, the backfill stiffness remains constant (Figure 5-11 positive displacement). Under negative uniform thermal loads, the backfill resistance is minimal and remains constant following a small displacement (Figure 5-11 negative displacement).

The analysis is performed under uniform thermal loads calculated from Procedure A and B and without interface friction. Resulting earth pressure due to backwall movement is calculated from the girder end displacements as given in Figure 5-11. For the earth pressure maximum effects, displacement under Procedure B positive uniform thermal load is used. Greater positive displacements in conjunction with higher K values increase backfill pressure on the backwall as depicted on Figure 5-11. Under negative uniform thermal load, Procedure A is more critical since the K value decreases with increased contracting displacements Figure 5-11.

Table 5-6. Girder End Displacements under Uniform Thermal Loads

Case	Uniform Positive Thermal	Uniform Negative Thermal
Procedure A	0.084	-0.315
Procedure B	0.205	-0.365

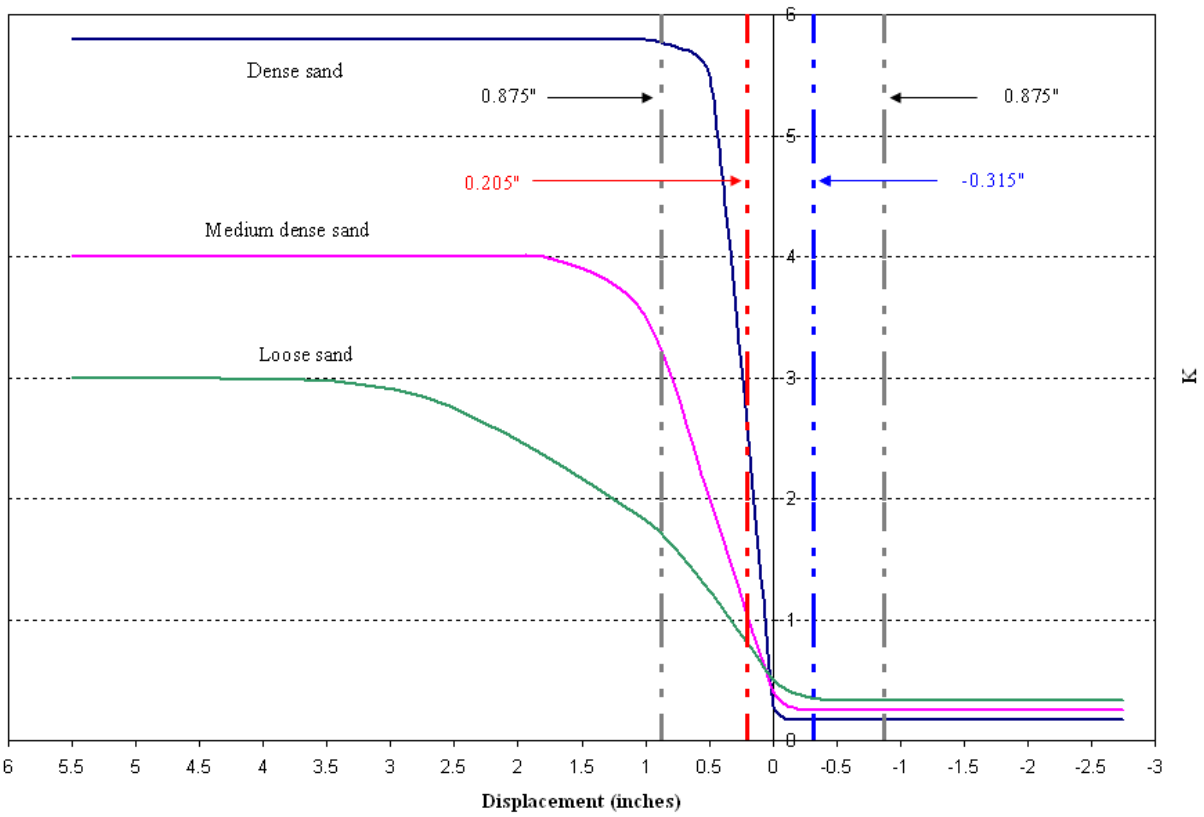

Figure 5-11. Relationship between displacement and lateral earth pressure coefficient (K)

5.2.2.1.2 Case II: Live load on approach slab + dead load of approach slab

Moments and axial force are obtained for dependent backwall cases. High stresses are concentrated at the approach slab mid-span (Figure 5-12 and Figure 5-13). A nominal moment of -2.8 ft-kips/ft is calculated at the deck section over the backwall (section B-B: apprend) for *EPS 1* analysis model (Table 5-7). The maximum nominal moment at the approach slab mid-span, "apprmid" (section A-A), of *EPS 2* analysis model is 11.2 ft-kips/ft.

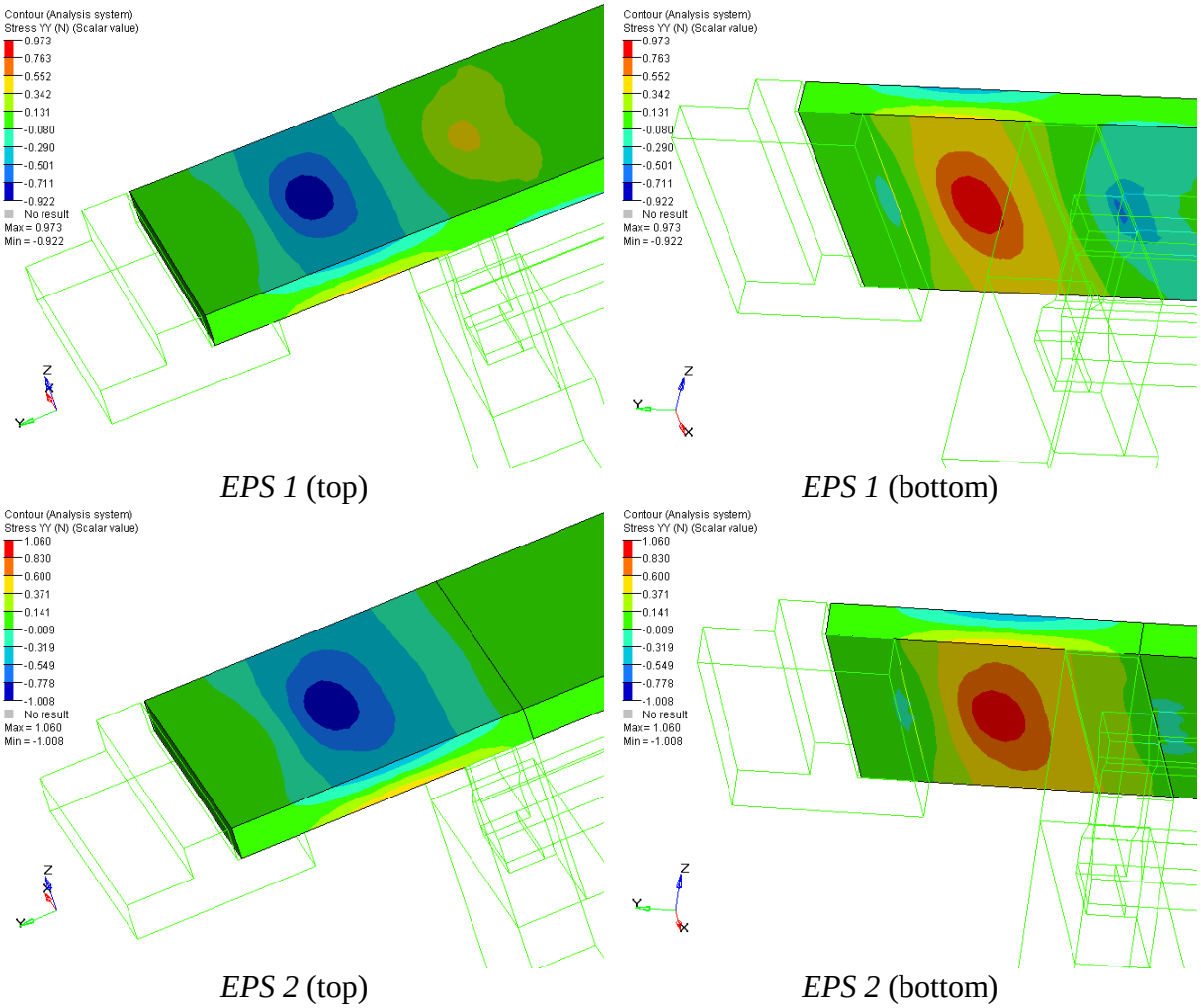

EPS 1 (top) *EPS 1* (bottom)

EPS 2 (top) *EPS 2* (bottom)

Figure 5-12. Stress YY developed under Case II loading – *EPS 1* and *EPS 2* configurations (ksi)

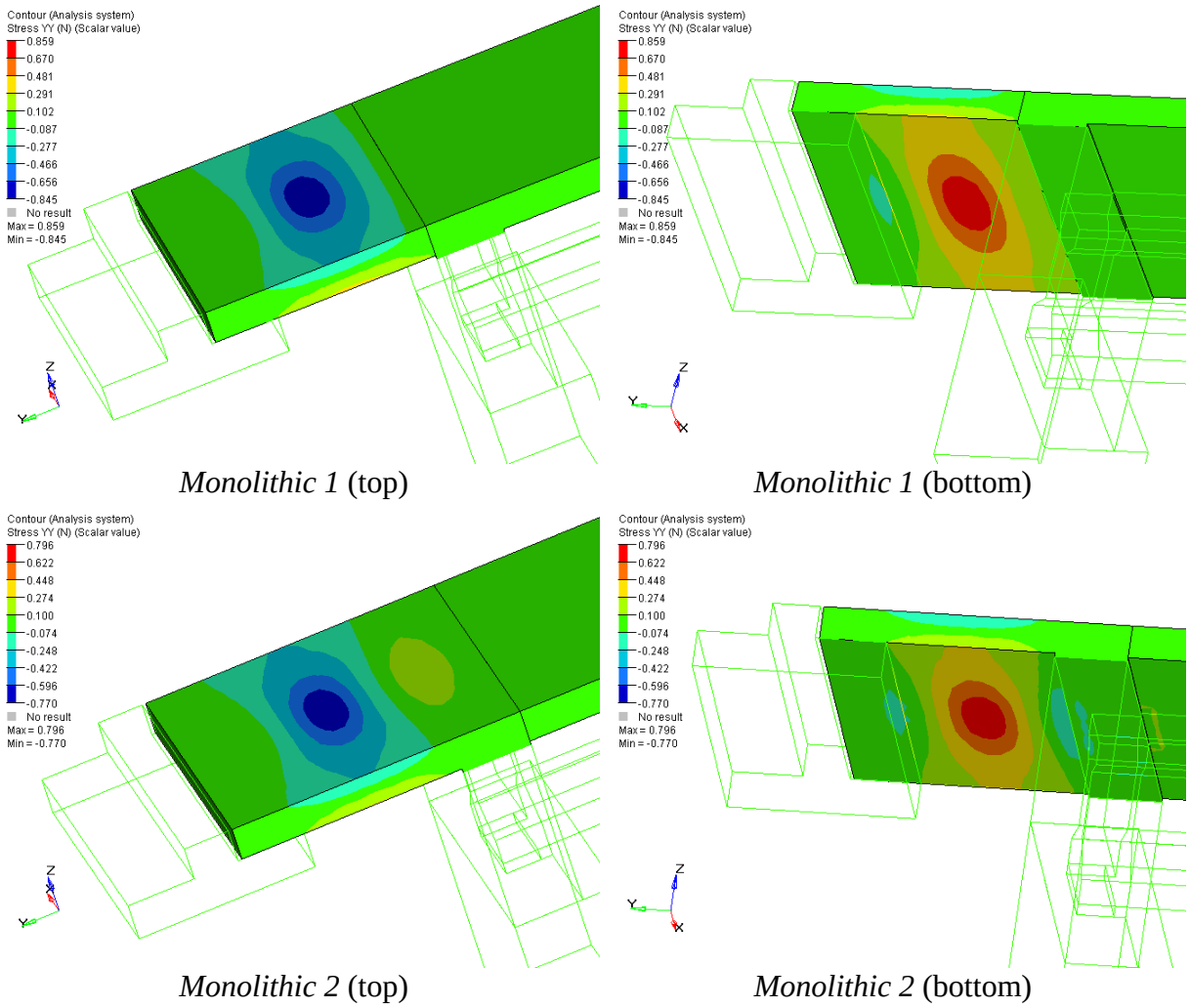

Figure 5-13. Stress YY under Case II loading – *Monolithic 1* and *2* configurations (ksi)

Table 5-7. Nominal Moment and Axial Force under Case II Loading with Different Friction Coefficient at Interfaces

Section	Analysis Case	EPS 1		EPS 2		Monolithic 1		Monolithic 2	
		M (ft-k/ft)	N (k/ft)	M (ft-k/ft)	N (k/ft)	M (ft-k/ft)	N (k/ft)	M (ft-k/ft)	N (k/ft)
Apprmid	A_1	9.8	0.0	11.2	0.0	8.4	0.0	7.4	0.0
	A_2	9.8	0.0	11.2	0.0	8.4	0.0	7.4	0.0
	A_3	9.8	0.0	11.2	0.0	8.4	0.0	7.4	0.0
	A_4	9.7	-0.8	10.8	-1.2	8.2	-0.6	7.3	-0.5
	A_5	9.7	-0.8	10.8	-1.2	8.2	-0.6	7.3	-0.5
Apprend	A_1	-2.8	0.0	0.9	0.0				
	A_2	-2.8	0.0	0.9	0.0				
	A_3	-2.8	0.0	0.9	0.0				
	A_4	-2.8	-0.8	0.6	-1.2				
	A_5	-2.8	-0.8	0.5	-1.2				

5.2.2.1.3 Case II-B: Live load on approach slab and span + dead load of approach slab

Under Case II-B loading, with the wheel load on the span, interface friction coefficient effects became more prominent. For the *EPS 1* backwall configuration, the maximum tensile stress of 843 psi, and compressive stress of -1153 psi are obtained at the approach slab section above the backwall. Top and bottom fiber compressive and tensile stresses developed at the approach slab mid-span section of *EPS 2* configuration are -1000 psi and 1053 psi, respectively. The maximum nominal moment calculated at the approach slab mid-span (section A-A: "apprmid") is 11.1 ft-kips/ft under *EPS 2* configuration. A nominal moment of -8.0 ft-kips/ft is calculated at the deck section over the backwall (section B-B: "apprend") for *EPS 1* configuration (Table 5-8).

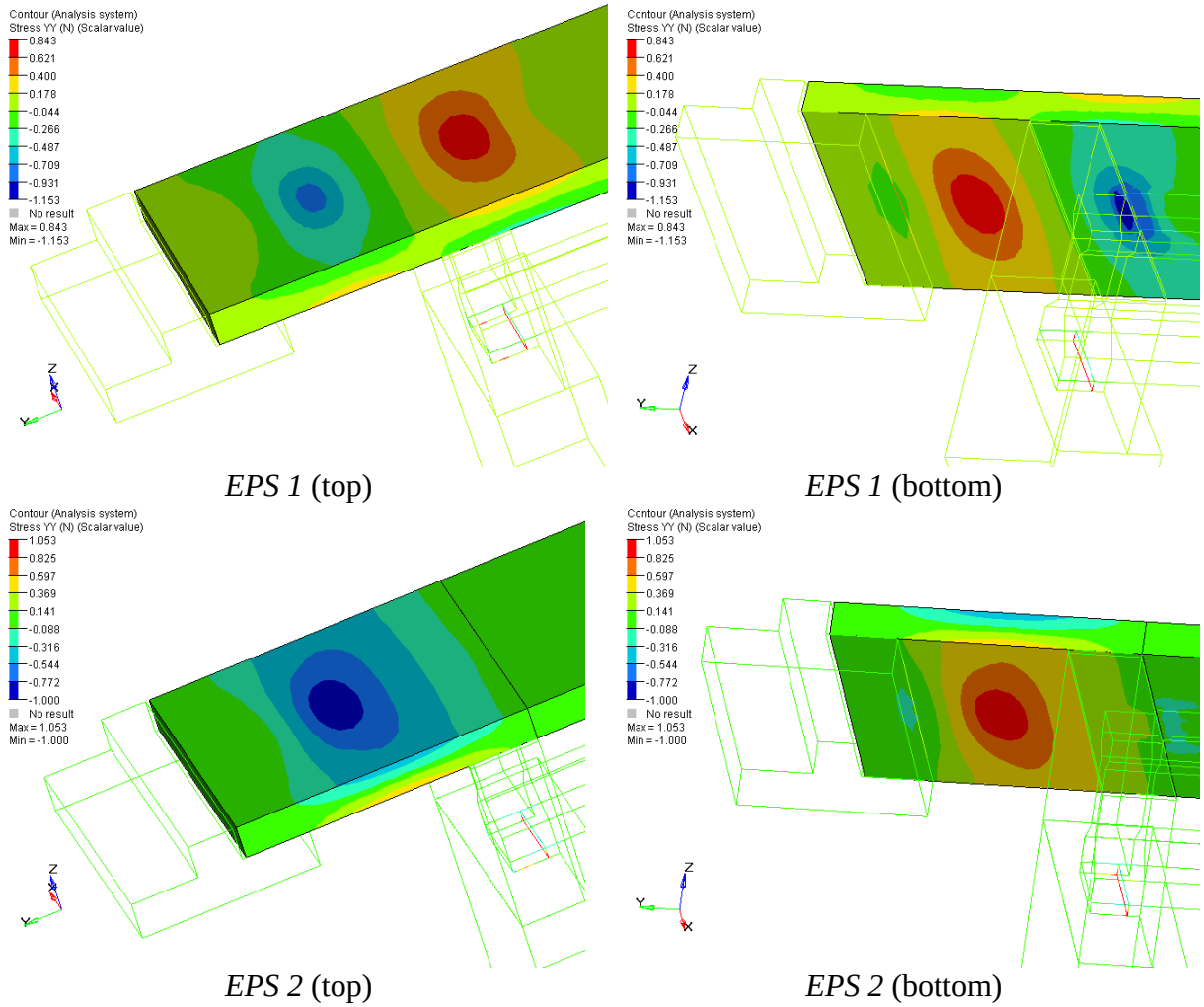

EPS 1 (top) *EPS 1* (bottom)

EPS 2 (top) *EPS 2* (bottom)

Figure 5-14. Stress YY under Case II-B loading – *EPS 1* and *EPS 2* configurations (ksi)

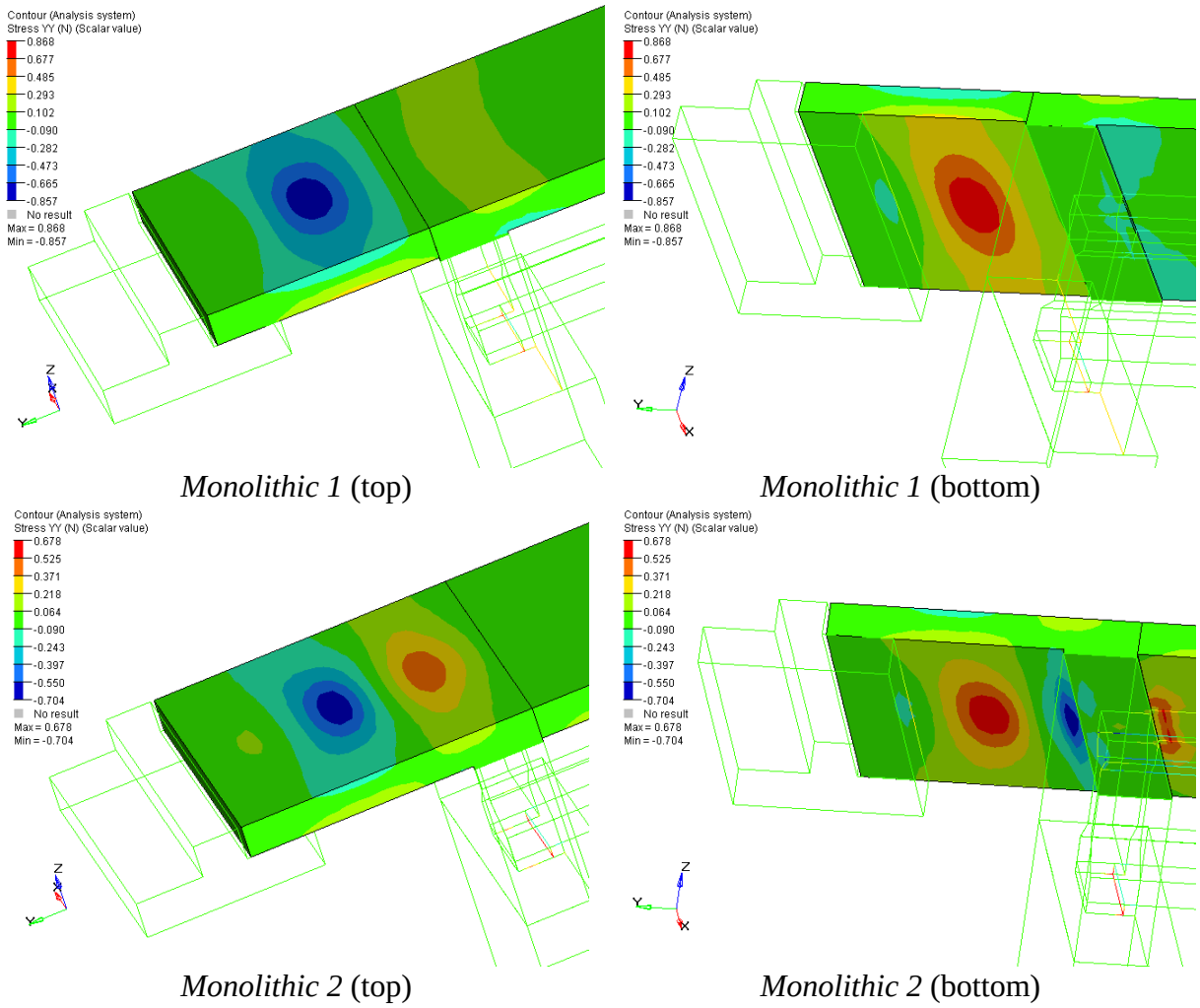

Monolithic 1 (top) *Monolithic 1* (bottom)

Monolithic 2 (top) *Monolithic 2* (bottom)

Figure 5-15. Stress YY under Case II-B loading – *Monolithic 1* and *2* configurations (ksi)

Table 5-8. Nominal Moment and Axial Force under Case II-B Loading with Different Friction Coefficient at Interfaces

Section	Analysis Case	EPS 1		EPS 2		Monolithic 1		Monolithic 2	
		M (ft-k/ft)	N (k/ft)	M (ft-k/ft)	N (k/ft)	M (ft-k/ft)	N (k/ft)	M (ft-k/ft)	N (k/ft)
Apprmid	A_1	7.8	0.0	11.1	0.0	8.5	0.0	5.5	0.0
	A_2	8.5	0.0	11.1	0.0	8.4	0.0	6.0	0.0
	A_3	8.7	0.0	11.1	0.0	8.4	0.0	6.4	0.0
	A_4	7.2	-3.2	9.5	-4.6	7.4	-3.5	4.9	-3.0
	A_5	8.7	-0.3	10.7	-1.2	7.9	-1.6	6.2	-1.0
Apprend	A_1	-8.0	0.0	0.8	0.0				
	A_2	-6.2	0.0	0.9	0.0				
	A_3	-5.7	0.0	0.9	0.1				
	A_4	-7.7	-3.2	-0.5	-4.6				
	A_5	-5.7	-0.2	0.5	-1.1				

5.2.2.1.4 Case IV-A and Case IV-B: Live load on approach slab + dead load of approach slab + Procedure A or Procedure B negative uniform thermal load

Under combined live, dead, and Procedure A negative uniform thermal loading, normal stress (YY) contours in Figure 5-16 and Figure 5-17 are generated for the zero friction analysis case (A_1). Analysis cases with different friction coefficients and load cases with Procedure B negative uniform thermal loading show similar stress contours with varying magnitudes. Nominal moment and axial force under various friction interfaces are presented in Table 5-9 and Table 5-10. First and second backwall configuration models where the EPS layer is present show similar stress contours and force resultants with Case II loading. An increase in mid-span moments is observed for all configurations as a result of friction between the sleeper slab-approach slab interface (Analysis cases A_4 and A_5). Under procedure B the thermal load's force resultants are not affected (less than % 2 for the most critical case),

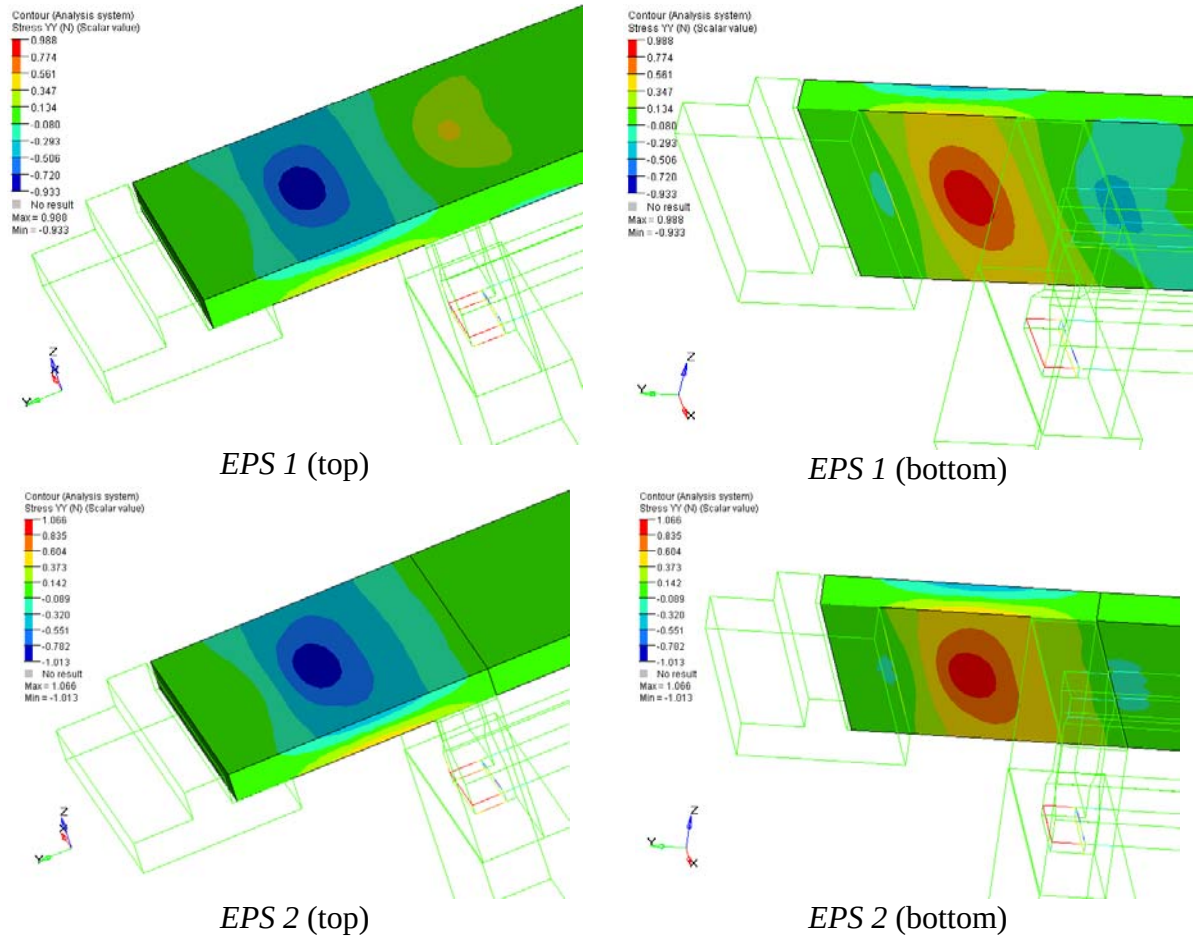

EPS 1 (top) *EPS 1* (bottom)

EPS 2 (top) *EPS 2* (bottom)

Figure 5-16. Stress YY under Case IV-A loading – *EPS 1* and *EPS 2* configurations (ksi)

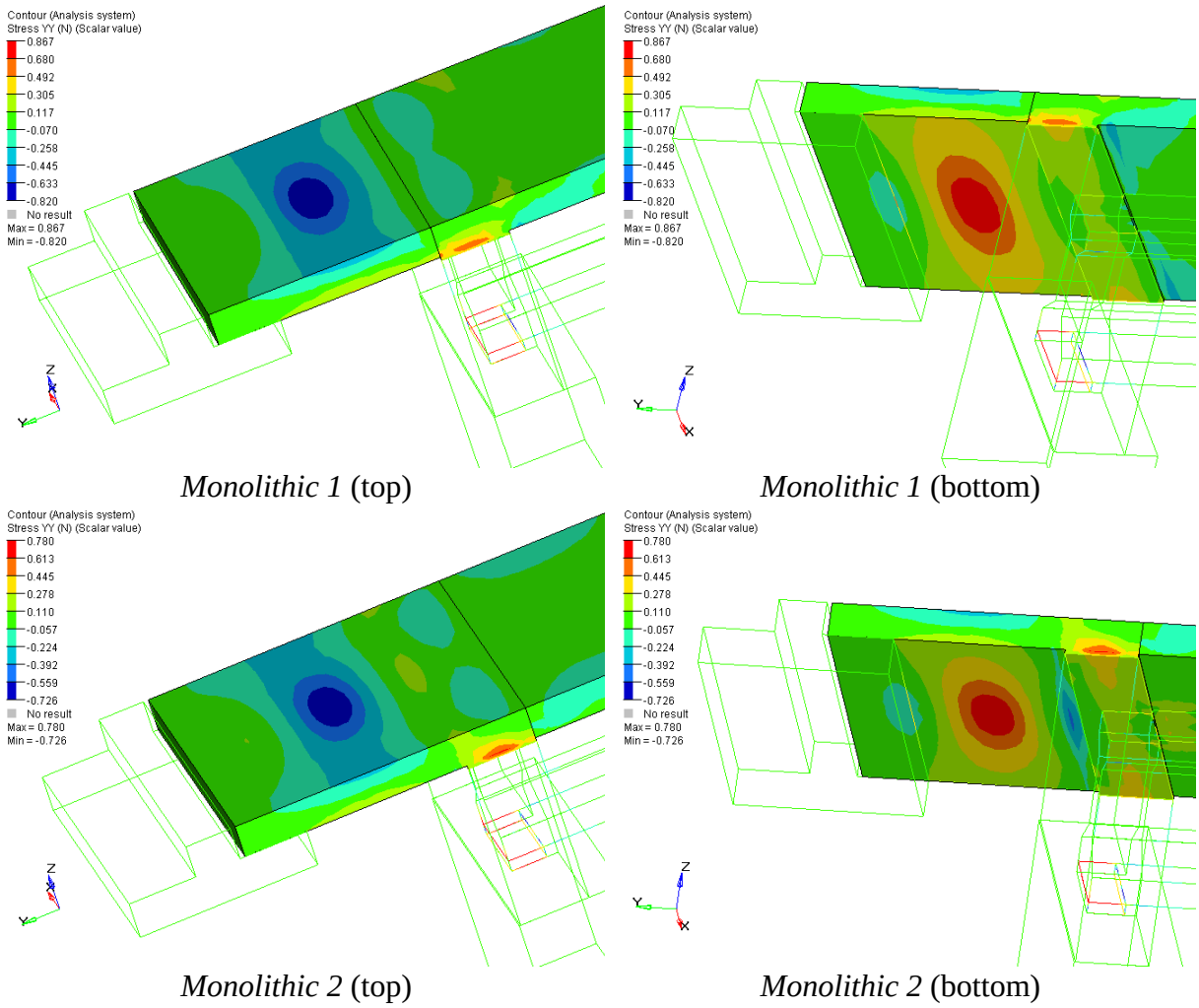

Monolithic 1 (top) *Monolithic 1* (bottom)

Monolithic 2 (top) *Monolithic 2* (bottom)

Figure 5-17. Stress YY under Case IV-A loading – *Monolithic 1* and *2* configurations (ksi)

Table 5-9. Nominal Moment and Axial Force under Case IV-A Loading with Different Friction Coefficient at Interfaces

Section	Analysis Case	EPS 1		EPS 2		Monolithic 1		Monolithic 2	
		M (ft-k/ft)	N (k/ft)	M (ft-k/ft)	N (k/ft)	M (ft-k/ft)	N (k/ft)	M (ft-k/ft)	N (k/ft)
Apprmid	A_1	10.0	0.0	11.3	0.0	8.4	0.0	6.9	0.0
	A_2	10.0	0.0	11.3	0.0	8.4	0.0	6.9	0.0
	A_3	10.0	0.0	11.3	0.0	8.4	0.0	6.9	0.0
	A_4	11.3	6.3	13.8	7.4	10.4	6.0	7.9	4.8
	A_5	11.3	6.3	13.8	7.4	10.4	6.0	7.9	4.8
Apprend	A_1	-2.5	0.0	0.9	0.0				
	A_2	-2.5	0.0	0.9	0.0				
	A_3	-2.5	0.0	0.9	0.0				
	A_4	-3.0	6.3	3.0	7.4				
	A_5	-3.0	6.3	3.0	7.4				

Table 5-10. Nominal Moment and Axial Force under Case IV-B Loading with Different Friction Coefficient at Interfaces

Section	Analysis Case	EPS 1		EPS 2		Monolithic 1		Monolithic 2	
		M (ft-k/ft)	N (k/ft)	M (ft-k/ft)	N (k/ft)	M (ft-k/ft)	N (k/ft)	M (ft-k/ft)	N (k/ft)
Apprmid	A_1	10.0	0.0	11.3	0.0	8.4	0.0	6.8	0.0
	A_2	10.0	0.0	11.3	0.0	8.4	0.0	6.8	0.0
	A_3	10.0	0.0	11.3	0.0	8.4	0.0	6.8	0.0
	A_4	11.3	6.3	13.8	7.4	10.4	6.0	7.8	4.7
	A_5	11.3	6.3	13.8	7.4	10.4	6.0	7.8	4.7
Apprend	A_1	-2.4	0.0	0.9	0.0				
	A_2	-2.4	0.0	0.9	0.0				
	A_3	-2.4	0.0	0.9	0.0				
	A_4	-3.0	6.3	3.0	7.4				
	A_5	-3.0	6.3	3.0	7.4				

5.2.2.1.5 Case IV-NG: Live load on approach slab + dead load of approach slab + negative thermal gradient load

Four different dependent backwall models (i.e., *EPS 1*, *EPS 2*, *monolithic 1*, and *monolithic 2*) are analyzed under combined effects of dead, live, and thermal loads, various sliding interface friction coefficients, and backfill effects. Stress distributions and the nominal moment and axial load for critical regions are calculated.

Under combined live, dead, and negative thermal gradient loading, stress distributions are similar to those observed under Case II-B loading. Tensile stresses are developed on the deck over the backwall in the *EPS 1* configuration model. Maximum approach slab mid-span moments occur in the *EPS 2* configuration model. This is expected since negative thermal gradient loading amplifies live load stresses. Normal stress (YY) contours presented in Figure 5-18 and Figure 5-19 are for the zero friction analysis case (A_1). Nominal moment and axial force under various friction coefficients are presented in Table 5-11.

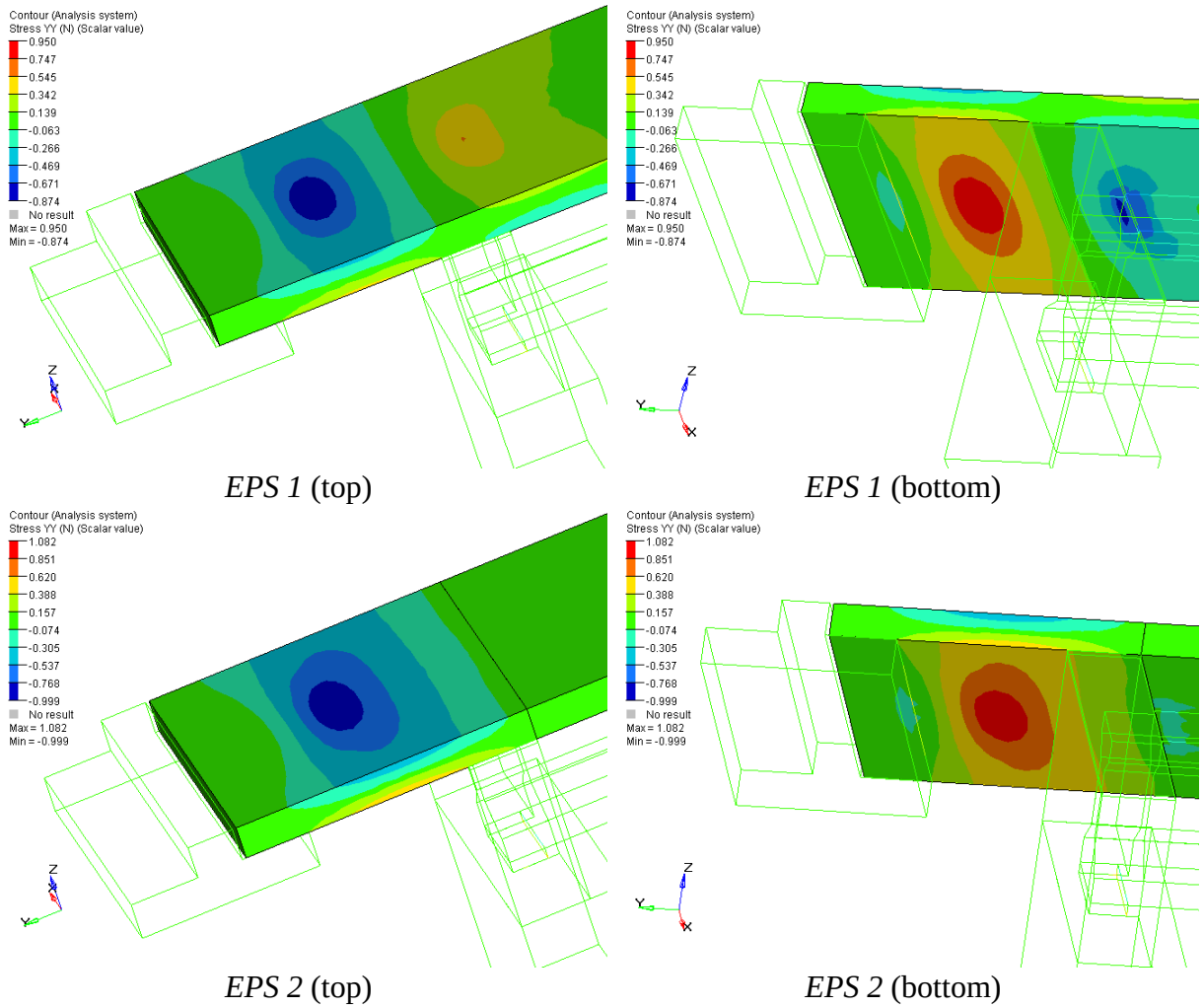

EPS 1 (top) *EPS 1* (bottom)

EPS 2 (top) *EPS 2* (bottom)

Figure 5-18. Stress YY under Case IV-NG loading – *EPS 1* and *EPS 2* configurations (ksi)

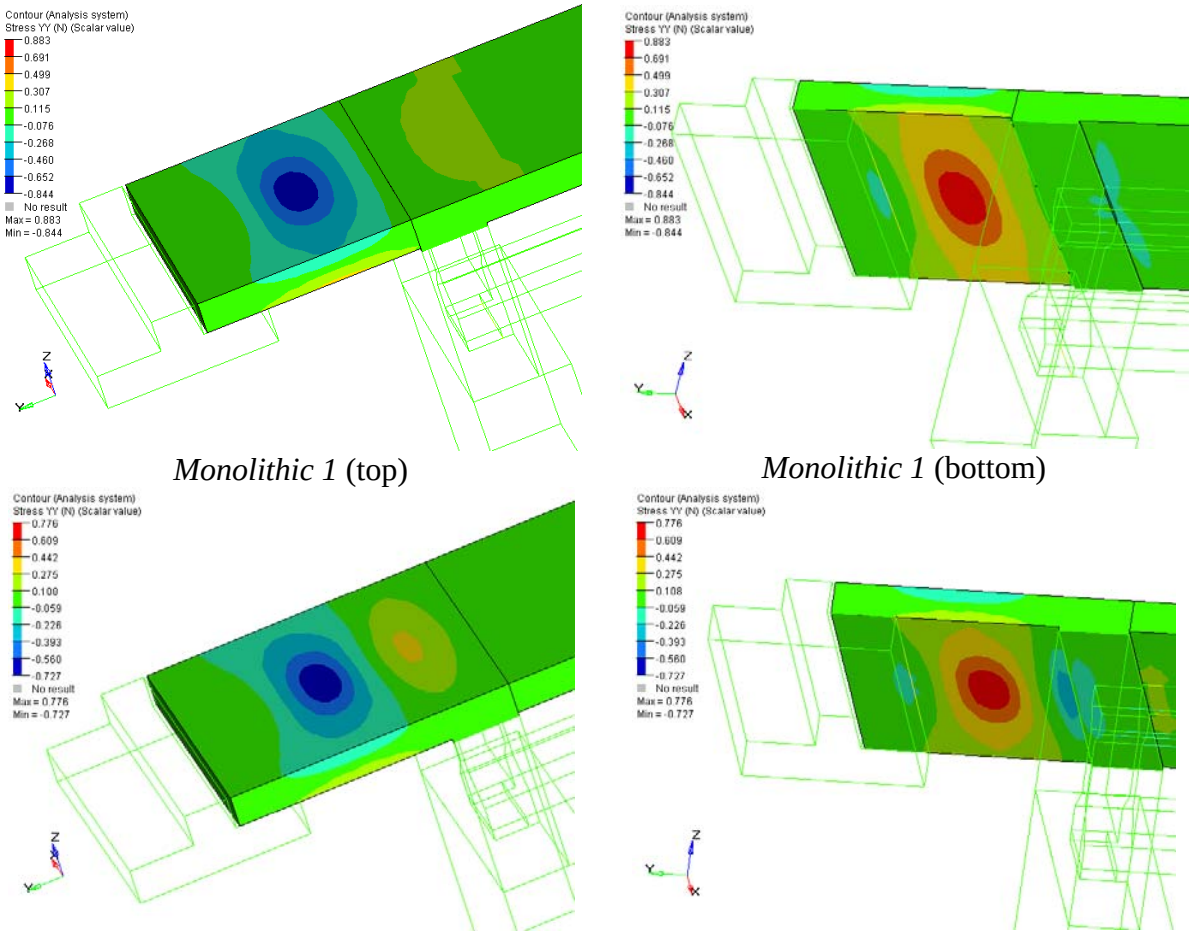

Monolithic 1 (top) *Monolithic 1* (bottom)

Monolithic 2 (top) *Monolithic 2* (bottom)

Figure 5-19. Stress YY under Case IV-NG loading – *Monolithic 1* and *2* configurations (ksi)

Table 5-11. Nominal Moment and Axial Force under Case IV-NG Loading with Different Friction Coefficient at Interfaces

Section	Analysis Case	EPS 1		EPS 2		Monolithic 1		Monolithic 2	
		M (ft-k/ft)	N (k/ft)	M (ft-k/ft)	N (k/ft)	M (ft-k/ft)	N (k/ft)	M (ft-k/ft)	N (k/ft)
Apprmid	A_1	9.1	0.0	11.2	0.0	8.4	0.0	6.7	0.0
	A_2	9.2	0.0	11.2	0.0	8.4	0.0	6.7	0.0
	A_3	9.2	0.0	11.2	0.0	8.4	0.0	6.7	0.0
	A_4	9.2	0.0	11.0	-0.7	8.4	0.0	6.7	-0.1
	A_5	9.2	0.2	11.0	-0.5	8.4	0.0	6.7	-0.1
Apprend	A_1	-4.6	0.0	0.9	0.0				
	A_2	-4.5	0.0	0.9	0.0				
	A_3	-4.5	0.0	0.9	0.0				
	A_4	-4.6	0.0	0.7	-0.7				
	A_5	-4.5	0.2	0.8	-0.5				

Under Case II loading dependent backwall behavior is similar to that of '*continuous*' independent backwall configurations, particularly for the *EPS 1* configuration. Changing the friction coefficient at the deck-EPS and bearing plate-abutment interfaces did not change the approach slab stresses or resultant forces (Cases A1 through A3). With the introduction of friction at the sleeper slab-approach slab interface, tensile stresses at the bottom of the approach slab decreased slightly (around 3%) due to an increase in restraint to movement (i.e., increased redundancy of the system). Approach slab mid-span moments are lowest in the '*monolithic 2*' configuration and largest in *EPS 2* configurations.

Case II-B loading is the most prominent load case. Stresses are affected by the backwall configuration type and different friction coefficients. *EPS 1* and '*monolithic 2*' configurations show the same trend under changing friction coefficients. Analysis results in Table 5-8 show that approach slab mid-span moments increase when friction at the bearing plate - abutment and deck-EPS interfaces increase (analysis cases A1 to A3). The same section moments decrease when friction is only present at the approach slab-sleeper slab interface. In the *EPS 2* and '*monolithic 1*' backwall configuration models, changing friction coefficient at the bearing plate-abutment interface did not change the approach slab stresses or resultant forces (analysis cases A1 through A3). The friction at the sleeper slab-approach slab interface slightly decreased the flexural stresses at the approach slab mid span due to an increase in restraint to movement.

In the *EPS 1* configuration, where the deck and approach slab are continuous over the backwall, wheel load on the span in load Case II-B creates a larger negative moment at the approach slab section over the backwall compared to that of load Case II. This is because the deck comes into contact with the backwall at regions towards the span side amplifying the concentration of stresses. In the '*monolithic 2*' configuration model, the construction joint is placed at the end of the approach slab aligned with the span side backwall face. Girder rotation due to wheel load, in Case II-B loading, also rotates the approach slab generating concentration of stress above the approach side of the backwall face.

In the '*monolithic 1*' model, a joint is placed at the approach span aligned with the approach side backwall face. Backwall rotation under Case II-B loading lifts the approach slab edge slightly, increasing the approach slab mid span moment when compared to the moment developed under

Case II loading. In the *EPS 2* configuration, the construction joint is placed at the end of approach slab aligned with span side backwall face as in the case of '*monolithic 2*' configuration. This time the approach slab mid span moment increased under Case II loading due to the compressibility of EPS that increased the approach span. However, the approach slab mid-span moment again decreases under Case II-B loading similar to the *EPS 1* and '*monolithic 2*' configuration models, but this time the decrease is only around 9% due to presence of EPS and the hinge joint.

In all dependent backwall configuration models, under Case IV-A and IV-B loading, where the effects of Case II loading is combined with negative uniform thermal load, the effect of friction at the approach-sleeper slab interface is far more pronounced than that of Case II loading. In Case IV-NG loading, the influence of interface friction is negligible.

Analysis results of four dependent backwall configurations show that in *EPS1* deck cracking could develop over the backwall under live and negative thermal gradient loading. In the case of *EPS 2*, there is no moment transfer between the span and the approach slab and is the preferred configuration over the *EPS1* configuration. The hinge connection between the deck and the approach slab can be detailed through a construction joint or by a saw cut with only the bottom rebar layer continuous.

Based on the above reason, *EPS 2*, '*monolithic 1*', and '*monolithic 2*' configurations will be further analyzed for the rocking effects of the sleeper slab.

5.2.2.1.6 Effects of sleeper slab rocking

The effect of sleeper slab rocking is investigated in *EPS 2* and '*monolithic 2*' configuration models. The *Monolithic 1* configuration is not included in this analysis since sleeper slab rocking only causes approach slab rotation over the backwall without influencing the bridge.

In cases where sleeper slab rocking is investigated, the soil stiffness beneath the sleeper slab is modeled following the procedure described by Hambly (1991). The soil stiffness below the sleeper slab is defined as follows:

$$K_z = \frac{2.5GA^{0.5}}{(1-\nu)} \quad \text{Vertical stiffness} \qquad (5\text{-}7)$$

$$K_x = 2G(1+\nu)A^{0.5} \quad \text{Horizontal stiffness} \qquad (5\text{-}8)$$

$$G = \frac{E}{2(1+\nu)} \quad \text{Shear modulus} \qquad (5\text{-}9)$$

where;

G = Shear modulus of soil,

E = Young's modulus of soil,

ν = Poisson's ratio of soil,

A = sleeper slab area = bd,

Shear modulus and Poisson's ratio of subgrade are taken as 30 ksi and 0.4 based on Ohio DOT pavement design guides (ODOT 1999). Calculated vertical and horizontal stiffness are distributed to the sleeper slab underside using the tributary area.

The analysis results show that with sleeper slab rocking, the approach slab mid-span nominal moment ('*apprmid*') is increased from 11.2 ft-kips/ft to 15.1 ft-kips/ft for *EPS 2* dependent backwall configuration models. Under Case II loading, the maximum nominal moment obtained at the sleeper section is 1.3 ft-kips/ft. For a simply supported span, one would expect lower mid-span moments when one side is over a flexible support. However, sleeper slab rotation under the rocking motion is about its left bottom corner at the pavement side (point A shown in Figure 5-20). Consequently, the effective span of the approach slab is increased resulting in a larger moment. Concentration of stress moves towards the sleeper slab. The approach slab in the *EPS 2* configuration model behaves as a simply supported slab (Figure 5-20 and Figure 5-21).

In the case of '*monolithic 2*' configuration, approach and backwall are monolithic and develop stresses near the approach-backwall interface region. There is a cracking possibility in that region if the backwall rotates. Thus, the '*monolithic 1*' configuration detail is preferred over '*monolithic 2*'.

EPS 2 and '*monolithic 1*' configuration models will be used for further analysis of the dependent backwall configuration.

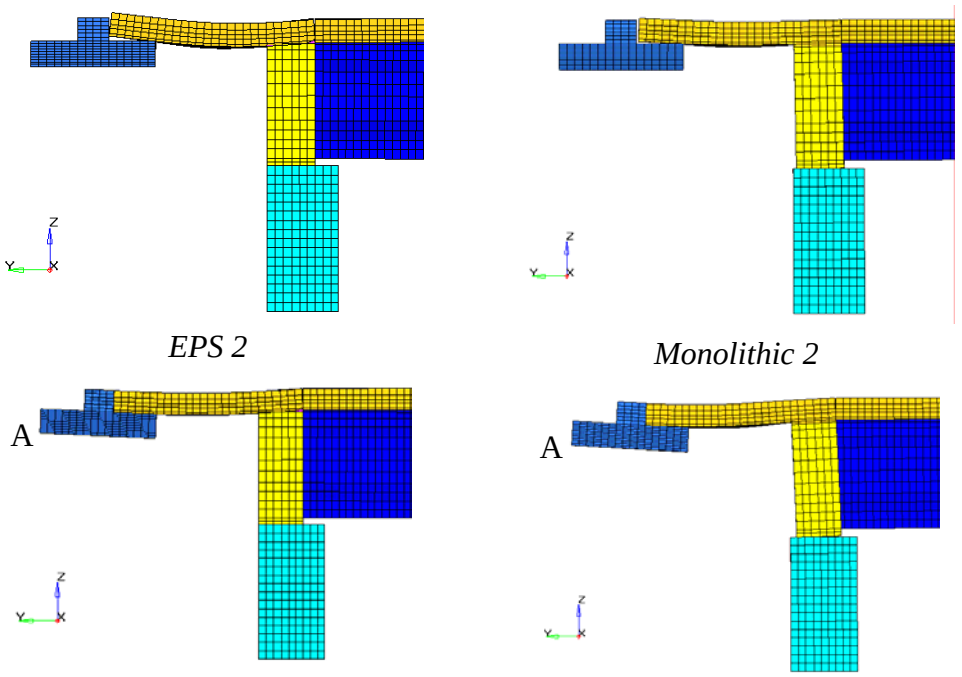

EPS 2 *Monolithic 2*

EPS 2 with sleeper slab rocking *Monolithic 2* with sleeper slab rocking

Figure 5-20. Deformed shape under Case II loading (with different scaling).

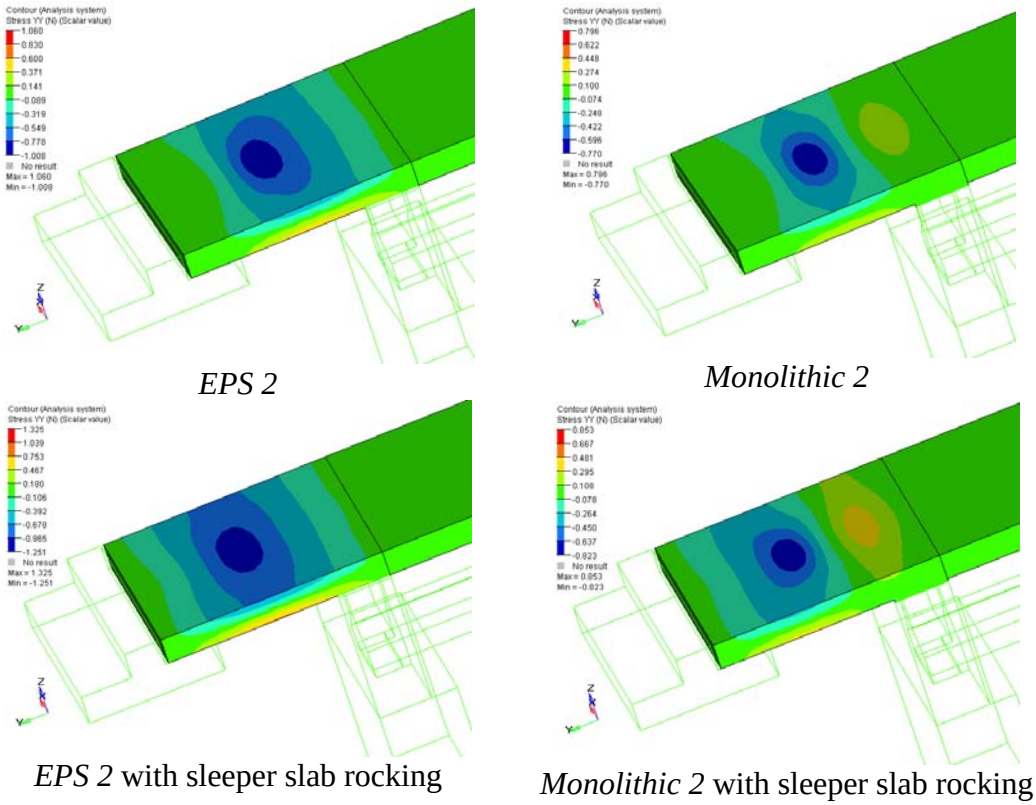

EPS 2 *Monolithic 2*

EPS 2 with sleeper slab rocking *Monolithic 2* with sleeper slab rocking

Figure 5-21. Stress YY under Case II loading – with and without sleeper slab rocking (ksi)

5.2.2.2 Abutment Region- Dependent Backwall

During field inspections, abutment cracking (D cracking) was documented directly under the bearings of two bridges that carry I-75 north and south over 13 mile road (Figure 5-22). Abutments transfer the superstructure dead load to the foundations. There is a possibility of generating large friction forces at the abutment-backwall interface due to the dead load of the superstructure in conjunction with uniform thermal contraction. This effect will be amplified if the live load is present on the approach. The abutment stresses are investigated in '*monolithic 1*' and *EPS 2* dependent backwall configuration models for the following load combination for assessing the causes of D-cracking.

CASE IV-B: Live load on approach slab + dead load of all components + Procedure A negative uniform thermal load

Figure 5-22. Abutment D-cracking

Further, the bearing under the beam is assumed frozen, and shear force developing on the abutment surface is the result of a friction coefficient of one. Resulting stress contours are shown in Figure 5-23. In the *EPS 2* configuration model, tensile stresses developed on the abutment close to the bearings under uniform thermal contraction loads, whereas concentration occurred underneath the backwall away from the bearings for '*monolithic 1*' configuration. Analysis results indicate that D-cracking is not a concern on retrofitted bridges.

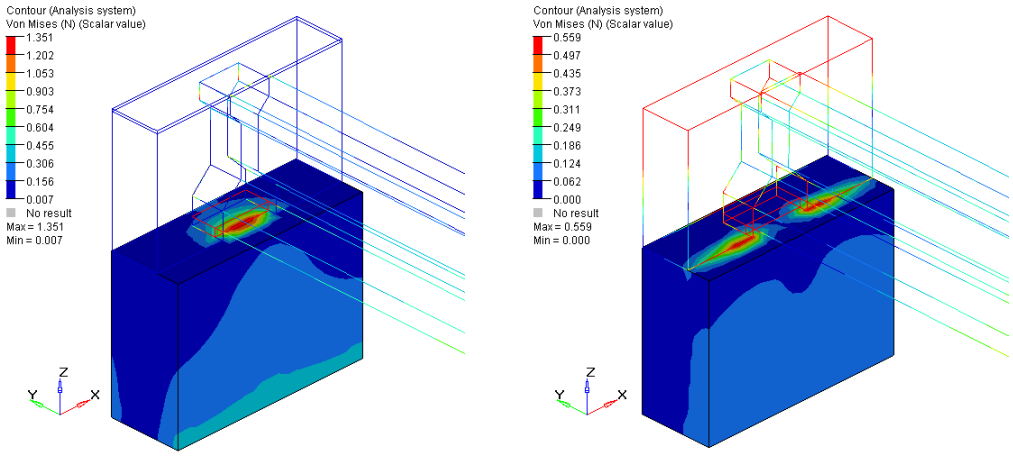

EPS 2 *Monolithic 1*

Figure 5-23. Von Misses stress distribution under Case IV-B loading for *EPS 2* and *Monolithic 1* configurations

5.2.3 Summary and Conclusion of Analyses of Approach Slab using Assemblage Models

FE analysis was performed on the following abutment configuration models:

Deck sliding over backwall configuration (independent backwall):

1. '*Continuous*'- the deck and approach slab are continuous over the backwall

2. '*Detached*' – the deck and approach slab are connected by a hinge simulating a construction joint with continuous bottom layer reinforcement. The construction joint is aligned with the span side backwall face.

Dependent backwall (semi-integral) configuration:

1. '*EPS1*'- the deck and approach slab are continuous over the backwall and EPS between backwall and the deck.

2. '*EPS2*' – the deck and approach slab are connected by a hinge simulating a construction joint with continuous bottom layer reinforcement. The construction joint is aligned with the span side backwall face.

3. '*Monolithic 1*' – The deck and backwall are monolithic. The approach slab is connected to backwall by a hinge simulating a construction where both top and bottom reinforcement layers are discontinuous. The construction joint is aligned with the approach side backwall face.

4. '*Monolithic 2*' – the approach slab and backwall are monolithic. The deck and approach slab are connected by a hinge simulating a construction joint with continuous bottom layer reinforcement. The construction joint is aligned with the span side backwall face.

According to the analyses results

1. Under live load and dead load on the approach slab, localized stresses occur at mid-span irrespective of backwall configuration. However, moment increases when the approach slab is connected through a construction joint with continuous bottom layer

reinforcement; the approach slab acts as a simply supported plate at two boundaries and can be designed accordingly.

2. The sub-grade effects under the approach slab are neglected in order to develop critical demands; nevertheless, the approach slab section capacity with both top and bottom reinforcements appears sufficient for the combined load effects. However, cracking can be expected at mid-span regardless of backwall configuration. Cracking is also expected at the deck section over the backwall when both approach slab and span are loaded (Case II-B) for '*continuous*' independent backwall configuration and *EPS1* and '*monolithic 2*' dependent backwall configurations. Axial load demand at the joints never exceeded the capacity.

3. The '*detached*' independent backwall configuration where deck and approach slab are detached and continuity is provided with a hinge at a section aligned with the span side backwall face should be favored over '*continuous*' detail.

4. For dependent backwall models where EPS is investigated, approach slab mid-span moments of the *EPS 2* configuration model, where a hinge connects the approach slab and the deck above the span side backwall face, are around 40% greater than that of *EPS 1* configuration. Yet, the *EPS 2* detail shows superior performance at the region over the backwall. A detail with a construction joint or a saw-cut aligned with the span side backwall face with continuous bottom reinforcement will reduce stress magnitudes over the backwall.

5. For monolithic dependent backwall configuration models, current construction detail (i.e., hinge between the deck and the approach above the approach side of backwall face – '*monolithic 1*') results in larger approach slab mid-span moment and axial force. Yet, it is superior to '*monolithic 2*' where the hinge is at the span side of the backwall face, by reducing stresses in the deck region over the backwall. Assuming the deck region is more critical, current MDOT detail should be favored. It should be noted that a diagonally placed reinforcement to tie the approach slab to the backwall will further reduce deck cracking potential within the vicinity of the abutment over the current MDOT detail with continuous bottom reinforcement.

6. Sleeper slab rocking creates an increase in approach slab mid-span moment by as much as 35%.

7. Modified-fixed bearings provide allowable displacement value of 0.875 inches, which are sufficient to accommodate expansion length of up to approximately 300 ft.

8. Additional restraints that may arise from the threshold friction between the approach slab and its subgrade or bearings did not generate any appreciable stress increase within the approach slab region.

9. In dependent backwall models, in the most critical load case, effects of backfill on stresses and displacements are around 5%.

10. Abutment D-cracking is not a concern with current retrofit applications.

5.3 FULL BRIDGE MODELS OF APPROACH SLAB REGION

The main objective of full bridge modeling is to simulate the structural system response and component interaction of the selected abutment region configurations under live and thermal loads (uniform and gradient). An additional objective is to document the structural system/component behavior and resultant forces and moments that cannot be investigated with single girder models such as torsion from asymmetric loading or bridge skew.

S12-3&4 of 25042 (two lane bridges) are selected for modeling. The side view of the full bridge model resembles that of single girder assemblage model as shown in Figure 5-1 for independent and dependent backwall configurations. The full bridge model consist of seven girders spaced at 76 in. with girder-deck cross-sections the same as given in Figure 4-12.

Live loading consists of two adjacent trucks placed on the approach slab (and deck, if applicable) similar to the case shown in Figure 4-13 to generate maximum torsion (M_{yy}) at the center of the approach slab following AASHTO LRFD restrictions. Actual loading defined in the FE models deviates slightly from what is presented in Figure 4-13 because of mesh limitations. Note that load eccentricity may be further increased by loading the shoulders; however, in this analysis trucks are positioned on design lanes (Figure 4-13).

Material properties, boundary conditions, and load cases are same as the single girder assemblage models. Analysis models developed for straight configurations are re-modeled incorporating a 20 degree skew investigating the skew effects.

One independent and two dependent backwall configurations selected after the analysis of single girder assemblage models are used for full bridge modeling. Three analysis load cases such as Case II, IV-A, and IV-B are selected out of the previously used five since they would be more critical for the set of selected backwall configurations. Furthermore, analysis cases are reduced to two as A_1 and A_4 for dependent backwall configurations, since the relative change among A_1-A_2-A_3 and between A_4-A_5 cases would not be significant. Analysis cases that represent utilization of varying friction interfaces are summarized in Table 5-3.

5.3.1 Full Bridge Analysis Model for Independent Backwall Configurations

The '*detached*' independent backwall configuration is modeled since it showed superior performance over the '*continuous*' with reduced deck stresses over the backwall. Elevation and isoparametric views of the configuration are shown in Figure 5-24.

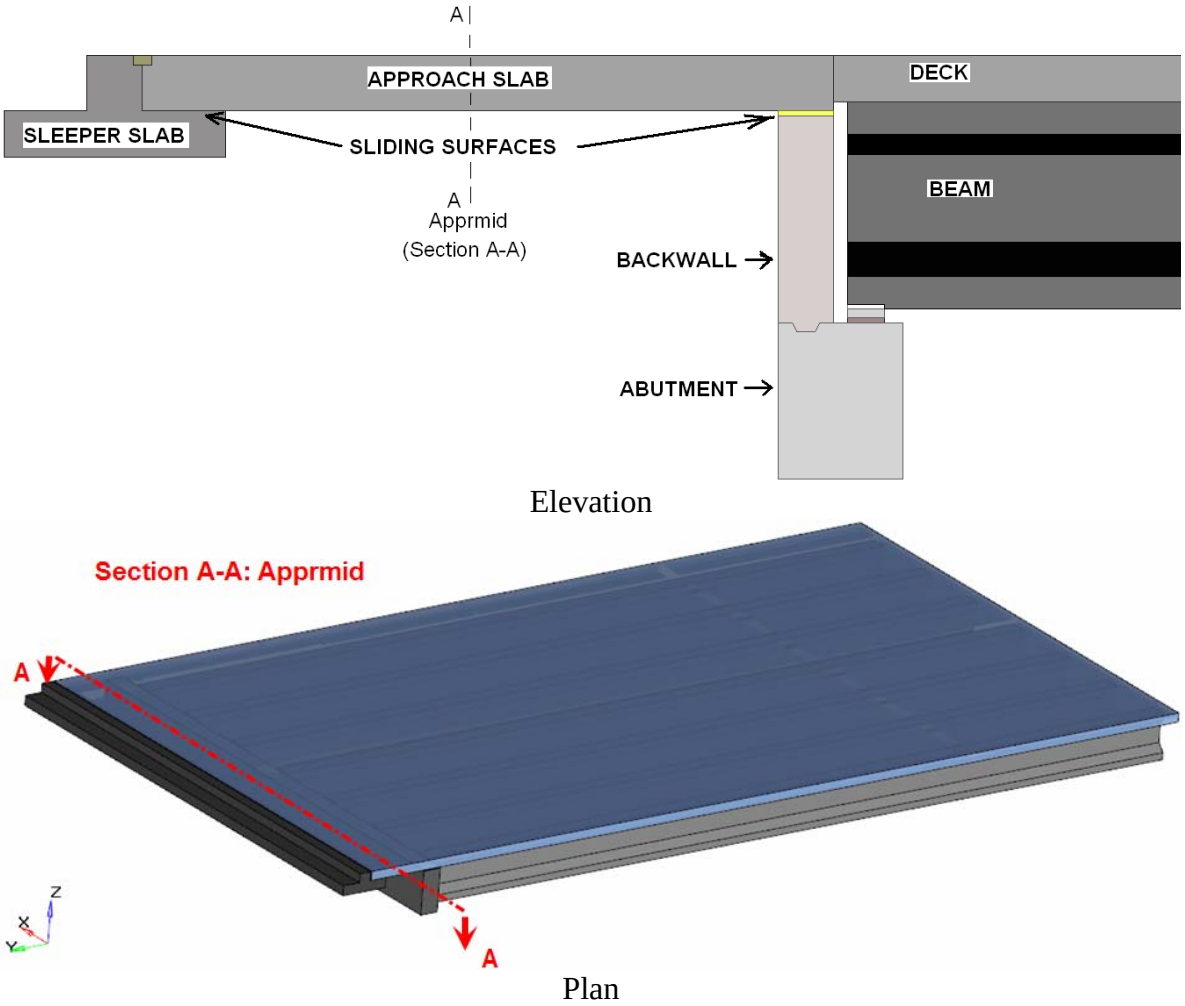

Figure 5-24. Approach slab region – independent backwall configuration

The model is analyzed for load configurations II, IV-A, and IV-B in conjunction with changing friction coefficients at the sleeper slab-approach slab and deck-EPS interfaces. Load configurations II-B and IV-NG are not considered since approach slab and span connectivity is by a hinge, eliminating moment transfer from span side to approach slab.

Nominal moments (M_{xx}, M_{yy}, and M_{zz}) and axial force (N) in longitudinal direction (YY) (Figure 4-12) are evaluated for the full bridge width at the approach slab mid span transverse cross-section, 'apprmid'. Additionally, moments and axial force for the primary strip width of 100

inches (M_{strip} and F_{strip}) for two traffic lanes under live and uniform thermal load combinations are also calculated. The results are presented in Table 5-12 and Table 5-13 for straight and 20° skew full bridges, respectively. Single girder analysis results are also included in the tables for comparison purposes.

Table 5-12. Moments and Axial Forces at '*Apprmid*' Cross-Section and within Primary Strip Width under Various Loading and Analysis Conditions for Straight Two Lane Bridge

Load Case	Analysis Case	Full Bridge (a)				Strip Width (b)		Single Girder (c)	
		M_{xx} (Bending)	M_{yy} (Torsion)	M_{zz} (Twist)	N (Axial Force)	M_{strip}	N_{strip}	M_{single}	N_{single}
		ft-kips	ft-kips	ft-kips	kips	ft-kips/ft	kips/ft	ft-kips/ft	kips/ft
Case II	A_1	94.4	66.9	0.0	0.0	11.3	0.0	11.2	0.0
	A_2	94.4	66.9	0.0	0.0	11.3	0.0	11.2	0.0
	A_3	94.4	66.9	0.0	0.0	11.3	0.0	11.2	0.0
	A_4	92.4	67.5	26.9	-5.6	11.1	-0.7	10.8	-1.1
	A_5	92.4	67.4	27.0	-5.6	11.1	-0.7	10.8	-1.1
Case IV-A	A_1	89.5	65.1	0.0	0.0	10.7	0.0	11.1	0.0
	A_2	88.8	64.8	0.0	0.0	10.7	0.0	11.1	0.0
	A_3	88.2	64.6	0.0	0.0	10.6	0.0	11.1	0.0
	A_4	114.8	59.4	257.4	73.0	13.8	8.8	13.6	7.3
	A_5	113.1	58.8	256.8	72.3	13.6	8.7	13.5	7.3
Case IV-B	A_1	88.8	64.8	0.0	0.0	10.7	0.0	11.1	0.0
	A_2	88.1	64.5	0.0	0.0	10.6	0.0	11.1	0.0
	A_3	87.4	64.2	0.0	0.0	10.5	0.0	11.1	0.0
	A_4	113.7	59.1	257.1	72.4	13.6	8.7	13.6	7.3
	A_5	111.8	58.4	256.4	71.4	13.4	8.6	13.5	7.3

(b) Calculated by dividing the total force on two traffic lanes by twice the primary strip width for one design lane as per AASHTO LRFD (2004) 4.6.1.2
(c) Single girder model resultants for '*detached*' independent backwall configuration as given in Table 5-5

Moments obtained for the strip width correlate well with the single girder assemblage results. Results are identical for load Case II and analysis cases A_1 through A_3. This is because AASHTO (2004) strip widths are defined empirically considering only gravity loading. Torsion is observed irrespective of load and analysis cases due to eccentric live load. Effects of changing interface friction on torsion are insignificant. The twist moment (M_{zz}) of the approach slab appeared when friction was introduced between the approach slab-sleeper slab interfaces (analysis cases A_4 and A_5), particularly under uniform thermal (Case IV-A and IV-B). This is

because non-uniform longitudinal reactions develop under eccentric live load in conjunction with uniform thermal load.

The analysis is repeated by remodeling the straight bridge model incorporating a 20 degree skew. The analysis is performed for the same load cases as well as the analysis cases of the straight bridge model. The results are presented below also including moment and axial forces calculated from single girder analysis:

Table 5-13. Moment and Axial Forces at '*Apprmid*' Cross-Section and within Primary Strip Width under Various Loading and Analysis Conditions for 20° Skew Two Lane Bridge

Load Case	Analysis Case	Full Bridge (a)				Strip Width (b)		Single Girder (c)	
		M_{xx} (Bending)	M_{yy} (Torsion)	M_{zz} (Twist)	N (Axial Force)	M_{strip}	N_{strip}	M_{single}	N_{single}
		ft-kips	ft-kips	ft-kips	kips	ft-kips/ft	kips/ft	ft-kips/ft	kips/ft
Case II	A_1	93.2	79.1	7.0	0.0	11.2	0.0	11.2	0.0
	A_2	93.2	79.1	7.0	0.0	11.2	0.0	11.2	0.0
	A_3	93.2	79.1	7.0	0.0	11.2	0.0	11.2	0.0
	A_4	91.7	80.9	7.6	-2.9	11.0	-0.3	10.8	-1.1
	A_5	91.7	80.9	7.6	-2.9	11.0	-0.3	10.8	-1.1
Case IV-A	A_1	89.1	82.1	7.1	0.0	10.7	0.0	11.1	0.0
	A_2	88.4	82.0	7.1	0.0	10.6	0.0	11.1	0.0
	A_3	87.7	81.8	7.1	0.0	10.5	0.0	11.1	0.0
	A_4	100.5	60.4	58.0	65.4	12.1	7.9	13.6	7.3
	A_5	99.3	60.1	61.6	64.7	11.9	7.8	13.5	7.3
Case IV-B	A_1	88.3	82.7	7.1	0.0	10.6	0.0	11.1	0.0
	A_2	87.4	83.2	7.2	0.0	10.5	0.0	11.1	0.0
	A_3	86.7	83.2	7.2	0.0	10.4	0.0	11.1	0.0
	A_4	99.5	61.1	57.3	64.6	11.9	7.8	13.6	7.3
	A_5	98.3	60.7	60.8	63.9	11.8	7.7	13.5	7.3

(b) Calculated by dividing the total force on two traffic lanes by twice the primary strip width for one design lane as per AASHTO LRFD (2004) 4.6.1.2
(c) Single girder model resultants for '*detached*' independent backwall configuration as given in Table 5-5

Comparing Table 5-12 and Table 5-13, nominal bending moments and axial force decreased with skew in all load and analysis cases considered. This decrease is more pronounced in cases where sleeper slab-approach slab friction is present and uniform temperature loads are involved. For the first three analysis cases (cases A_1 through A_3), the decrease in bending moments with skew is only about 1%. Under Case IV-A and Case IV-B loading and A_4 and A_5 analysis cases, the

decrease is around 12%. In all load and analysis cases, twist about the center of the approach slab's mid-span occurs, yet the magnitudes are only around 25% of those observed in straight bridges. Torsion increased with skew unlike bending and twist. The most pronounced increase in torsion occurred for the first three analysis cases (A_1 through A_3) with magnitudes around 25% higher compared to the straight bridge. It is expected that the twist would increase with skew and friction at the sleeper slab-approach interface. This is because the reaction at the wide corner support is greater than the reaction at narrow corner under a uniformly distributed load. However, the analysis performed in this project consisted of a live load that is placed close to the narrow corner. This load configuration changed the vertical reaction distribution one would expect from a skew bridge and resulted in lower twist than expected.

5.3.2 Full Bridge Analysis Model for Dependent Backwall Configurations

'*Monolithic 1*' and '*EPS 2*' dependent backwall configurations are incorporated in full bridge models since they showed superior performance by reducing stress magnitudes at the deck area over the backwall. Elevation and isoparametric views of the configurations are shown in Figure 5-25 and Figure 5-26. The models are again modified to include skew for further analysis.

Nominal moments (M_{xx}, M_{yy}, and M_{zz}) and axial force (N) in longitudinal direction (YY) are evaluated at the approach slab mid span transverse cross-section ('*apprmid*') for the full bridge width. Additionally, the bending moments and axial force for a primary strip width of 100 inches are calculated (M_{strip} and F_{strip}) and presented in Table 5-14 and Table 5-15 for straight and skew bridge models. Single girder analysis results are also included in these tables for comparison purposes.

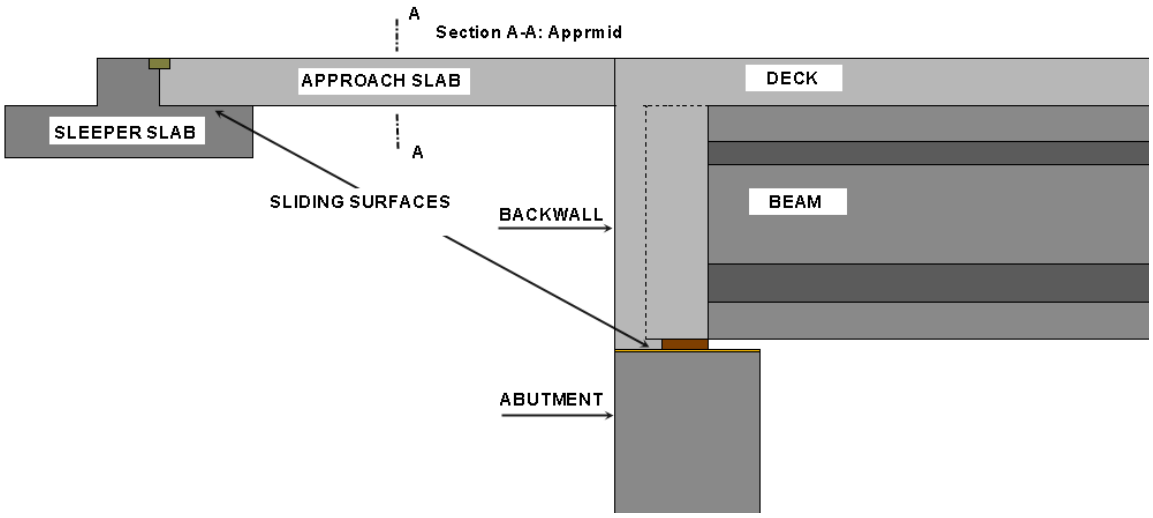

Elevation

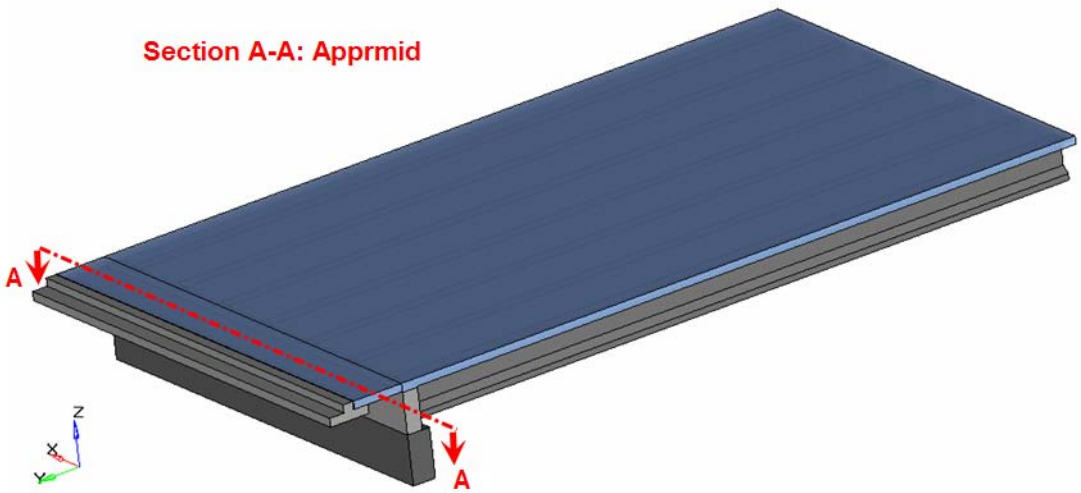

Plan

Figure 5-25. Approach slab region –dependent backwall '*monolithic 1*'configuration

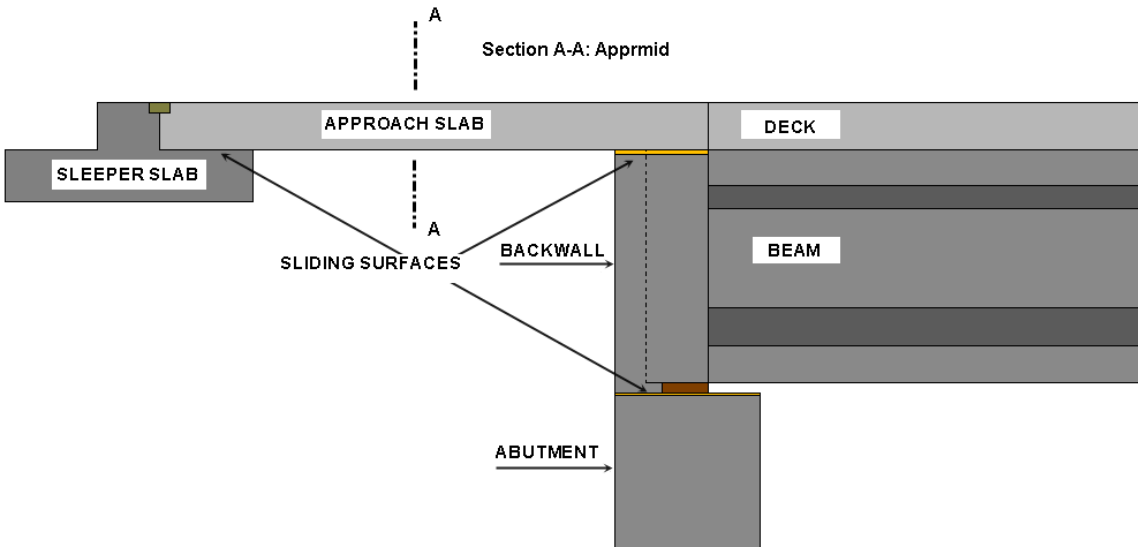

Elevation

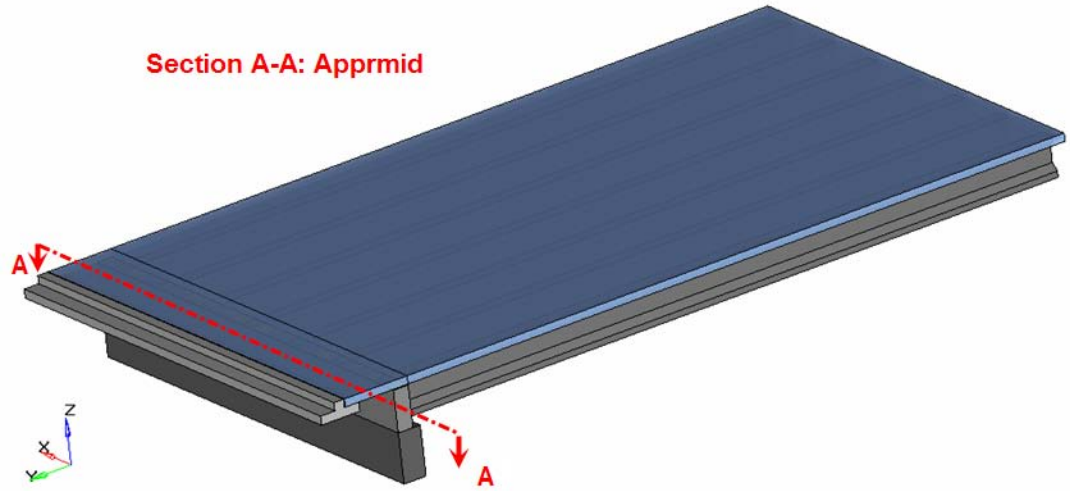

Plan

Figure 5-26. Approach slab region –dependent backwall '*EPS 2*'configuration

Table 5-14. Moments and Axial Force at '*Apprmid*' Cross-Section and within Primary Strip Width under Various Loading and Analysis Conditions for Straight and 20° Skew Two Lane Bridge with '*monolithic 1*' Configuration

STRAIGHT									
Load Case	Analysis Case	Full Bridge (a)				Strip Width (b)		Single Girder (c)	
		M_{xx} (Bending)	M_{yy} (Torsion)	M_{zz} (Twist)	N (Axial Force)	M_{strip}	N_{strip}	M_{single}	N_{single}
		ft-kips	ft-kips	ft-kips	kips	ft-kips/ft	kips/ft	ft-kips/ft	kips/ft
Case II	A_1	71.9	113.8	0.0	0.0	8.6	0.0	8.4	0.0
	A_4	71.1	114.0	12.2	-2.9	8.5	-0.3	8.2	-0.6
Case IV-A	A_1	85.4	23.7	0.0	0.0	10.3	0.0	8.4	0.0
	A_4	99.5	23.1	169.8	53.9	11.9	6.5	10.4	6.0
Case IV-B	A_1	85.9	23.4	0.0	0.0	10.3	0.0	8.4	0.0
	A_4	100.0	22.8	169.6	53.9	12.0	6.5	10.4	6.0
20° SKEW									
Load Case	Analysis Case	Full Bridge (a)				Strip Width (b)		Single Girder (c)	
		M_{xx} (Bending)	M_{yy} (Torsion)	M_{zz} (Twist)	N (Axial Force)	M_{strip}	N_{strip}	M_{single}	N_{single}
		ft-kips	ft-kips	ft-kips	kips	ft-kips/ft	kips/ft	ft-kips/ft	kips/ft
Case II	A_1	48.4	22.5	2.5	0.0	5.8	0.0	8.4	0.0
	A_4	48.2	23.2	1.6	-1.8	5.8	-0.2	8.2	-0.6
Case IV-A	A_1	62.6	21.5	2.7	0.0	7.5	0.0	8.4	0.0
	A_4	65.4	2.7	29.0	46.8	7.8	5.6	10.4	6.0
Case IV-B	A_1	61.3	20.5	2.4	0.0	7.4	0.0	8.4	0.0
	A_4	64.3	2.4	24.7	45.9	7.7	5.5	10.4	6.0

(b) Calculated by dividing the total force on two traffic lanes by twice the primary strip width for one design lane as per AASHTO LRFD (2004) 4.6.1.2

(c) Single girder model resultants for '*monolithic 1*' dependent backwall configuration as given in Table 5-7, Table 5-9, and Table 5-10

Table 5-15. Moments and Axial Force at '*Apprmid*' Cross-Section and within Primary Strip Width under Various Loading and Analysis Conditions for Straight and 20° Skew Two Lane Bridge with '*EPS 2*' Configuration

STRAIGHT									
Load Case	Analysis Case	Full Bridge (a)				Strip Width (b)		Single Girder (c)	
		M_{xx} (Bending)	M_{yy} (Torsion)	M_{zz} (Twist)	N (Axial Force)	M_{strip}	N_{strip}	M_{single}	N_{single}
		ft-kips	ft-kips	ft-kips	kips	ft-kips/ft	kips/ft	ft-kips/ft	kips/ft
Case II	A_1	101.5	172.9	0.0	0.0	12.2	0.0	11.2	0.0
	A_4	99.5	173.3	26.0	-6.3	11.9	-0.8	10.8	-1.2
Case IV-A	A_1	112.6	61.8	0.0	0.0	13.5	0.0	11.3	0.0
	A_4	133.9	60.8	248.2	74.6	16.1	9.0	13.8	7.4
Case IV-B	A_1	114.0	61.1	0.0	0.0	13.7	0.0	11.3	0.0
	A_4	135.0	60.2	245.4	74.2	16.2	8.9	13.8	7.4
20° SKEW									
Load Case	Analysis Case	Full Bridge (a)				Strip Width (b)		Single Girder (c)	
		M_{xx} (Bending)	M_{yy} (Torsion)	M_{zz} (Twist)	N (Axial Force)	M_{strip}	N_{strip}	M_{single}	N_{single}
		ft-kips	ft-kips	ft-kips	kips	ft-kips/ft	kips/ft	ft-kips/ft	kips/ft
Case II	A_1	95.6	80.9	7.2	0.0	11.5	0.0	11.2	0.0
	A_4	95.0	82.7	7.0	-3.2	11.4	-0.4	10.8	-1.2
Case IV-A	A_1	105.0	96.3	8.3	0.0	12.6	0.0	11.3	0.0
	A_4	109.5	65.3	79.3	63.5	13.1	7.6	13.8	7.4
Case IV-B	A_1	103.5	92.3	8.0	0.0	12.4	0.0	11.3	0.0
	A_4	107.8	61.9	75.3	62.7	12.9	7.5	13.8	7.4

(b) Calculated by dividing the total force on two traffic lanes by twice the primary strip width for one design lane as per AASHTO LRFD (2004) 4.6.1.2

(c) Single girder model resultants for '*EPS 2*' dependent backwall configuration as given in Table 5-7, Table 5-9, and Table 5-10

Similar to the independent backwall configuration analysis, in loading Case II, straight full bridge dependent backwall configurations primary strip width results correlate well with single girder bending moment resultants. This again is due to the fact that AASHTO (2004) primary widths are defined empirically for gravity loading only. Both configurations have a twisting response similar to that of an independent backwall; significant magnitudes are observed at the approach slab's mid-span under the approach slab-sleeper slab interface friction, and under uniform thermal (Case IV-A and IV-B). Twist calculated in '*EPS 2*' configurations are around

45% higher than those obtained for '*monolithic 1*' configurations; whereas, '*EPS 2*' dependent and detached independent backwall configurations do not differ more than 3%. Torsion is observed irrespective of load case and appeared independent of friction coefficient at the sliding interfaces. Under uniform thermal (Case IV-A and IV-B), torsion is reduced.

Similar to the results obtained from the '*detached*' independent backwall configuration model, bending moments and axial force decreased with skew in all load and analysis cases. In load Case II, for the first analysis case (A_1), the decrease in bending moment magnitudes are 33% and 6% for '*monolithic 1*' and '*EPS 2*' configurations, respectively. Under load Cases IV-A and IV-B, in conjunction with analysis case A_5, the decrease is around 36% and 20% for the '*monolithic 1*' and '*EPS 2*' configurations respectively. Twist about the center of the approach slab's mid-span occurs irrespective of analysis and load cases, yet the magnitudes are only between 18% and 30% of those calculated from straight bridge models. The torsional response of the two dependent backwall configurations is quite different with skew depending on the load and analysis case. In both configurations, torsion decreased significantly under load Case II independent of friction at the sleeper slab-approach slab interface. The torsional moment magnitudes are only about 27% and 47% of those calculated from straight bridge models. In load cases where uniform thermal is included (Case IV-A and IV-B), torsion decreased in the '*monolithic 1*' configuration but increased in '*EPS 2*' configuration. '*Monolithic 1*' configuration results are affected mainly by sleeper slab-approach slab interface friction (case A_4), whereas deck-EPS interface friction (case A_1) is more pronounced in '*EPS 2*' configurations.

The skew bridge analysis results show lower twist and torsion than that calculated from the straight bridge. The reasons for deviation of expected results are discussed at the end of the previous section. Skew bridge response also changes with the configuration used in the analysis. Further study on skew jointless bridge approach slab regions is suggested for detailed investigations of the design parameters.

5.3.3 Summary and Conclusion of Full Bridge Analyses of Approach Slab Region

Moment and force demands were evaluated in the approach slab for both straight and 20^o skew two-lane bridges under transversely asymmetric live loads, dead load of approach slab, and

combinations with uniform thermal. The '*detached*' independent backwall configuration and '*monolithic 1*' and '*EPS 2*' dependent backwall configurations were modelled investigating the effects of changing sliding interface friction coefficients. The moment and axial force calculated for a primary strip width (M_{strip} and N_{strip}) of two-lane full bridge models are compared with single girder assemblage results.

Based on the analysis results the following conclusions are reached:

1. The AASHTO (2004) primary strip width method can be used for the design of approach slab. Dead load of the approach slab should be used in conjunction with live load. The approach slab can be analyzed as a simply supported beam with a clear span between the approach side backwall face and edge of the sleeper slab where the approach slab sits. For cases where EPS is used, a clear span should also include the length at which EPS is placed, i.e., width of backwall.

2. In all the backwall configuration models, the longitudinal bending moment and axial force decrease with skew angle irrespective of load or analysis case.

3. Significant twisting of the approach slab occurred with including approach slab-sleeper slab interface friction (analysis cases A_4 and A_5,), particularly with uniform thermal (Case IV-A and IV-B) in both independent and dependent backwall models. This is due to higher longitudinal reactions developed under uniform thermal load. With skew, twisting about the center of the approach slab's mid-span occurred irrespective of analysis and load case, yet the magnitudes in Case IV loading is only between 18% and 30% of those calculated in straight bridge models. The cause of this reduction in twist is placing the live load close to the narrow corner that generated vertical as well as horizontal reactions due to friction at the approach slab-sleeper slab interface, which is different from what is expected from a skew bridge.

4. Each backwall configuration showed unique torsional response with high sensitivity to analysis and load cases. The reasons for the differences need to be further investigated.

6 SUMMARY, CONCLUSIONS, AND RECOMMENDATIONS

6.1 SUMMARY AND CONCLUSIONS

Three tasks were performed in this project. The first task was to review and synthesize information related to the behavior, performance, design, and analysis of jointless bridges with link slabs. A thorough literature review was conducted to identify specific design configurations with records of better performance. One of the examples identified was the first link slab bridge in North Carolina. A crack was documented with a width wider than estimated and was attributed to effects of debonding. This link slab was designed with two layers of continuous reinforcement. Another example is the deck sliding over backwall detail developed by MDOT with a construction joint aligned with the span side of the backwall face. The MDOT detail includes top layer reinforcement to be continuous through the construction joint. The analysis performed in this project showed that a better detail will be to eliminate the continuity of the top reinforcement in order to eliminate the development and transfer of negative moment across the joint. In integral and semi-integral abutment details, detaching the deck from the approach slab and tying the approach slab to the backwall with the use of diagonally placed reinforcement was found superior. This detail appeared to reduce deck cracking in the vicinity of the abutment by allowing the joint to act as a hinge and accommodate its inevitable rotation over the backwall (Burke 1999, Weakley 2005, and Yannotti et al. 2005).

The second task was to document the distress at the sleeper slab and bearings in Michigan jointless bridges associated with the link slab, approach slab, abutments, pier caps, and expansion joints. Field inspection was performed on five unique and three similar jointless bridges with link slabs and deck sliding over the backwall or the backwall sliding over abutment details. Inspection documented that full depth link slab cracking was common to all bridges irrespective of bridge girder type and span length and regardless of whether or not the link slab was saw cut directly over the pier centerline. When stay-in-place forms hindered the inspection of the deck underside, inspection of the deck overhang helped identify these full-depth cracks. Vertical cracks on the abutment wall were also common to all inspected bridges. D-cracking on the abutment directly under the beam supports were documented only on two of the eight bridges. However, most of the documented abutment

distress was present before the repair activity and was not due to the parameters of jointless bridge design. Short horizontal cracks on the backwall near the bearings were documented in six out of eight bridges inspected. In addition, distressed bearings were documented on five bridges. Joints at the sleeper slab were functioning in all the bridges inspected.

The third and final task of the project was to develop analysis models of the jointless bridge deck system including the link slab, bearings, abutment types (deck sliding over backwall and backwall sliding over abutment), the approach slab, and the sleeper slab. The purpose of the analytical models was to simulate the response and interaction between components under selected load conditions, including volume change loads. This was accomplished by developing independent models for the link slab region and the approach slab region. Support conditions, girder size, span length, adjacent span ratio, and debonded length were the design parameters considered in the finite element models of the link slab region. The approach slab region was modeled with the adjacent span and included the backwall and the sleeper slab. Two independent and four dependent backwall configurations were modeled and analyzed to evaluate their comparative response under critical load cases. The model parameters included friction forces generated by the sliding interfaces, subgrade effects on the approach slab, and backfill effects on the sliding abutment.

Link slab assemblage analysis showed that support conditions underneath the link slab influence the design moments and axial force of the link slab. In principle the link slab is subjected to combined axial force and moment with RHHR support configuration and needs to be designed by accounting for their interaction. Analysis also showed that drying and thermal hydration shrinkage strains generate cracks of which the width equals the expected magnitude under a live load. Negative thermal gradient loading is additive to a live load, whereas positive gradient loading could alone exceed the positive moment section capacity at the link slab. Current link slab design is based on the moment demand due to a live load. AASHTO LRFD (2004) Service I limit state requires the combined effect of live and thermal load in calculating link slab moment demand. A new analysis procedure is proposed for calculating link slab design moment and axial load from thermal gradient load and is presented in Appendix F. Furthermore, the existing modified-fixed bearings reserve capacity was sufficient for girder-end displacements. In addition, full bridge link slab assemblage

models revealed that torsional moment arises in link slabs of skew bridges irrespective of support conditions. Finally, lower and upper bound bearing stiffness had a greater influence on torsion and twisting moments than bending moments and axial forces.

Details including construction joints are recommended with a continuous bottom reinforcement layer where deck sliding over the backwall or the backwall sliding over the abutment is incorporated. A modification is proposed to the current MDOT detail for new semi-integral construction, where the backwall and approach slab are connected with continuous bottom layer reinforcement. The detail proposed is to connect the approach slab to the backwall by providing a diagonal reinforcement layer.

6.2 RECOMMENDATIONS

Based on the literature review, field inspection data analysis, and finite element modeling and subsequent simulations of the numerous models developed in this project, four design recommendations are developed. One recommendation deals with the link slab design, and the remaining three address the backwall and approach slab region.

6.2.1 Link Slab Details

Current link slab details include only the continuous top layer reinforcement over the pier centerline. It is recommended that continuous top and bottom reinforcements are used irrespective of support conditions underneath the link slab. Additional moment and axial force under thermal gradient loads should be included in the link slab design using the procedure given in the Appendix F. This procedure is essential for the analysis of the AASHTO LRFD (2004) Service I limit state load case. The current link slab detail, though implemented in bridges, is not standardized. Link slab details given in S12-25042 bridge plans were modified as shown in Figure 6-1 illustrating recommended link slab reinforcement detail. Three saw cuts are recommended: one at each end of link slab and the other is directly over the pier centerline.

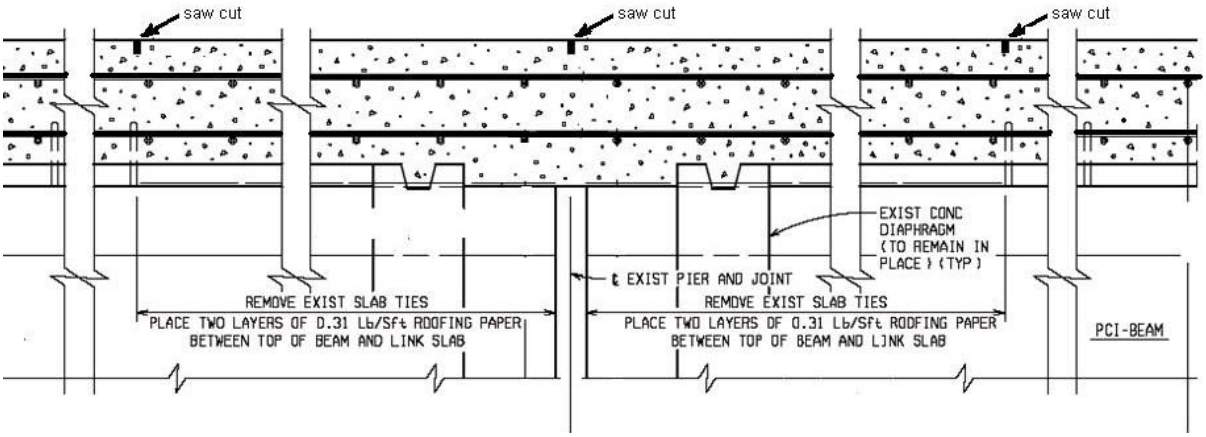

Figure 6-1. Proposed link slab details; both reinforcement layers are continuous with three saw cuts

6.2.2 Deck Sliding over Backwall – Design Application for Repair Activity

Modification is proposed to the current MDOT independent backwall detail at the construction joint between the deck and the approach. The MDOT Bridge Design Guide sheet 6.20.03A standard detail consists of continuous top layer reinforcement through the construction joint while bottom layer reinforcement is discontinued. It is proposed that the bottom reinforcement layer remain continuous through the construction joint while discontinuing the top layer. The modification proposal to MDOT Bridge Design Guide 6.20.03A is shown in Figure 6-2. The proposed detail in standard MDOT Bridge Design Guide format is presented in Appendix G.

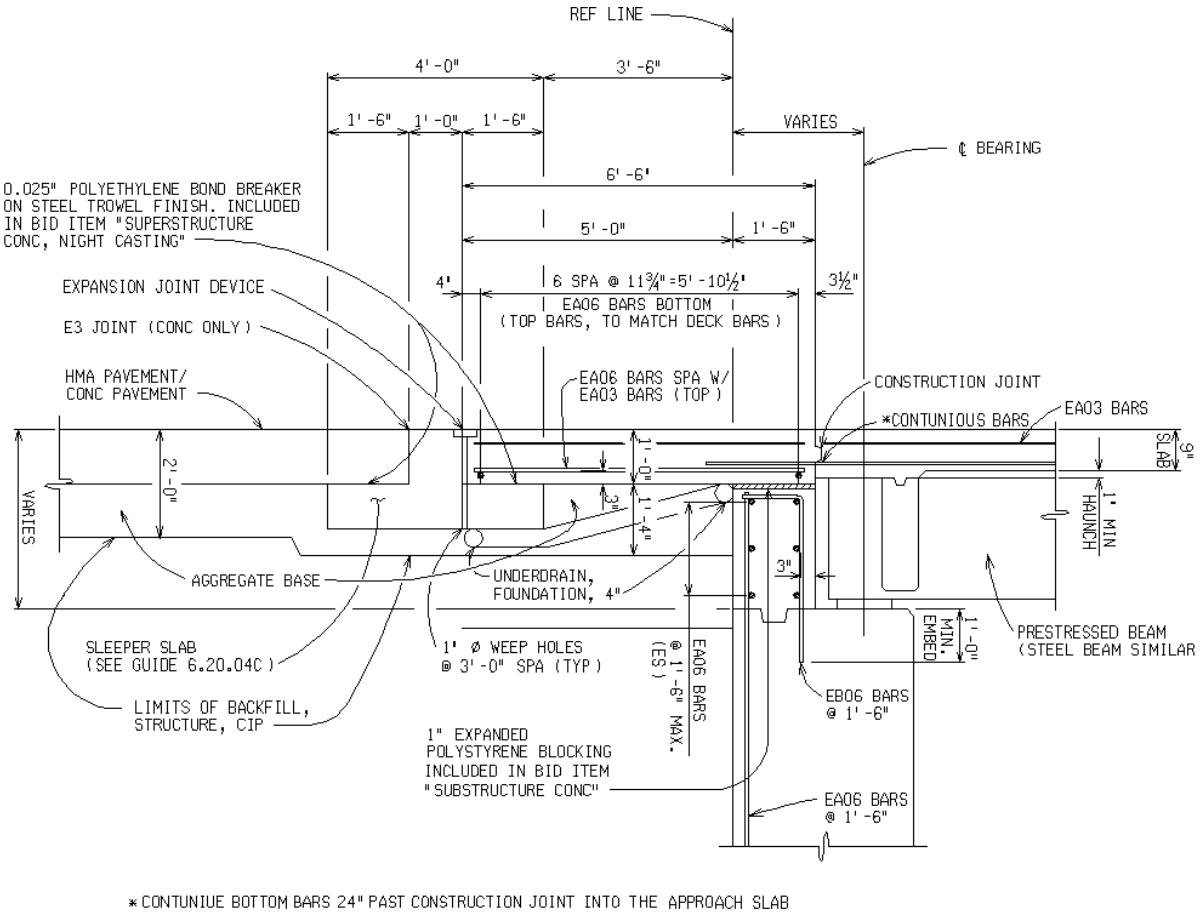

Figure 6-2. Proposed independent backwall configuration with deck sliding over backwall, i.e. continuous bottom layer reinforcement with discontinued top layer

6.2.3 Dependent Backwall Configuration – Design Application for Repair Activity

Dependent backwall retrofit details implemented in S12-25042, S04-63174, and B01-10042 bridges were not standardized. Details show continuous top and bottom layer reinforcements connecting the deck and approach slab over the backwall. Also, a saw cut or a construction joint at the deck-approach slab interface is not required. Based on the documented cracking on the bridge deck during field inspection and FE analysis results, it is recommended to implement a construction joint in conjunction with a continuous bottom reinforcement layer for current repair design applications. The proposed detail is shown in Figure 6-3. The proposed detail in standard MDOT Bridge Design Guide format is presented in Appendix G.

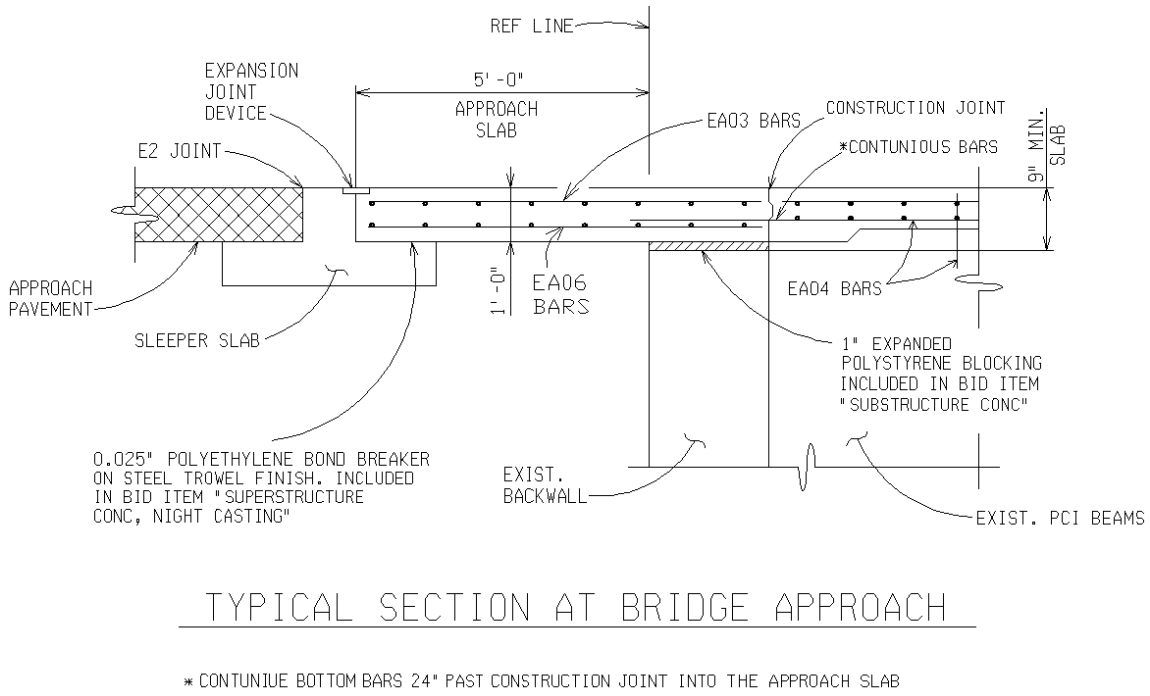

Figure 6-3. Proposed dependent backwall configuration, i.e. construction joint over the backwall face at the span side with continuous bottom reinforcement

6.2.4 Dependent Backwall Configuration – New Construction

MDOT Bridge Design Guide sheet 6.20.04 standard detail consists of continuous bottom layer reinforcement through the optional construction joint between the approach and the deck while top layer reinforcement is discontinued. Further, if the optional construction joint is not provided, a saw cut is required at the same location. Based on literature review and finite element analysis results, it is proposed that the approach slab is fully detached from the deck with a construction joint, both top and bottom reinforcement layers are discontinued, and a diagonal reinforcement layer is used for establishing connection between the approach and the backwall. The modification proposal to MDOT Bridge Design Guide 6.20.04 is shown in Figure 6-4. The proposed detail in standard MDOT Bridge Design Guide format is presented in Appendix G.

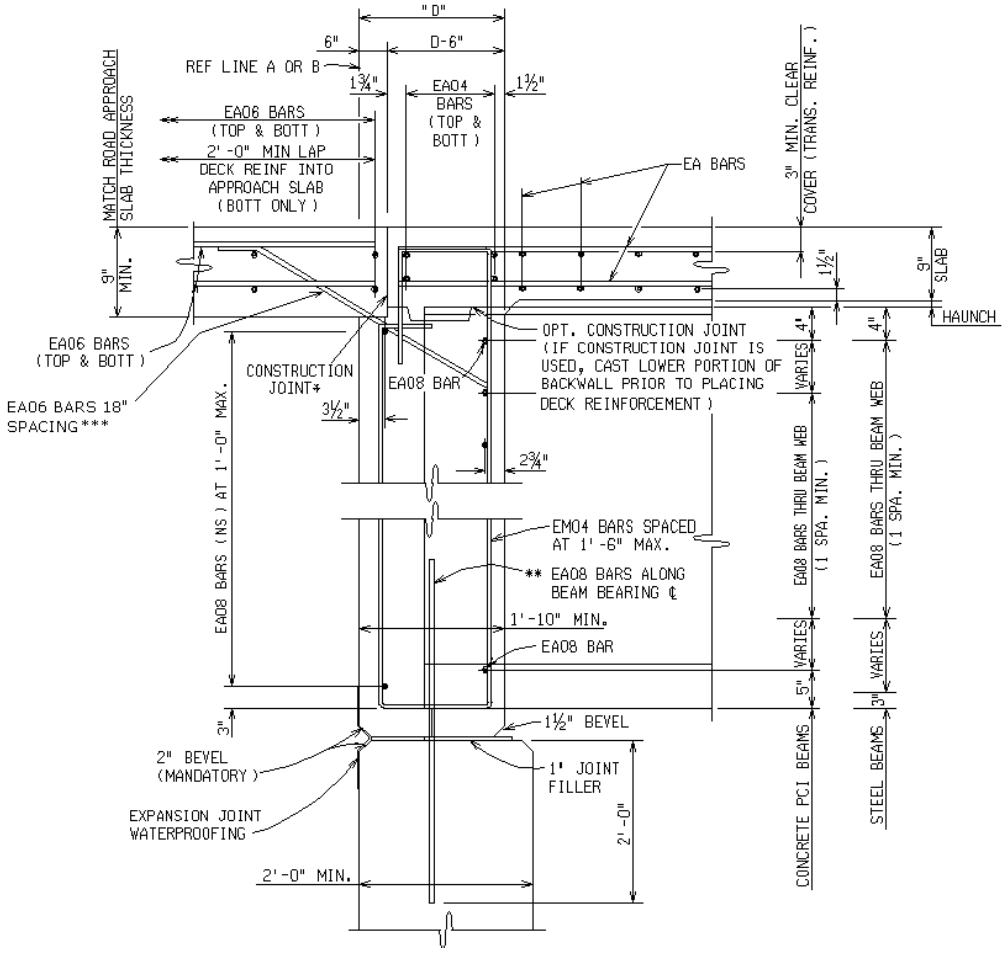

Figure 6-4. Proposed dependent backwall details for new construction; i.e., top and bottom reinforcements discontinuous through the construction joint and diagonal reinforcements are provided between approach slab and backwall

7 SUGGESTIONS FOR FUTURE RESEARCH

The focus of this work has been the investigation of current design details in Michigan jointless bridges with link slabs and decks sliding over the backwall or a deck-backwall combination sliding over abutment. We made design modification proposals for some of the existing configurations and attempted to understand the reasons for link slab cracking by developing analytical models and conducting a load response analysis for single girder and full bridge models. As with most research projects, several questions remain unanswered, and future work is needed. The following list of tasks that should be considered is outlined below.

- Research presented in this report demonstrates the support configuration influence on the link slab force demands. Current analysis procedures fail to account for the influence of support configuration. Development of a refined simple analysis method that incorporates the influence of support configurations on the link slab load demand is recommended. Design load combinations should be reevaluated considering thermal gradient loading. The crack width criteria should also be reevaluated since it is known that the z-factor approach for crack control used in the current procedure is excessively restrictive when concrete covers exceed 2 inches.
- Link slab cracks develop due to hydration thermal loads and drying shrinkage. New cementitious material that can tolerate these loads should be developed.
- Investigation of the high skew effect on jointless bridges with link slabs needs to be investigated.
- Future work is required to benchmark the proposed details. Instrumentation and monitoring of a newly constructed bridge would provide data to verify the behavior and loads predicted from analytical models.

REFERENCES

AASHTO (2002). *Standard Specifications for Highway Bridges*, 17th Edition, Washington, DC, 2002.

AASHTO (2004). *AASHTO LRFD Bridge Design Specifications*, Third Edition, Washington, DC, 2004

ABAQUS/Standard User's Manual - Version 6.7. (2007). Hibbitt, Karlson & Sorensen, Inc., Pawtucket, RI.

ACI Committee 209 (1992). "Prediction of Creep, Shrinkage, and Temperature Effects in Concrete Structures." *Report No. ACI 209R-92*, ACI, Detroit, MI, 1992.

Aktan, H.M., Fu, G., Dekelbab, W., and Attanayake, U. (2003). "Investigate Causes and Develop Methods to Minimize Early-Age Deck Cracking on Michigan Bridge Decks," *MDOT RC-1437*, *CSD 2003-02*, Report to the Michigan Department of Transportation, Detroit, MI 48226.

Aktan, H., Koyuncu, Y., Rutyna, J., Ahlborn, T.M., & Kasper, J.M. (2002). *Causes and cures for prestressed concrete I-beam deterioration*. Research report RC-1412, Michigan Department of Transportation, Lansing, Michigan.

Alampalli, S. and Yannotti, A.P. (1998). "In-Service Performance of Integral Bridges and Jointless Decks." *Transportation Research Record 1624,* Paper No. 98-0540, pp.1-7.

Altair HyperWorks User's Manual – Version 8.0. (2007). Altair Engineering, Inc., 1820 E Big Beaver, Troy, MI 48083-2031.

Badwan, I. Z. and Liang, R. Y. (2007). "Reactin Distribution in Highly Skewed Continuous Steel Girder Bridge." *Transportation Research Record: Journal of the Transportation Research Board, No. 2028*, Washington, D.C.

Burke, M. P., Jr. (1994). "Semi Integral Bridges: Movements and forces." *Transportation Research Record 1460*, Transportation Research Board, Washington, D.C., pp.1–7.

Burke, M. P., Jr. (1997). “Structure Movement Systems Approach to Effective Bridge Design.” *Transportation Research Record 1594*, Transportation Research Board, Washington, D.C., pp.147-153.

Burke, M. P., Jr. (1998). “Pavement Pressure Generation: Neglected Aspect of Jointed Pavement Behavior.” *Transportation Research Record 1627*, Transportation Research Board, Washington, D.C., pp.22-28.

Burke, M. P., Jr., (1999), “Cracking of Concrete Decks and Other Problems with Integral-Type Bridges.” *Transportation Research Record 1688*, Paper No. 99-0104.

Cai, C.S., Shi, X.M., Voyiadjis, G.Z., and Zhang, Z.J. (2005). “Structural Performance of Bridge Approach Slabs under Given Embankment Settlement.” *Journal of Bridge Engineering*, Vol. 10, No. 4. pp.482-489.

Caner, A. (1996). “Analysis and Design of Jointless Bridge Decks supported by simple-span girders.” *PhD Dissertation*, North Carolina State University, Raleigh, NC.

Caner, A. and Zia, P. (1998). “Behavior and Design of Link Slab for Jointless Bridge Decks.” *PCI Journal*, May-June, pp.68-80.

Chun, B.S., Lim, H.S., Sagong, M., and Kim, K. (2004). “Development of a hyperbolic constitutive model for expanded polystyrene (EPS) geofoam under triaxial compression tests.” *Geotextiles and Geomembranes*, 22 (2004), 223-237.

Clough, G. W., and Duncan, J. M. (1971). “Finite Element Analysis of Retaining Wall Behavior.” *Journal of Soil Mechanics and Foundations Division*, ASCE, Vol. 97, SM12, Dec 1971, pp. 1653-1673.

Clough, G. W., and Duncan, J. M. (1991). ‘‘Earth Pressures.’’ Chapter 6, *Foundation Engineering Manual*, 2nd Ed., H. Y. Fang, ed., Van NostrandReinhold, New York, 223–235.

Conboy, D., and Stoothoff, E. (2005). “Integral Abutment Design and Construction: The New England Experience.” *Proceedings of the IAJB 2005*, March 16-18 2005, Baltimore, Maryland.

El-Safty, A.K. (1994). “Analysis of Jointless Bridge Decks with Partially Debonded Simple Span Beams.” *Ph.D Dissertation*, North Carolina State University, Raleigh, NC.

Emerson, M. (1976). “Bridge Temperatures Estimated from the Shade Temperatures.” *TRRL Laboratory Report 696*, TRRL, Crowthorne, Berkshire, Great Britain, 1976.

Faraji, S., Ting, J.M., Crovo, D.S., and Ernst, H. (2001). “Nonlinear Analysis of Integral Bridges: Finite-Element Model.” *Journal of Geotechnical and Geoenvironmental Engineering*, Vol. 127, No. 5, pp.454-461.

Fennema, J.L., Laman, J.A., and Linzell, D.G. (2005). “Predicted and Measured Response of an Integral Abutment Bridge.” *Journal of Bridge Engineering*, Vol. 10, No. 6, pp.666-677.

Gardner, N.J., and Lockman, M.J. (2001). “Design provisions for drying shrinkage and creep of normal strength concrete. ” *ACI Materials Journal*, Vol. 98, No.2, pp. 159-167.

Gastal, F., and Zia, P. (1989). “Analysis of Bridge Beams with Jointless Decks.” *Proc. of International Association for Bridge and Structural Engineering (IABSE) Symp.*, Lisbon, Portugal, pp.555–560.

Gilani, A., and Jansson, D. (2004). “Link Slabs for Simply Supported Bridges: Incorporating Engineered Cementitious Composites.” *Draft Report No. MDOT SPR-54181*, Michigan Department of Transportation, Lansing, Michigan.

Gnip, I.Y., Vejelis, S., Kersulis, V., and Vaitkus, S. (2007). “Deformability and tensile strength of expanded polystyrene under short-term loading.” *Polymer Testing*, 26 (2007), 886-895.

Hambly, E.C. (1991). *Bridge Deck Behavior*, Second Edition, Van Nostrand Reinhold, 115 5th Avenue, New York NY 10003.

Hani, N., Suksawang, N., and Mohammed, M. (2003). “Effects of curing methods on early age and drying shrinkage of high performance concrete.” *TRB 2003 Annual meeting CD-Rom*.

Hadidi, R., Saadeghvaziri, M. A., and Hsu, C. T. T. (2003). "Practical Tool to Accurately Estimate Tensile Stresses in Concrete Bridge Decks to Control Transverse Cracking." *Practical Periodical on Structural Design and Construction*, Vol. 8, No. 2, pp. 74-82.

Imbsen, R.A. (1985). "Thermal Effects in Concrete Bridge Superstructures." *NCHRP Report 276*, TRB, Washington, DC, September 1985.

Kunin, J. and Alampalli, .S. (2000). "Integral Abutment Bridges: Current Practice in United States and Canada." *Journal of Performance of Constructed Facilities*, Vol.14, No.3, pp.104-111.

Li, V.C. (PI), Fischer, G., Kim, Y., Lepech, M., Qian, S., Weimann, M. and Wang, S. (2003). "Durable Link Slabs for Jointless Bridge Decks Based on Strain-Hardening Cementitious Composites." *MDOT Research Report RC-1438*, Michigan Department of Transportation, Lansing, Michigan.

Maberry, S., Camp, J., and Bowser, J. (2005). "New Mexico's Practice and Experience in Using Continuous Spans for Jointless Bridges." *Proceedings of the IAJB 2005*, March 16-18 2005, Baltimore, Maryland.

Maruri, R., and Petro, S. (2005). "Integral Abutment and Jointless Bridges (IAJB) 2004 Service Summary." *Proceedings of the IAJB 2005*, March 16-18 2005, Baltimore, Maryland.

MDOT (2003a). *Bridge Design Guide*. Michigan Department of Transportation, Lansing, MI.

MDOT (2003b). *Standard Specifications for Construction*. Michigan Department of Transportation, Lansing, MI.

MDOT (2005). *Bridge Design Manual*. Michigan Department of Transportation, Lansing, MI.

Menassa, C., Mabsout, M., Tarhini, K. and Frederick, G. (2007). "Influence of Skew Angle on Reinforced Concrete Slab Bridges." *Journal of Bridge Engineering*, Vol. 12, No. 2, pp.205-214.

Mistry, V. (2005). “Integral Abutment and Jointless Bridges.” *Proceedings of the IAJB 2005*, March 16-18 2005, Baltimore, Maryland.

Mokarem, D.W., Weyers, R.E., and Lane, D.S. (2003). “Development of Portland cement concrete shrinkage performance specifications.” *TRB 2003 Annual meeting CD-Rom.*

Mourad, S. and Tabsh, S.W. (1999). “Deck Slab Stresses in Integral Abutment Bridge.” *Journal of Bridge Engineering*, Vol. 4, No. 2, pp.125-130.

Nassif, H., Abu-Amra, T., and Shah, N. (2002). “Finite Element Modeling of Bridge Approach and Transition Slabs.” *FHWA NJ 2002-007*, Piscataway, NJ.

Needham, D. and Juntunen D. (2000).“Link Slab Design w/ Steel I-beam Girders.” *Hand Calculations*.

National Cooperative Highway Research Program (NCHRP) (1991). “Manuals for the design of bridge foundations.” R. M. Barker, J. M. Duncan, K. B. Rojiani, P. S. K. Ooi, C. K. Tan, and S. G. Kim, eds. *Rep. 343*, Transportation Research Board, Washington, D.C.

Oesterle, R.G., Tabatabai, H., Lawson, T.J., Refai, T.M., Voltz, J.S., and Scanlon, A. (1999). “Jointless and Integral Abutment Bridges.” *Summary Report,* Final Report to Federal Highway Administration, Washington D.C.

Oesterle, R.G., Refai, T.M., Volz, J.S., Scanlon, A., and Weiss, W.J. (2005), “Jointless Bridges, Analytical Research and Proposed Design Procedures.” *Volume II*, Final Report to FHWA, February 2005.

Okeil, A.M., and ElSafty, A. (2005). “Partial Continuity in Bridge Girders with Jointless Decks.” *Practice Periodical on Structural Design and Construction*, Vol. 10, No. 4.

PCI (2003). *Precast Prestressed Bridge Design Manual*. Precast/Prestressed Concrete Institute, 175 W. Jackson Boulevard, Chicago, IL 60604.

Purvis, R. L. (1989). “Prevention of Cracks in Concrete Bridge Decks.” *Wilbur Smith Associates*, Report on Work in Progress.

Richardson, D.R., (1989). “Simplified Design Procedures for the Removal of Expansion Joints from Bridges using Partial Debonded Continuous Decks.” *Master’s Thesis*, North Carolina State University, 1989.

Saadeghvaziri, M. A. and Hadidi, R. (2002). “Cause and Control of Transverse Cracking in Concrete Bridge Decks.” Final Report, *FHWA-NJ-2002-019*, New Jersey Department of Transportation, Trenton, NJ.

Scanlon, A., Patel, I.C., and Angelo, S. (1994). “Bridge Superstructure Research, Task 3: Final Designs and Details for Simple-Span Bridges Made Continuous”, *Final Report Research Project 90-11*, PennDOT, 1994.

Shah, S. P., Marikunte, S., Yang, W., and Aldea, C. (1996). “Control of cracking with shrinkage-reducing admixtures.” *Transportation Research Record*, pp. 25.

Tabatabai, H., Oesterle, R.G., and Lawson, T.J. (2005). “Jointless Bridges, Experimental Research and Field Studies.” *Volume I*, Final Report to FHWA, August 2005.

Thiagarajan, G. and Roy, S. (2005). “Finite Element Modeling of Reinforced Concrete Bridge Decks with ABAQUS.” *Report No. UTC R111*, Center for Infrastructure Engineering Studies/ UTC Program, University of Missouri, Rolla.

Thippeswamy, H. K., GangaRao, H. V. S., and Franco, J. M. (2002). “Performance Evaluation of Jointless Bridges.” *Journal of Bridge Engineering*, Vol. 7, No. 5, pp.276-289.

Tindal, T.T. and Yoo, C.H., (2003). “Thermal Effects on Skewed Steel Highway Bridges and Bearing Orientation.” *Journal of Bridge Engineering*, Vol. 8, No. 2, pp.57-65.

U.S. Department of the Navy. (1971). ‘‘Design manual—Soil mechanics, foundations, and earth structures.’’ NAVFAC DM-7, Naval FacilitiesEngineering Command, Alexandria, VA.

Wasserman, E.P., and Walker, J.H. (1996). "Integral Abutments for Steel Bridges," *Highway Structures Design Handbook*, VII, Chapter 5, American Iron and Steel Institute, 1996.

Weakley, K. (2005). "VDOT Integral Bridge Design Guidelines." *Proceedings of the IAJB 2005*, March 16-18 2005, Baltimore, Maryland.

Wetmore, J. and Peterson, B. (2005). "Case Study – Jointless Bridge Beltrami County State Aid Highway 33 Over Mississippi River in Ten Lake Township, Minnesota." *Proceedings of the IAJB 2005*, March 16-18 2005, Baltimore, Maryland.

Wing, K.M. and Kowalsky, M.J., (2005)."Behavior, Analysis, and Design of an Instrumented Link Slab Bridge." J*ournal of Bridge Engineering*, Vol. 10, No. 3, pp.331-344.

Yazdani, N., Eddy, S. and Cai, C.S., (2000). "Effect of Bearing Pads on Precast Prestressed Concrete Bridges." *Journal of Bridge Engineering*, Vol. 5, No. 3, pp.224-232.

Zederbaum, J. (1969). "Factors Influencing the Longitudinal Movement of Concrete Bridge System With Special Reference to Deck Contraction," *Concrete Bridge Design*, ACI Publication No. SP-23, ACI, Detroit, MI, 1969.

Zia, P., Caner, A. and El-Safty, A.K. (1995). "Jointless Bridge Decks." Center for Transportation Engineering Studies, *Report No. FHWA/NC/95-006*, September 1995, pp.117.